LARGE-AREA SOIL PHYSICAL DEGRADATION ASSESSMENT USING GIS, REMOTE SENSING, AND INFRARED SPECTROSCOPY IN ARID AND SEMI-ARID KENYA

CHRISTIAN THINE OMUTO

UNIVERSITY OF NAIROBI

2006

LARGE-AREA SOIL PHYSICAL DEGRADATION ASSESSMENT USING GIS, REMOTE SENSING, AND INFRARED SPECTROSCOPY IN ARID AND SEMI-ARID KENYA

BY

CHRISTIAN THINE OMUTO

(B.Sc., M.Sc. Agricultural Engineering)

A

THESIS

Submitted in the fulfilment for the award of the Degree of

Doctor of Philosophy

of the University of Nairobi

2006

DECLARATION

This thesis is my original work and has not been presented for a degree in any other university.

.... 7/3/07 ....

Christian Thine Omuto   Date

This thesis has been submitted for examination with our approval as University Supervisors for the award of the Degree of Doctor of Philosophy in the Department of Environmental and Biosystems Engineering in the Faculty of Engineering of the University of Nairobi.

.... 15/3/2007 ....

Professor Lawrence O. Gumbe   Date

.... 12-03-07 ....

Dr. Keith D. Shepherd   Date

.... 8/3/07 ....

Dr. George Okwach   Date

DEDICATIONS

This thesis is dedicated to my beloved and Almighty GOD. You have never let me down on any issue.

ACKNOWLEDGEMENTS

Relentlessly asking questions and seeking answers have achieved writing this thesis. Many institutions and individuals facilitated my achievements and I express my gratitude most sincerely to all of them. Painfully, I confront the fact that I cannot acknowledge everyone individually. Necessarily, however, I have to be transparent about key facilitation without which this thesis would not have been a product for the public. To Dr. Keith Shepherd: You fuelled me to putting my thoughts on paper and ensuring my entry into a network with the World Agroforestry Centre (ICRAF). I was more than your student and I know deeply that this piece of work is certainly with a heavy input from you. To Dr. Markus Walsh: I am a proud product of your scientific endeavours and refereeing. To Professor Lawrence Gumbe: I will not forget your academic acumen. In addition, the burning desire to copy your admirable efforts in all manner of life, academics, and professionalism kept me through the studies without any sign of stress. To Mr. Ric Coe: You are my mentor and who took me many places during the development of the scientific form of this thesis. I will also not forget Dr. George Okwach who built around me a fatherly confidence. You have stirred in me the philosophical nature of a PhD-holder that cannot be exhaustively summarized by simple writing on paper.

This study benefited from generous financial support from ICRAF, The University of Nairobi, The Rockefeller Foundation, and International Fund for Agricultural Research, IFAR. I also thank International Training Centre (ITC), in The Netherlands for support in the acquisition of the remote sensing images. I benefited directly or in-kind from contributions from Kenya Agricultural Research Institute (KARI)-Katumani. I also thank Alex Awiti, Stephen Ichami, Elvis Weullow, and Andrew Sila all from ICRAF. This study was also supported in a huge way from my family members. I single out my loving brother Fredrick Opere for his sustained effort during the period. God bless you all and may your effort not end in future.

TABLE OF CONTENTS

LIST OF FIGURES

LIST OF TABLES

LIST OF SYMBOLS AND ABBREVIATIONS

List of abbreviations

CI – Crust Index
DEM – Digital elevation model
DN – Digital Numbers
DSR – Diffuse Spectral Reflectance
FAO – Food and Agriculture Organization
GI – Gini Index of impurity
GIS – Geographic Information System
ICRAF – International Centre for Research in Agroforestry
LST – Land Surface Temperature
NDV – Normalized Difference Vegetation Index
NIR – Near Infrared
NLME – Nonlinear Mixed Effects model
PDI – Physical Degradation Index
RSE – Residual Standard Error
SA – Percentage of stable aggregates
SAR – Sodium Absorption Ratio
TOA – Top of the Atmosphere
WHC – Water Holding Capacity

Symbols

Letters

A_G – Amplitude
C_s – Volumetric heat capacity
d – Earth-Sun distance
E_o – Extraterrestrial solar irradiance
f_c – Steady infiltration rate
h_a – Air-entry potential (m)

L_p – Atmospheric path radiance

$L_{atm}^{\uparrow}$ – Upwelling radiance

$L_{atm}^{\downarrow}$ – Down welling radiance

L_{sat} – Top of the atmosphere radiance

n – Pore-size distribution index

z – Soil depth

Greek symbols

α – Alpha parameter (m^{-1}). The inverse of air-entry potential

ρ_b – Bulk density

θ_s – Saturated soil moisture content (cm^3/cm^3)

θ_r – Residual coil moisture content (cm^3/cm^3)

ϕ – Solar zenith angle

τ – Atmospheric transmittance

ω – Frequency

κ_s – Thermal conductivity

LARGE-AREA SOIL PHYSICAL DEGRADATION ASSESSMENT USING GIS, REMOTE SENSING, AND INFRARED SPECTROSCOPY IN ARID AND SEMI-ARID KENYA

By

Omuto Christian Thine

(University of Nairobi)

ABSTRACT

Soil physical condition controls several important soil functions such as support for biomass production, water cycling, filtering pollutants, and land surface energy balance. However, physical degradation undermines this ability. Currently, there is lack of rapid and repeatable methods that can facilitate timely large-area assessment for effective monitoring and control of soil degradation. This study tested the combined applications of point-measurements of physical properties, soil diffuse spectral reflectance (DSR), and remote sensing to spatially assess the degradation in a large watershed (4500 km^2) in semi-arid areas in eastern Kenya.

Indicators of the degradation were determined from 540 point-measurements of infiltration and water retention and field observations of the visible signs of soil physical degradation. The physical properties included steady-state infiltration rates, sorptivity, water-holding capacity, pore distribution index, bulk density, and air-entry potential. The parameters describing these properties were derived using a nonlinear mixed effects (NLME) approach, which was also used to test for the effects of other covariates such as land use and geographic features. A screening protocol was then developed that took evidence of degradation from visible assessments in the field, estimated soil physical properties, and rapid soil tests based on soil DSR to predict the degradation cases. Over 90% sensitivity

and specificity was achieved with a mixed effect logistic model based on a one-third holdout sample. The screening results showed that soil DSR was a powerful tool for detecting early warning indicators of degradation that were not readily discernable from field observations.

In addition to the point-estimates of likelihood of physical degradation, time-integrated remote sensing indicators were also tested for power of spatial prediction of the trends of the degradation in the study area. The standardized deviations of land surface temperature (LST) and Normalized Difference Vegetation Index (NDVI) from time-series Landsat scenes were used to study the thermal and vegetation conditions of the degradation at sampled points. These indices effectively predicted the likelihood of the degradation of the held-out samples with 80% accuracy of ground reference data and were used to map the degradation in the whole study area.

The approach developed in this study showed promising opportunity for spatial prediction of physical degradation at high spatial resolution over large areas and could be a useful tool for guiding policy decisions on sustainable land management especially in the tropics where land use policies lack scientific support.

CHAPTER ONE

1. INTRODUCTION

1.1 Background

Soil physical condition determines several important soil functions including the soil's capacity to store or transmit water and nutrients, removal of contaminants from the environment, heat transfer between the soil and the atmosphere, provision of suitable habitat for soil biota, and anchorage for plant root development (Lal, 2000a). Especially in the upper layer, soil structure controls the flux of nutrients, water, gases, and heat to and from the underlying soil profile (Poesen and Nearing, 1993; Blum *et al.,* 1998; Park *et al*, 2004). Thus, soil physical constraints are important for agronomic production as well as environmental quality and global climate circulation. Although much research has been conducted to offer opportunities for prevention and control of soil degradation, the problem still continues worldwide (Pagliai and Jones, 2002). This is in part due to the lack of appropriate soil testing for early-warning signs and large-area assessment protocols that can permit comparisons over time. Particularly in tropical watersheds where soil degradation is threatening food security, rapid soil testing for the physical constraints and landscape assessment procedures are urgently needed to guide land use policy (Lal, 2000a).

Soil physical degradation, though a process that evolves through many stages before it can be observed in the field, affects many soil and plant properties in a way that can be utilized to monitor the trends of the degradation. For example, since the degradation adversely affects soil iron oxide and carbon content, these properties can be used to monitor progress of degradation (West *et al.*, 2004). However, because measurements of iron oxide and carbon are relatively expensive for large sample-sizes, rapid techniques such as reflectance spectroscopy can be used as a proxy (Baumgardner *et al.*, 1985; Shepherd and Walsh, 2004; West *et al.*, 2004).

Physical degradation also influences soil thermal admittance that regulates LST (Campbell and Norman, 1998). Thermal admittance is governed by soil bulk density, volumetric heat capacity, and thermal conductance and their alterations affect LST. By monitoring variations of LST, inferences can be made about soil surface physical conditions (Park *et al.*, 2004). LST and vegetation greenness measured through NDVI, are both detectable with remote sensing (Liang, 2004) and can provide a good opportunity for use of remote sensing in detecting soil physical degradation. This study aimed at testing the opportunities for use of soil physical properties, spectral reflectance, and remote sensing for rapid detection of physically degraded sites in the Upper Athi river basin in Eastern Kenya.

1.2 Problem statement and justification

Soil physical degradation negatively affects agronomic productivity, causes adverse off-site effects such as siltation of surface water and reduction of soil depth needed to filter pollutants, and also has negative impacts in environmental sustainability (Lal, 2000a). The need to curb the degradation has therefore been a serious concern to agriculturalists, environmentalists, engineers, and also political establishments (Horn *et al.*, 1995). However, the characteristic slow processes of the degradation beguile researchers and land managers who begin to act when the degradation is at its advanced and most expensive stage to control (Dexter, 2004). Recently, scientists have discovered the need to establish early warning signs and find solutions for timely prevention of physical degradation (Paglia and Jones, 2002; Dexter, 2004). One of the principal research problems in this study was to contribute to the call for detection of early warning signs of soil physical degradation and increase knowledge that will help in the timely prevention of degradation at appropriate management scales.

Early detection of soil physical degradation, however, can be an elusive undertaking given that; (1) the effects of the incipient degradation can be easily masked by agronomic inputs such as manure, fertilizers or irrigation (Watts and Dexter, 1998; Breuer and Schwertmann, 1999) and (2) it can take many years to notice changes in the soil physical properties that index the degradation (Deuchers *et al.*, 1999). Although physical properties are ideal in diagnosing long-term changes in soil physical conditions (Dexter, 2004), their measurement not only suffers from the problem of being too expensive for large-area measurements but also from delayed response to changes in the soil matrix. One way of overcoming these limitations is through the combined use of physical properties and other soil properties that are integral of many functional capacities related to physical degradation but that can be measured rapidly and cheaply. A prominent soil property that has been widely shown to integrate many functional processes is the soil's DSR (Janik *et al.*, 1998; Sanchez *et al.*, 2003; Shepherd and Walsh, 2004). Soil spectral reflectance is a characteristic pattern of the electromagnetic radiations after interaction with the soil medium (Ben-Dor *et al.*, 1999). Many researchers have successfully been able to link spectral reflectance to various soil constituents with the help of high spectral resolution detectors and multivariate calibration techniques (Chang *et al.*, 2001; Shepherd and Walsh, 2002). Recently, Ben-Dor *et al.* (2003) and Eshel *et al.* (2004) used the technique to diagnose soil structural degradation. This study intended to combine soil physical properties, field observations of the degradation, and soil spectral reflectance to develop a classification protocol for early detection of the physical degradation in a tropical watershed.

Although soil spectral reflectance and point-measurements of physical properties have the promise of explaining physical degradation, land managers and land users understand the degradation at the landscape level. Consequently, all research aimed at aiding management decision on the degradation need to consider landscape-level scales in their studies (Lal, 2000a). The use of remote sensing and GIS has been very valuable for this scale of study (De Jong, 1994). Especially with detectable features such as NDVI and LST, the use of remote sensing has been able to capture spatial and temporal changes in soil quality

(Farrar *et al.*, 1994; Park *et al.*, 2004). It was hypothesized in this study that soil physical degradation could have marked influence on LST and NDVI in a way that can allow use of remote sensing for monitoring the degradation.

1.3 Objectives

The broad objective of this study was to develop a rapid protocol for the assessment of soil physical degradation in large-basins in arid and semi-arid areas of Kenya.

The specific objectives of the study were:

i. To identify pertinent soil physical properties that index physical degradation.
ii. To develop a case-definition of soil physical degradation using the properties identified in (i) above.
iii. To develop calibration models between cases of physical degradation in (ii) above and visible-infrared spectral reflectance as a rapid screening tool for early detection of degradation.
iv. To calibrate soil physical degradation to indices derived from remote sensing for spatial prediction in the study area.

CHAPTER TWO

2. LITERATURE REVIEW

2.1 The nature of soil physical degradation

Soil physical degradation is a component of land degradation in which the soil texture and structure are adversely affected with negative impacts on agronomic productivity, environmental quality, and water quality (Jones, 2003). Land degradation is the broad term that describes the reduction in the potential of land to sustain the provision of utility of natural resources (De Jong, 1994). FAO (1979) distinguished six main components of land degradation as water erosion, wind erosion, excess salts, chemical degradation, physical degradation, and biological degradation. However, Chatres (1987) argues that erosion and salinization are soil physical processes and suggested only three components of land degradation as physical, chemical, and biological degradation.

2.1.1 Characteristics of soil physical degradation

The concept of soil physical degradation, though it varies depending on the author, is always associated with soil structure or physical quality. As an example, according to Dexter (2004), soil physical degradation results when the soil exhibits physical qualities like poor infiltration, runoff water from the soil surface, hard-setting, poor aeration, poor rootability, and poor workability, while according to Munkholm and Schjonning (2004), physical degradation is the diminution of the soil structure. Despite the differences in the definitions, the physical degradation may be seen to manifests itself in such forms as compaction, or disaggregation, surface deformation, and the exposure of soil profiles underlying the topsoil (Figure 2.1). Physical degradation can also be characterized by salt nodules in the profile and/or their accumulation in places where irrigation is practiced or at least where evaporative demands are high, surface (Metternicht and Zinck, 2003).

Soil compaction refers to a specific phenomenon in which the amount of soil solids in a given cross-sectional area is increased at the expense of the pore spaces (Ball *et al.*, 1997). According to Fies and Bruand (1998), there are two types of soil pores: structural pores and textural pores. The structural pores, which may result from tillage, traffic, climate, or biological activity, are largely affected by compaction while textural pores that are the results of arrangement of the elementary soil particles are not easily affected by compaction (Richard *et al.*, 2001). However, the influence of compaction on the textural pores as reported by Coulon and Bruand (1989) could be an indication of severe physical degradation.

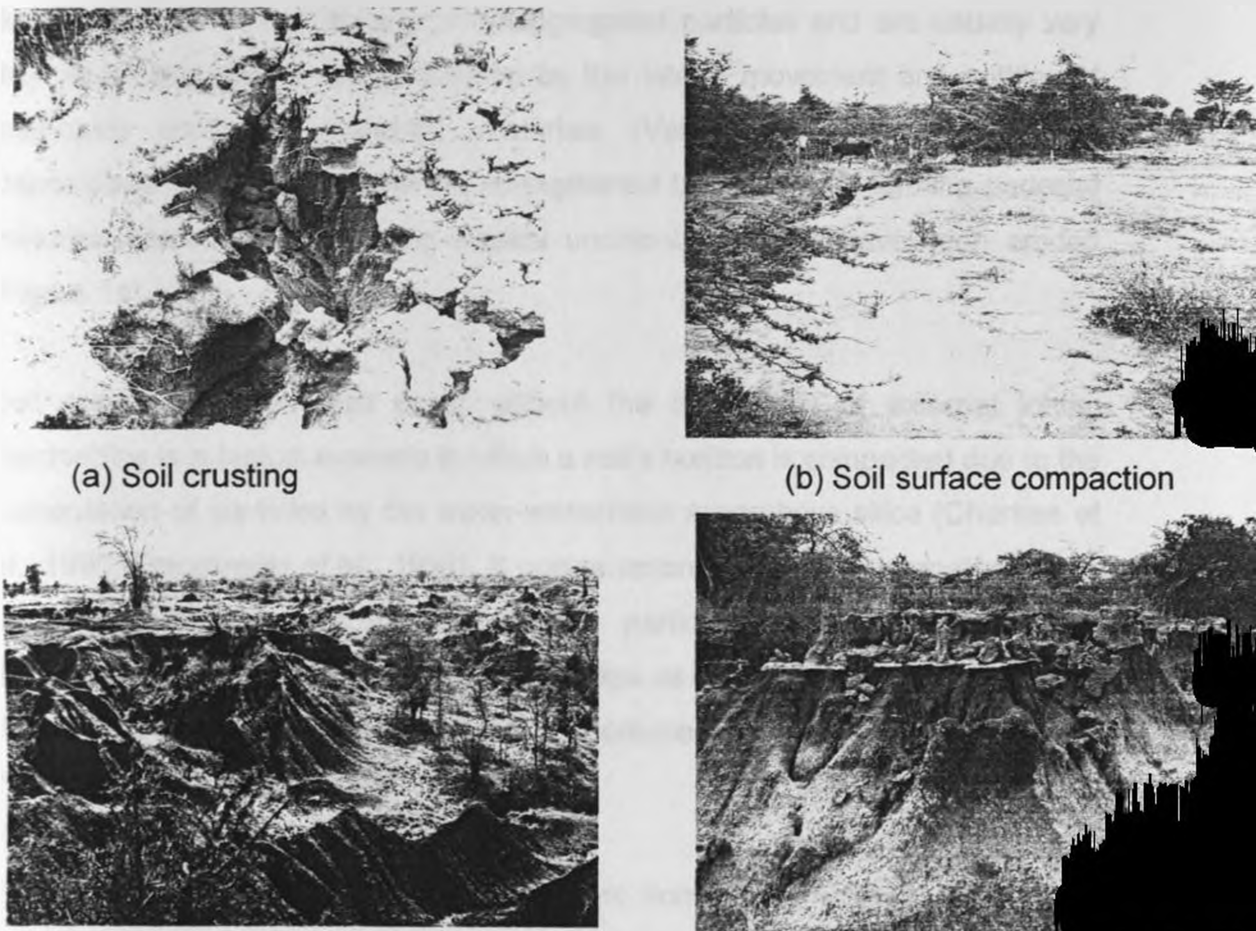

(a) Soil crusting (b) Soil surface compaction

(c) Surface soil loss (d) Exposure of subsoil

Figure 2.1. Characteristic types of soil physical degradation

Soil compaction on the surface can lead to the formation of surface seals or crusts. This phenomenon arises when the soil aggregates at surface are broken down, re-arranged, and finer particles pushed to clog the spaces between larger particles (Agassi *et al.*, 1981). Whereas soil surface seals are formed by the orientation and packing of dispersed particles due to raindrop impact, crusts are formed by deposition of fine sediments or by trampling by livestock or compaction through traffic by machinery (Chen *et al.*, 1980; Mapfumo *et al.*, 1999). Crusts formed by trampling or vehicular compaction are known as structural crusts while those that are formed by deposition of eroded materials are known as depositional crusts (Valentin and Bresson, 1992). Structural crusts develop by the vertical sorting of disaggregated particles and are usually very thin while depositional crusts develop by the lateral movement and settling of previously eroded fine-grained materials (Valentin and Bresson, 1992). Depositional crusts may further be strengthened by algae thus forming pedestal features where the surrounding weaker uncolonized crusts have been eroded (Figure 1a).

Soil compaction can also occur without the application of external loads. Hardsetting is a typical example in which a soil's horizon is compacted due to the cementation of particles by the water-extractable amorphous silica (Chartres *et al.*, 1990; Franzmeier *et al.*, 1996). It occurs among unstable aggregates where the iron oxides, organic matter, and fine particles are rearranged to form structural connections between sand particles as the soil dries (Mullins *et al.*, 1987). The strength of these connections increases with drying to finally form a hard mass of compacted soil.

Soil salinity or sodicity is somewhat different from the other forms of physical degradation. Salinity arises due to accumulation of salts from ions dissolved in the soil-water or from precipitation of minerals, while sodicity accrues from the replacement of other cations in the adsorption complex by sodium (Van Beek and Van Breeman, 1963). These forms of soil degradation are different from acidification and toxicity, which are forms of chemical degradation (FAO, 1979).

Soil erosion, as a form of physical degradation, is the loss of the upper layer of the soil profile (Figure 1d). Although there are many categories of soil erosion, the most significant ones are accelerated erosion and tillage erosion (Govers *et al.*, 1996). Accelerated erosion occurs when soil particles are detached and moved away by action of water, wind, gravity, or glaciers (Hudson, 1993). Suresh (2002) has discussed different types of accelerated erosion that include splash, sheet, rill, and gully erosion. Tillage erosion occurs during tillage when implements completely or partially turn the soil upside down and making it vulnerable for translocation over the landscape (Govers *et al.*, 1996).

The occurrence of soil erosion is an indication of advanced physical degradation process. For instance, Tiffen *et al.* (1994) observed that most of the gullies in Ukambani in Kenya developed from former cattle tracks. These cattle tracks must have suffered animal trampling as an initial form of physical degradation before gradually developing into gullies. Quine *et al.* (1997) observed tillage erosion from structural deterioration induced by mechanical tillage.

2.1.2 What influences soil physical degradation

Soil degradation varies considerably even within similar soil mapping units. The variations in magnitude and extent of physical degradation have been widely cited in literature to be due to soil type, climatic, and management factors (Oldeman *et al.*, 1991; Marshall *et al.*, 1996; Young *et al.*, 2001).

Among the soil factors influencing physical degradation, the content of readily dispersible clay is most prominent (Heil *et al.*, 1997). The structure of soils with readily dispersible clay may collapse and lose large pores when wet and hardset when dry. This homogenization of soil can result into compaction (Dexter and

Czyz, 2000). In addition to dispersible clays, presence of plinthite and high amount of exchangeable sodium and potassium can also influence soil physical degradation. According to Lal (2000b), plinthite that hardens irreversibly on exposure is also partly the reason for a soil's susceptibility to compaction. Especially in the tropical region, majority of subsoils have plinthite that is responsible for a large number of compaction cases (Lal, 2000b). Research by Quirk (1986) showed that soil's vulnerability to physical degradation is eminent when sodium ions (Na^+) constitute a significant part of the exchangeable complex. Na^+ is considered the exchangeable cation responsible for clay dispersion (Quirk, 1986). However, for soils with low Na^+, Auerswald *et al.* (1996) found positive correlation between exchangeable potassium with soil erodibility.

Although soils may differ in terms of their susceptibility to physical degradation, climate can aggravate this vulnerability. Climatic patterns that permit rapid wetting and drying may impose uneven internal strain in soils, which can weaken their structural stability and consequently making them prone to physical degradation (Lal, 2000a). Also, depending on soil tilth and rainfall characteristics raindrop impact may either detach soil particles or cause compaction. Initiation of soil degradation by raindrop impact has been well researched (for example Rousseva *et al.*, 2002).

Land management practices can also influence soil physical degradation. Whereas soil conservation can retard or prevent some forms of physical degradation, adverse management practices such as agricultural extensification can lead to rapid physical degradation (Hudson, 1971). For example, Alegre *et al.* (1986) showed that the conversion of fragile soils from natural to agricultural ecosystems could accelerate the physical degradation. Munkholm and Schjonning (2004), while observing an increase in the structural deterioration by working wet sandy loam soils, concluded that land preparations done at the onset of rains could cause serious physical damage to the soils. This could be valid since soils significantly lose their strength with increase in wetness.

Auerswald *et al.* (1996) also found out that excessive fertilization with potassium could damage the soil's physical condition since exchangeable potassium promotes soil erodibility.

2.1.3 Occurrence and direct drivers of soil physical degradation

A first step in any diagnostic study is to quantify the prevalence and incidences of degradation cases. These characteristics provide useful guidelines for the prevention and monitoring of the degradation (Jones, 2002). Incidence is a measure of the degradation condition either at a time or over time while prevalence is an indication of the extent of the degradation.

Salinity and sodicity

The prevalence of salinity/sodicity in a soil profile may be attributed to the migration of salts with soil-water movement. Especially for salinization, accumulation of salts is largely due to high evaporation rates compared to both supply and storage of the soil-water. Salinity/sodicity may also be associated with certain soil types. For example, soils classified as Solonchaks contain excess soluble salts while Solonetz contain excess exchangeable sodium (FAO, 1971-1981). The prevalence of these soils combined with other factors can determine the occurrence of the world salt-affected soils. Although the statistics relating to distribution of saline/sodic soils are varied according to authors, there is a general trend of increase in the world's salinity/sodicity across literatures. Lal (2000b) approximates salinity in the arid tropics at about 317 M ha, while Ghassemi *et al.* (1995) estimates global extent of primary salt-affect soils at about 955 M ha and 77 M ha for secondary salinization.

Although all soils contain some soluble salts, salty soils show high contents of various kinds of salt and/or excess exchangeable sodium. When the salt contents are observable in the field, the degradation may be severe. According to Smedma and Rycroft (1983), the efflorescence phenomena in saline soils and occurrence of a dark film on the surface of sodic soils are typical signs of severe physical degradation.

Soil salinity exerts additional binding forces of soil-water above the normal moisture retention forces thus reducing the readily available water for the plant roots. It may also cause unfavourable toxic conditions to soil biota, plant development, or unsafe water for human consumption (Gupta and Abrol, 1990). Unlike salinity that may encourage flocculation, sodicity can cause easy dispersion of soil colloids and consequently contributing to structural deterioration (Marshall *et al.*, 1996).

Compaction

Soil compaction also varies in its prevalence and incidences across contents. Oldeman *et al.* (1991) has shown a typical distribution of the world's soil compaction in which the total compacted area in Europe (33 million hectares) and Africa (18 million hectares) are higher than those of other regions. According to Van Lynden (2000), the extent of compaction in Europe is attributable to mechanized agriculture. In Africa, the extent of compaction is attributable to the occurrence of susceptible soils (Lal, 1997) as well as high livestock-stocking rates (Mapfumo *et al.*, 1999).

There are varied reasons for the occurrence of surface sealing, crusting, and hardsetting. Some authors attribute the prevalence of these forms of physical degradation to certain physical, chemical, and mineralogical soil properties (Mullins *et al.*, 1990; Heil *et al.*, 1997; Breuer and Schwertman, 1999). They argue that higher percentage of fine soil particles, the presence of low activity clays, and lack of aggregating agents such as metal hydroxides and organic matter encourage the degradation. Other authors, however, point out a combination of climate and land use systems to cause surface sealing, crusting, and hardsetting (Lal and Sanchez, 1992; Lal, 2000b). Although these claims come from different geographic backgrounds, De Jong, (1994) observed that sufficient spatial data is still lacking to support the claims on crusting or hardsetting.

Soil compaction, whether of the profile or at the surface, affects plants, soil workability, and environment. Especially for plant growth and root development, soil compaction can be both beneficial or an impediment depending on the type of plant. In rice production, subsoil compaction may be a requirement while for many other plants it inhibits root growth through mechanical impedance and inadequate nutrient supply (Whalley *et al.*, 1995). In addition to restricting seedling germination, compaction on the soil surface also retards infiltration and consequently limiting supply of moisture to root-zone. Compacted soils are also difficult to work thus reducing the production efficiency. They have been shown to significantly contribute to the production of the noxious greenhouse gases in two ways (Horn *et al.*, 1995): increasing engine emissions in mechanized agriculture due to increased energy requirement to work hard soils and emissions from soils in anaerobic condition due to improper drainage. Furthermore, by reducing the soil's bulk thermal conductivity soil compaction has the potential of contributing to the build-up of the surface thermal flux (Campbel and Norman, 1998).

Erosion

Unlike other forms of soil physical degradation, the distribution of erosion has been well researched. Estimates are both available for the global scale (Oldeman *et al.*, 1991) and regional scales (Van Lynden and Oldeman, 1997; Van der Knijff *et al.*, 1999). Although these reports are largely based on expert opinion, they give an overall impression of the status of soil degradation in different regions. The estimates have also been used to determine the effect of the degradation on the global/regional agronomic productivity and environmental quality. Oldeman (1998) estimated the productivity losses at 25% for Africa, 13% for Asia, and 37% for Central America. Lal (1998) estimated global yield loss of 10% in cereals, 5% in soybeans and pulses, and 12% in root and tubers due to soil erosion.

Soil erosion also degrades environmental quality. With soil movement by erosion, nutrients such as phosphorous and agrochemicals adsorbed onto the surfaces of the clay particles move by overland flow, through drains and in streams or rivers. This can result in algal blooms and other forms of water pollution (Hesketh *et al.*, 2001). In addition, the sedimentation of low-lying areas due to upland erosion may undermine the agricultural productivity of these areas. Even though sediments may be chemically fertile, their agricultural productivity is inferior because of adverse physical characteristics such as poor water retention, poor aeration, and susceptibility to compaction. Soil erosion can also degrade environmental quality by the development of badland that have little further value for agricultural production. The soil loss during erosion reduces the soil-profile depth in varied scales across landscapes thus causing badlands. In addition, the reduced soil depth may affect the soil's capacity to filter pollutants and buffer atmospheric heat that may result in higher land surface temperature.

2.2 Evolution of research in soil physical degradation

2.2.1 Research activities

As indicated in the previous sections of this thesis, physical degradation ranges from structural deterioration to soil loss through erosion. Research on these manifestations of soil physical condition has not waned over the years. Pagliai and Jones (2002) noted that for the last few decades a lot of research has been constituted to study soil degradation in many parts of the world and the results published in various journals, books, theses, and presentations in scientific conferences. Young *et al.* (2001) reviewed the literatures between 1991 and 1999, albeit with a bias towards soil structure. The approach they used clearly showed varied levels of research activities in different aspects of soil physical condition. Similarly, a bibliographic search was conducted in this study to review recent research on soil physical degradation in journal articles published in the following main areas: compaction, crusting, hardsetting, salinity, and erosion. It should be appreciated that online publications in peer-reviewed journals are not full representation of on-going research but rather some sort of indication to the direction of the research activities in a given field. In this study, the online journal search engine (OJOSE) (http://www.ojose.com/) was used. The search was conducted from among the mainstream refereed journals including: European journal of soil science (European JSS), American journal of soil sciences (SSSAJ), Agriculture, Ecosystems and Environment (AEEnv), Geoderma, Soil and Tillage Research (S&TR), Soil Science, Australian Journal of Soil Science (Australian JSS), Catena, and Soil Biology and Biochemistry (SB&B). In order to remove the errors associated with online access in some journals, the search period was limited to between 2000 and 2005. Figure 2.2 shows the results in which the vertical axis represents the percent of the papers that dwelt with a specific degradation issue across the journals.

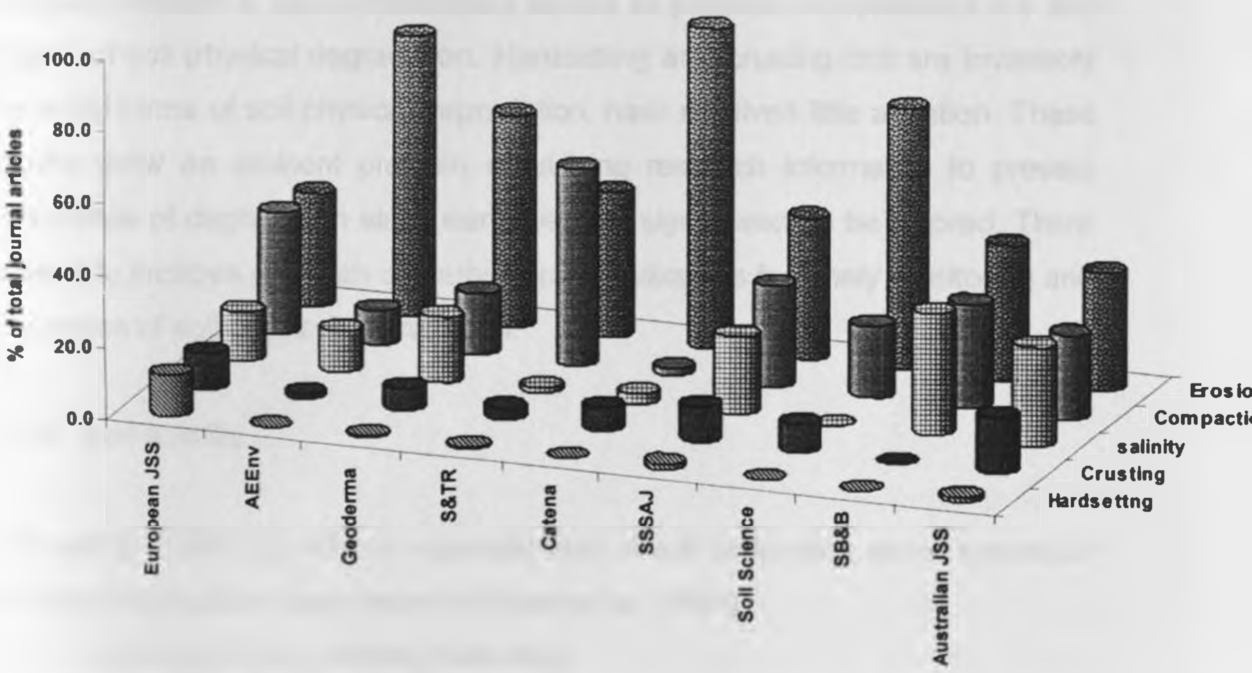

Figure 2.2. Distribution of on-line articles in aspects of physical degradation

It appears from the search results that soil erosion has been extensively studied. The first seminal work on erosion was done by Hudson (1971) who described the causes, types, and management of soil erosion. Since then, the research has tackled numerous aspects of erosion (Oldeman, 1994). Recently, Govers (1999) described emerging forms of erosion – tillage and land leveling erosion – in which the term *soil loss* assumes different meaning compared to Hudson's geological and accelerated erosion. All these impetus in erosion studies could be attributed to certain key reasons. For example, Lal (1998) observed that apart from the easy conceptualization of erosion measurements, the readily observable erosion features make the problem more distinct compared to other subtle forms of physical degradation. Second, a lot of donor funding has gone into facilitating research in soil erosion (FAO and ISRIC, 2000). According to Oldeman (1998), the impetus in erosion studies is driven by the belief that it is the major threat to food security.

Although erosion is much researched across all journals, it represents the late stages of soil physical degradation. Hardsetting and crusting that are invariably the initial forms of soil physical degradation, have received little attention. These results show an eminent problem of utilizing research information to prevent occurrence of degradation since early warning signs seem to be ignored. There is need to improve research on early warning indicators for timely monitoring and prevention of soil physical degradation.

2.2.2 Soil quality

Soil quality is the capacity of a specific kind of soil to function within natural or managed ecosystem boundaries to (Doran *et al.*, 1994):

1. sustain plant and animal productivity
2. maintain or enhance water and air quality
3. support human health and habitation

Soil function describes what the soil does and includes (Seybold *et al.*, 1998):

1. sustenance of biological activity, diversity, and productivity
2. regulation and partitioning of water and solute flow
3. filtering and buffering soil chemicals
4. providing support of socio-economic structures and protection of archaeological treasures associated with human habitation

Since soils vary naturally in their capacity to function, the term soil quality may be specific to each kind of soil. The concept of soil quality therefore encompasses two interconnected parts: inherent and dynamic qualities. Characteristics such as texture and mineralogy are innate soil properties determined by soil forming factors collectively form the inherent quality. For example, if all things remain the same, a loamy soil will have higher water holding capacity than a sandy soil and hence has higher inherent quality than the sandy soil. In this context, soil quality can be generally regarded as the soil capacity (Karlen *et al.*, 1997). Recently, soil quality has been defined as changing nature of soil resulting from human use and management (Sanchez *et al.*, 2003). Some management practices such as the use of cover crops, increase in organic matter can have positive effects on soil quality. Soil quality that has three aspects: physical quality, chemical quality, and biological quality can be assessed through the use of indicators (Karlen *et al.*, 1997; Dexter, 2004).

2.2.3 Indicators of physical soil quality

Soil quality indicators are measurable properties that influence the capacity of soil to perform physical, chemical, and biological function (Karlen *et al.*, 1997). The soil physical quality refers to the physical arrangement of soil solids and pores (Stephen, 2002). Many scientists have worked on developing a set of basic soil characteristics that can serve as key physical quality indicators (Oldeman *et al.*, 1991; McGarry, 1993; Hartemink, 1998; Stott *et al.*, 1999). These indicators need to be sensitive to changes in both the management and climatic effects on soil physical conditions (Dexter, 2004). Many researchers have suggested that the best indicators are those that show significant changes between 1 and 3 years, with 5 years being the upper limit (Stott *et al.*, 1999).

While discussing attributes of soil quality, Stephen (2002) suggested that physical quality indicators should include texture, water holding capacity, dry bulk density, porosity, aggregate stability and strength, and steady infiltration rate. Many studies in literature seem to support this suggestion. For example, Sanchez *et al.* (1997) used water holding capacity, stable aggregates, particle size, and organic matter to index soil physical degradation. These soil properties have been widely reported to be sensitive to soil structural condition and therefore appropriate in indexing structural degradation. Greene *et al.* (2002) used clay mineralogy to predict soils with hardsetting problems in Gascoyne in Western Australia while Fabiola *et al.* (2003) used tensile strength and penetration resistance to distinguish hardsetting soils. Although tensile strength and penetration resistance are popular among section of literature, a lot of care is needed in their use since they are sensitive to soil moisture content (Dirksen, 1999).

Although some researchers have used bulk density to assess soil compaction (see for example Horn *et al.*, 1995 and references therein). However, Flowers and Lal (1998) observed that bulk density is not a sensitive indicator of compaction especially for heavy-textured soils. Green and Chong (1983) proposed the use of sorptivity as suitable indicator of soil compaction while Lal (2000a) strongly suggested the use of infiltration rates.

Even though many researchers have used infiltration and retention to characterize soil crusting and surface seal (Roulier *et al.*, 2002), the formation of the crusts or seals has been shown to be largely due to the soils' chemical and mineralogical composition (Chen *et al.*, 1980). Consequently, integral indicators such as soil spectral reflectance have been proposed (Baumgardner *et al.*, 1985). Recently, Ben-Dor *et al.* (2003) and Eshel *et al.* (2004) successfully tested near-infrared (NIR) soil spectral reflectance for detection of crusting. These studies show the potential for accurate and quantitative ways of detecting structural crusts and seals.

Soil salinity or sodicity are forms of physical degradation characterized by imbalanced salt accumulations. There are relationships between salinity/sodicity and cationic composition in form of exchangeable sodium percent (ESP), electrical conductivity (ECe) or soil pH (Dane and Klute, 1977). Consequently, some researchers have successfully used ESP, pH, and ECe to characterize physical degradation due to salinity or sodicity (Triantafilis, 1996; Condom *et al.*, 1999).

Soil erosion, which is the ultimate form of physical degradation, is often characterized by the amount of soil lost or presence of surface deformation characteristics (Gobin *et al.*, 1999). Oldema *et al.* (1991) and King and Delpont (1993) used surface deformation signs such as presence of sheet erosion, rills, or gullies to characterize severity of soil erosion. According to De Jong (1994), these soil surface signs can easily permit the application of GIS and remote sensing in assessment and monitoring of soil physical degradation. Although surface characteristics provide quick and easy method of erosion assessment, traditional researchers still advocate for the measurement of sediment yield to quantify soil loss (De Jong, 1994). However, this is of little value for early detection of soil physical degradation.

2.2.4 Assessment of soil physical degradation

The aim of assessment of soil degradation is to provide opportunity for planning the reclamation strategies and for setting up preventive measures for sustainable agriculture. Especially for warning indicators of degradation problems, assessment can give vital information for mitigation measures before it becomes expensive and difficult to correct the effects of the degradation. Assessments may be made through direct measurement of the indicators or through modelling of the indicators with factors affecting the degradation processes (for example topography, soil type, land cover). In these cases, the methods applied may vary in their complexity owing to: (i) difficulty and cost in the measurements, (ii) sample representation of true field characteristics, (iii) analytical formulation linking the independent variable and soil physical degradation, and (iv) methodological and technical problems associated with time and space. Besides the measurements approach, some studies have used expert opinion to develop protocols for field assessment (Oldeman, 1994; Van Lynden, 2000). Although they offer advantages in terms of speed and scale of representation so that detailed and targeted survey can be planned, they are largely not accurate the (Lal, 2000a).

2.2.5 Assessment of on-site degradation

Owing to its small-scale nature, the assessment of on-site soil physical degradation can be reliably made using point-measurements or small-scale modelling with surrogate variables. There are many examples, however, a few can be cited to illustrate their applicability and data requirements. Sanchez *et al.* (1997) used particle size, water holding capacity, and aggregate stability to derive an index of soil physical degradation given by,

$$PDI = \frac{CI}{SA + WHC} \qquad (2.1)$$

where PDI is the physical degradation index, CI is the crust index, SA is the percentage of stable aggregates, and WHC is the water holding capacity. The crust index that also signifies the crusting form of degradation was given by,

$$CI = \frac{1.5FS + 0.75CS}{CL + 10 * OM} \qquad (2.2)$$

where FS is the percentage of fine silt, CS is the percentage of course silt, CL is the percentage of clay, and OM is the percentage of organic matter. By considering the aggregates and porosity, equation (1) caters for the soils structural condition. In addition, the inclusion of crust index as well as fine particles takes into consideration the factors that degrade soil physical condition.

Dexter (2004) developed the S-theory from water retention characteristics to index soil physical quality. In this model, the *S* index can be obtained as the slope of the retention curve at inflection point. For example, using the van Genuchten (1980) function the *S* index can be given by,

$$S = -n(\theta_s - \theta_r)\left[1 + \frac{1}{m}\right]^{-(1+m)} \qquad (2.3)$$

where θ_s is the saturated moisture content, θ_r is the residual moisture content, and *n* and *m* are empirical constant in the retention model. Since this index takes into consideration the soil pore structure, it can be used to determine changes in the soil structure especially with respect to aeration and moisture retention.

Pagliai (1988) used the image analysis of thin soil sections to derive indices of soil structural degradation. According to this method, a soil can be classified as in Table 2.1 where the total porosity represents the percentage of area of the thin section occupied by pores larger than 50 μm. The choice of 50 μm was based on the classification of soil pore by Greenland (1981) in which pores greater than 50 μm included storage pores, transmission pores, and fissures. These categories of pores have useful effects on plant-root penetration, water storage for plants and microorganisms, and for movement of water in the soils.

Table 2.1. Classification of structural degradation (Adapted from Pagliai, 1988)

Degree of compaction	**Total porosity (%)**
Extremely porous	> 40
Highly porous	25 – 40
Moderately porous	10 – 25
Compact	5 - 10
Very compact	< 5

In characterizing soil salinity or sodicity, Richards (1954) has shown that typical sodic soils have a pH > 8.5, ECa < 4.0 dSm^{-1}, sodium absorption ration (SAR) > 13 -15, and ESP > 15. Ayers and Westcot (1985) used these guidelines to determine water quality for irrigation and its susceptibly to cause physical degradation. Recently, Mzezewa *et al.* (2003) used the same guidelines to characterize sodic soils in Zimbabwe. These studies show opportunities for indexing the susceptibility of soils to physical degradation due to salinity or sodicity.

On-site assessment of soil loss is a little challenging since most of the impacts are felt off-site. However, some techniques have been successfully devised. Hudson (1993) proposed the use of erosion pins, paint collars, bottle tops, and pedestals to index the one-dimensional soil loss in terms of change in surface levels following erosion incidences. Quine *et al.* (1997) used Cs^{137} tracer method. ^{137}Cesium is one of radioisotopes of caesium that was released into the stratosphere by the testing of above ground thermonuclear weapons in the late 1950s and early 1960s (Wallbrink *et al.*, 1999). Its high affinity to fine soil particles makes it possible to track soil particles when they move from one point to another. Morgan *et al.* (1980) used aerial photo analysis to determine land morphology changes due to soil loss in croplands. They used digital terrain models (DEM) derived from aerial photos taken in different years to establish changes on land morphology over the years.

2.2.6 Prospects for large-area protocols

Since impacts of physical degradation are often felt at field scale, their assessments require a large-scale approach. Some authors have used geostatistics on point-measurements at various locations in the landscape to extrapolate for large-scale assessment (Hengl *et al.*, 2004). The potential for using GIS on point-measurements requires well-spread sampling in addition to sufficient data that can widen the prediction range. Furthermore, applications of GIS can permit use of surrogate variables that are easy to sample but which can explain as much information as the primary indicators of the degradation (McBratney *et al.*, 2003).

There are also numerous cases where plot-level models have been fitted with spatial databases to derive national or regional maps of soil degradation. This technique has been widely used with erosion models developed at plot levels or hillside scale (Jetten *et al.*, 1999). Bazzofi (2002) has tabulated the commonly used models. The models can be fitted with input from soil database (such as SOTER, UNEP/ISSS/ISRIC/FAO (1995)), spatial climate database, remote sensing vegetation characteristics, and topographic maps to derive maps of soil loss. For example, Jones (2002) used USLE with European soil database, rainfall map, 250-m DEM, and NOAA AVHRR images for vegetation to derive a preliminary erosion risk map for Italy. Dwivedi *et al.* (1997) used a combination of remote sensing images, erosion model, GIS ancillary information to derive erosion map of Tripura district in India. Although the approach demonstrated in these studies may not be very accurate, they offer preliminary information that can permit targeted survey for detailed assessment of the degradation.

Oldeman *et al.* (1991) and Van Lynden and Oldeman (1997) used expert opinion to develop large-scale maps of erosion. Using a team of over 250 local experts, they identified primary and secondary causes of erosion, degree, and extent of each cause for homogenous natural physiographic areas and finally linking the information in a GIS environment to map the degradation (Feddema, 1998).

Despite their rapid nature and good spatial coverage, the above off-site assessment protocols still lack the much needed accuracy that come with point measurements in the on-site assessments. Likewise, even though the on-site assessments are accurate they are limited in spatial coverage and therefore not sufficient for policy decision-making. These two contrasting points illustrate the opportunities for research to utilize the advantages of each protocol for the benefit of land management. Opportunities should be explored with techniques that offer relative accuracy for point sampling, ease in sampling and analysis of numerous samples from multiple points in the landscape, and be able to link these with spatial techniques such as GIS and remote sensing. Recently, infrared spectroscopy has been suggested to aid rapid analysis of plant and soil samples (Shepherd and Walsh, 2002; Shepherd *et al.*, 2003) in a way that can permit fertility capability classification (Sanchez *et al.*, 2003) as well as provide possibility to link with remote sensing (Liang, 2004). Thus, there is promise that a robust and widely replicable approach can be adopted with infrared spectroscopy to assess soil physical degradation.

2.2.7 Conclusions on the indicators of soil physical quality

From the above literature, it can be concluded that indicators of soil physical quality need to relate to the arrangement of soil solids and pores and they also need to be easily measurable both in the field and in a laboratory on samples taken from the field. The infiltration and water retention characteristics stand out to be the most favourable soil properties that can be logically evaluated both in the field and in a laboratory.

2.3 Infiltration characteristics

2.3.1 Models of infiltration

Infiltration is the entry of water into the soil surface (Marshall *et al.*, 1996). There are two forces that define the water entry: The gravitational force on water molecules and the matric suction from soil matrix. According to Kutilek and Nielsen (1994), the two forces are complementary: matric forces dominating the initial rates while gravitational forces dominating the late-stage rates. Therefore, models that describe the infiltration rates often have two components for these forces. At long infiltration times, these models can be expressed as:

$$i(t) = ct + b \qquad (2.4)$$

where *c* represents matric force component while *b* represent gravitation force component. Figure 2.3 shows the complementary effects of the two forces in infiltration curves.

Although when water enters the soil surface its flow characteristic is three-dimensional in nature (Chow *et al.*, 1988), most models avoid the complications of equations in three dimensions and only prefer one-dimensional characteristics. Table 2.2 shows some of the common infiltration models in literature. Some of the parameters of the infiltration models in Table 2.2 do not have any physical meaning and therefore known as empirical models. However, models such as the Green and Ampt and the Philip's models have parameters with physical meaning and are known as physical models (Kutilek and Nielsen, 1994). Since the wetting front suction potential, φ, of the Green and Ampt model is often difficult and involving in determination, the Philip's model has been popularly adopted (Dingman, 2002).

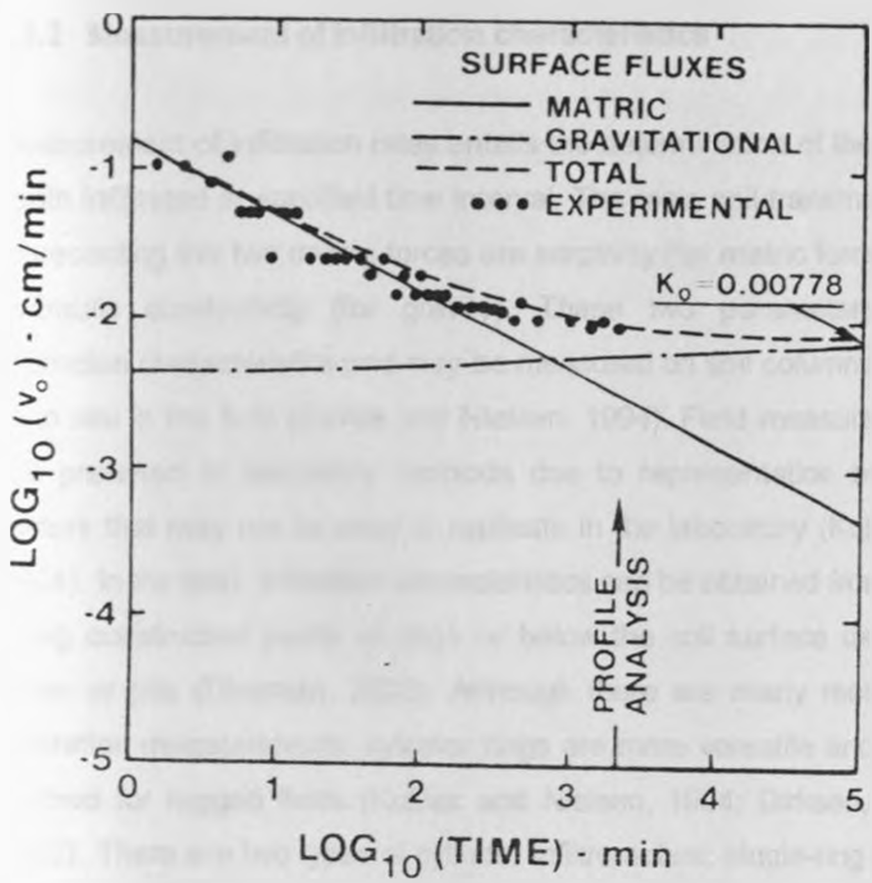

Figure 2.3. Effects of matric and gravitation forces in infiltration flux (v_0) (Adapted from Kunze & Kar-Kuri, 1983). K_o is the saturated hydraulic conductivity.

Table 2.2. Infiltration models. *z* is the cumulative depth infiltrated

Model	Parameters	Model name	Reference
$i(t) = (f_o - f_c)e^{-kt}$	k, f_c, f_o	Horton	Horton, (1933)
$i(t) = 0.5St^{-0.5} + f_c$	S, and f_c	Philip	Philip (1957)
$i(t) = K\varphi\Delta\theta / z + K$	K, φ, $\Delta\theta$	Green-Ampt	Chow *et al.* (1988)
$i(t) = akt^{n-1} + f_c$	a, k, n, f_c	Kostiakov	Kostiakov (1932)
$i(t) = aS_s^{1.4} + f_c$	S_a, f_c, a	Holtan	Holtan (1961)
$i(t) = akt^{a-1}$	a, and k	SCS	USDA (1974)
$i(t) = \frac{kt_c\{Atan(t/t_c)\}^{-0.5}}{2(t_c^2 + t^2)} + f_c$	k, t_c, A	Collis-George	Collis-George (1977)

2.3.2 Measurement of infiltration characteristics

Measurement of infiltration rates entails the determination of the amount of water depth infiltrated at specified time interval. The main soil transmission parameters representing the two driving forces are sorptivity (for matric forces) and saturated hydraulic conductivity (for gravity). These two parameters determine the infiltration characteristics and may be measured on soil columns in the laboratory or in situ in the field (Kutilek and Nielsen, 1994). Field measurement techniques are preferred to laboratory methods due to representation and complexity of factors that may not be easy to replicate in the laboratory (Kutilek and Nielsen, 1994). In the field, infiltration characteristics can be obtained from the soil surface using constructed ponds or rings or below the soil surface using shallow bore holes or pits (Dingman, 2002). Although there are many methods for surface infiltration measurements, cylinder rings are more versatile and commonly used method for rugged fields (Kutilek and Nielsen, 1994; Dirksen, 1999; Dignman, 2002). There are two types of cylinder infiltrometers: single-ring and double-rings infiltrometers (Reynolds and Elrick, 1990). Single rings should be preferred when large-areas need to be surveyed, for many replicate measurements, and where infiltration water is limiting (Reynolds and Elrick, 1990; Omuto, 2003). Furthermore, they present higher relative accuracy over double-rings given that the differences in pressure-heads in double rings are likely to introduce unaccounted errors (Wu *et al.*, 1997).

2.4 Water retention characteristics

2.4.1 Models of water retention

Water retention model is defined as the relationship between water content and suction for the soil (Williams, 1982). The water content defines the amount of water contained in the pores of the soil while the suction represents matric forces plus osmotic potential. Figure 2.4 shows characteristic features of water retention curve. θ_s is the saturated moisture content while θ_r is the residual moisture content. Numerous empirical equations have been proposed to simulate the curve in Figure 2.4. Among the earliest is an equation proposed by Brooks and Corey (1964) of the form:

$$\theta(h) = \theta_r + (\theta_s - \theta_r)(\alpha h)^\lambda \quad (2.5)$$

where α is the inverse of air-entry potential (h_a) and λ is the pore distribution index.

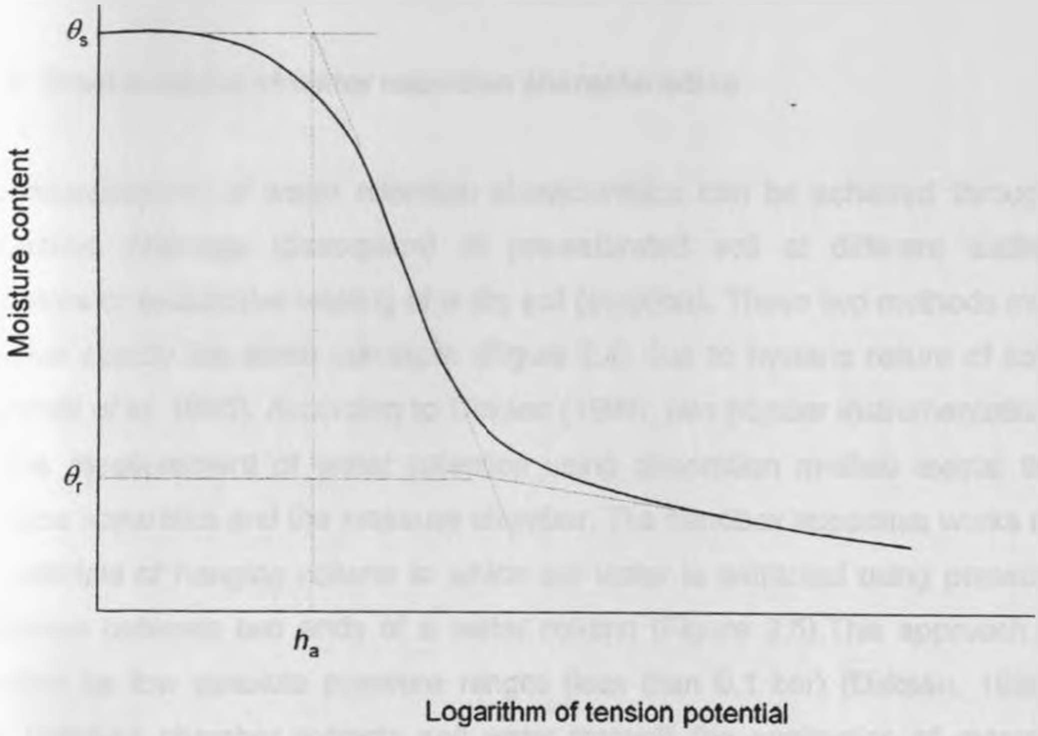

Figure 2.4. Characteristic curve of water retention

Equation (2.5) has been reviewed through several studies and new models proposed (Gardner *et al.*, 1970; Rogowski, 1971; Campbell, 1974; Clapp and Hornberger, 1978; McCuen *et al.*, 1981; Williams *et al.*, 1983). The following linear relationship between logarithm of water content and suction potential was used by Williams *et al.* (1983) to describe water retention in Australian soils:

$$\log h = a + b \log \theta \tag{2.6}$$

where *a* and *b* are fitting parameters. Another frequently used form of water retention model is that given by Van Genuchten (1980) model is given by:

$$\theta(h) = \theta_r + (\theta_s - \theta_r)[1 + (\alpha h)^n]^{(1-n)/n} \tag{2.7}$$

where *n* is a fitting parameter. Although these models are somewhat related to the features in Figure 2.4, they have not been proven with physical laws.

2.4.2 Measurement of water retention characteristics

The measurement of water retention characteristics can be achieved through: successive drainage (desorption) of pre-saturated soil at different suction pressures or successive wetting of a dry soil (sorption). These two methods may not give exactly the same curvature (Figure 2.4) due to hysteric nature of soils (Marshall *et al.* 1996). According to Dirksen (1999), two popular instrumentations for the measurement of water retention using desorption method exists: the sandbox apparatus and the pressure chamber. The sandbox apparatus works on the principle of hanging column in which soil water is extracted using pressure difference between two ends of a water column (Figure 2.5).This approach is effective for low absolute pressure ranges (less than 0.1 bar) (Dirksen, 1999). The pressure chamber extracts soil water through the application of external pressure. It is useful in extracting soil water held at high-pressure heads. In the case of sorption water retention characteristics, the tensiometers have been extensively used (Marshall *et al.*, 1996). These devices hold water at specific tension and release the water through porous plate into the soil. During the water release, the moisture level of the soil changes and can be measured using any method for moisture determination while the tension level is recorded from the tensiometer (Marshall *et al.*, 1996).

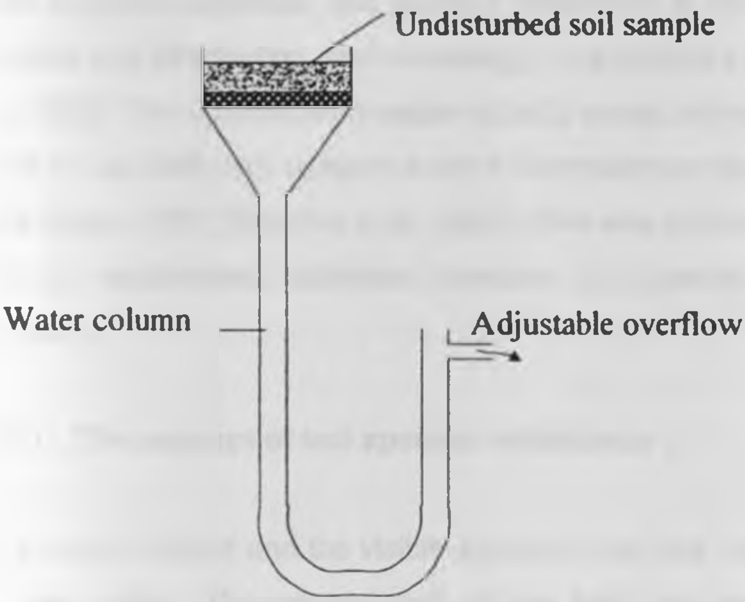

Figure 2.5. The principle of hanging water column in retention measurement

2.5 Soil spectral reflectance

Due to the fact that soil physical properties are influenced by the textural characteristics and organic matter content, many researchers have developed relationships between physical properties and soil texture (McBratney *et al.*, 2003). The basic reason here is that soil texture provides the building blocks while organic carbon cements the blocks. Recent developments in soil infrared spectroscopy have also shown promising alternatives for predicting soil physical properties (Janik et al., 1998; Shepherd & Walsh, 2002). Soil spectral reflectance is the response of soils upon interaction with electromagnetic radiation (Ben-Dor *et al.*, 1999). Since its development, many soil scientists have established predictive calibrations between soil spectral reflectance and numerous soil properties (Janik *et al.*, 1997; Chang *et al.*, 2001; Shepherd and Walsh, 2002; Dematte *et al.*, 2003; Eshel *et al.*, 2004).

Like physical properties, soil spectral reflectance is affected by carbon content, particle size distribution, soil mineralogy, and moisture content (Baumgardner *et al.*, 1985). The spectral information of soils across entire solar illumination region (400 nm to 2500 nm) contains a lot of information on these properties (Shepherd and Walsh, 2002; Ben-Dor *et al.*, 2003). One way of capturing such information is through multivariate calibration between soil spectral reflectance and target property.

2.5.1 The concept of soil spectral reflectance

The nature of light and the visible spectrum are only one part of what is needed to see colour. The second part of the triad has something to do with the interaction of light and matter and involves a partial reflection of light from that object. When light strikes an object it will react in one or more of the following ways depending on whether the object is transparent, translucent, opaque, smooth, rough, or glossy: It will either be transmitted, absorbed or reflected (Ben-Dor *et al.*, 1999). Transmission takes place when light passes through an object without being essentially changed. Light that strikes a transparent object is transmitted in part and reflected in part. But when light strikes an opaque object (that is, an object that does not transmit light), the object's surface plays an important role in determining whether the light is fully reflected, fully diffused, or some of both (Liang, 2004). Finally, some or all of the light may be absorbed depending on the pigmentation of the object. Pigments are natural colorants that absorb some or all wavelengths of light (Ben-Dor *et al.*, 1999).

Just as spectral power distributions are a property of a light source, the spectral reflectance or transmittance curve in the visible range is a property of a colored object. According to Liang (2004), spectral reflectance refers to the amount of light at each wavelength reflected from an object as compared to a pure reflection (for example, from a pure white object that reflects 100% at all wavelengths) (Ben-Dor *et al.*, 1999). Spectral transmittance refers to the amount of light at each wavelength that is transmitted through an object as compared to the amount transmitted through a clear medium such as air (Ben-Dor *et al.*, 1999).

During reflectance and absorbance, the changes in energy cause electronic transition of atoms of matter and vibrational stretching and bending of structural groups of atoms that form molecules and crystals. The transition and vibrations of atoms at higher levels of energy give reflectance with fundamental features, which may spread over a span of wavebands (Figure 2.6). The relationship between reflectance or absorbance and wavelength has been termed a 'spectrum' (Ben-Dor and Benin, 1990).

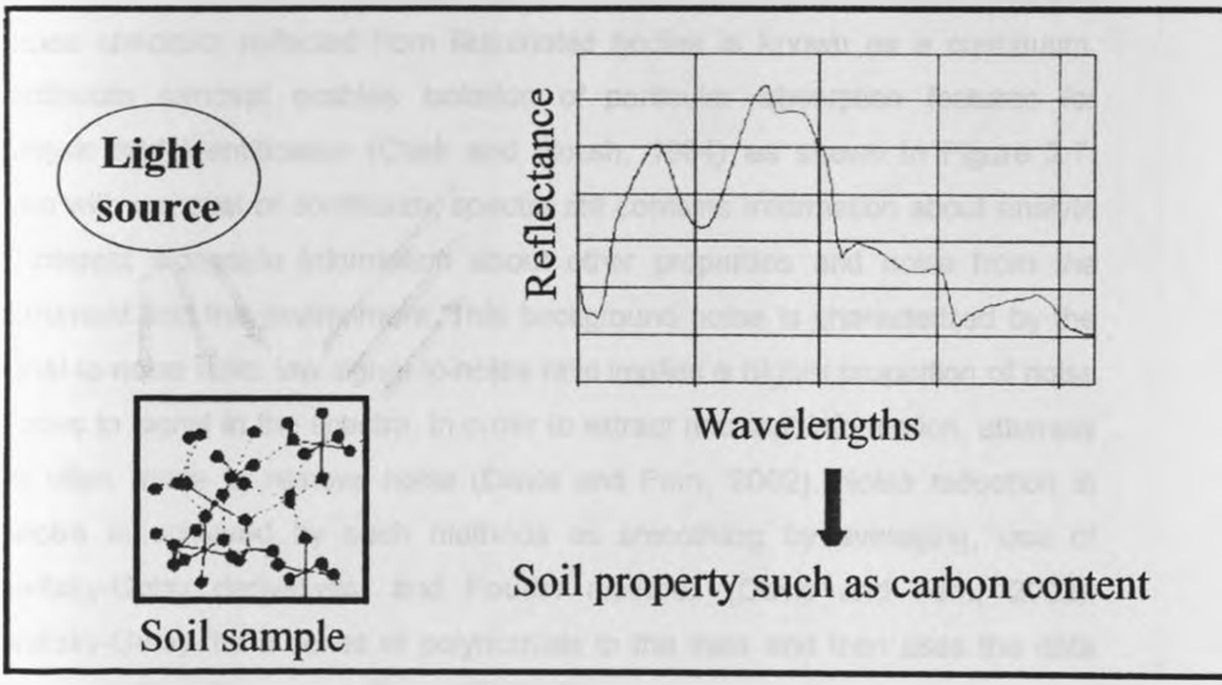

Figure 2.6. Spectral reflectance of light

In soils, these features occur in the visible range (V, 400 nm – 700 nm), near infrared range (NIR, 700 nm – 1000 nm) and the short wave infrared (SWIR, 1000 nm – 2500 nm) ranges. Certain qualitative relationships between these spectra and soil properties have been well recognized by scientists (Ben-Dor *et al.*, 1999). The scientific concept of using spectral reflectance to describe object features has often been referred to as reflectance spectroscopy (Ben-Dor and Benin, 1990). In soil science, reflectance spectroscopy has proven invaluable in characterizing the surface of soils of the earth for purposes as varied as mineral exploration (Cudahy and Ramanaidou, 1979) or soil property determination (Ben-Dor *et al.*, 1999).

2.5.2 Characterization of soil spectral reflectance

Most spectral reflectance emitted from illuminated bodies have background absorption, which mask meaningful identification of their features. The mask that drapes spectrum reflected from illuminated bodies is known as a continuum. Continuum removal enables isolation of particular absorption features for analysis and identification (Clark and Roush, 1984) as shown in Figure 2.7. Even with removal of continuum, spectra still contains information about analyte of interest alongside information about other properties and noise from the instrument and the environment. This background noise is characterized by the signal-to-noise ratio: low signal-to-noise ratio implies a higher proportion of noise relative to signal in the spectra. In order to extract relevant information, attempts are often made to remove noise (Davis and Fern, 2002). Noise reduction in spectra is achieved by such methods as smoothing by averaging, use of Savitzky-Golay derivatives, and Fourier methods (Davis and Fern, 2002). Savitzky-Golay fits a series of polynomials to the data and then uses the data computed from the curves (Fern, 2002). Fourier removes high frequency noise by computing a Fourier transformation and setting a large proportion of higher frequency coefficient to zero (Cowe and McNicol, 1985). The simple moving average is by far the most popular. Other noise reduction methods also often used through pre-processing include: derivatives, multiple scatter correction (MSC), standard normal variate (SNV), optimised scaling (OS) and orthogonal signal correction (OSC) (Davis and Fern, 2002).

Soil spectral reflectance can be acquired in the laboratory or directly from the field. Reflectance data acquired from the field involve additional difficulties such as low signal-to-noise ratio (Tsai and Philipot, 1998). In addition, problems associated with artificial-light source in the field include variable moisture content, soil surface structure and small area (point-measured) scanning. Thus, laboratory oriented spectral scanning has gained popularity over the decades as spectral data acquired from the laboratories are often done under controlled conditions (Ben-Dor *et al.*, 1999).

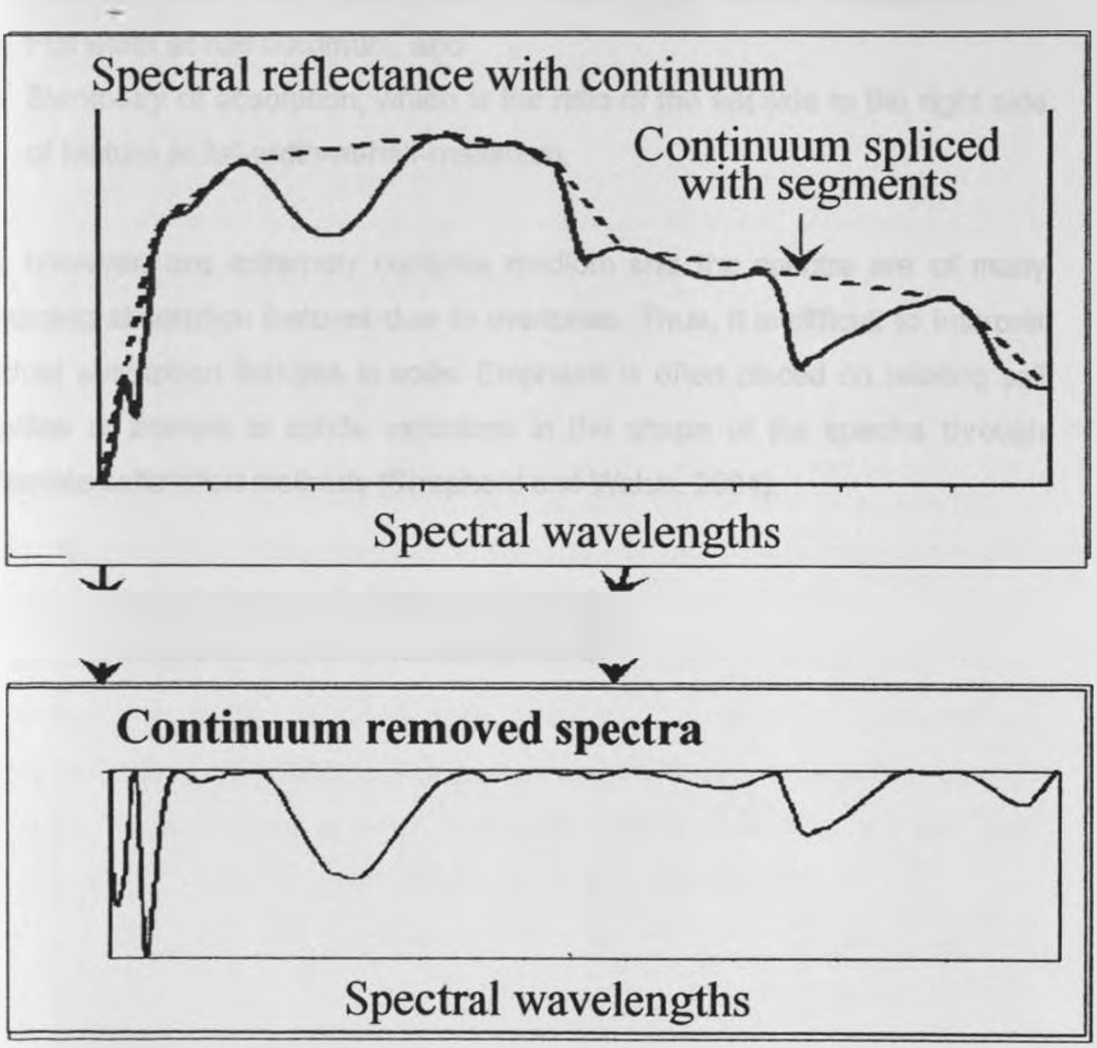

Figure 2.7. Process of continuum removal (Montero *et al.*, 2001)

Spectral characterization is normally done to objectively describe spectral reflectance signatures with a view of identifying principal absorption areas (Tsai and Philpot, 1998). Characterization of spectral features (Figure 2.8) involves determination of:

1. Center of absorption, which is the wavelength of the most intensely absorbed radiation feature
2. Depth of absorption feature or spectral contrast, which is the difference between lowest and highest point of feature in the units of reflectance
3. Full width at half maximum, and
4. Symmetry of absorption, which is the ratio of the left side to the right side of feature at full-width-at-half-maximum.

Soils, however, are extremely complex medium and the spectra are of many overlapping absorption features due to overtones. Thus, it is difficult to interpret individual absorption features in soils. Emphasis is often placed on relating soil properties of interest to subtle variations in the shape of the spectra through multivariate calibration methods (Shepherd and Walsh, 2004).

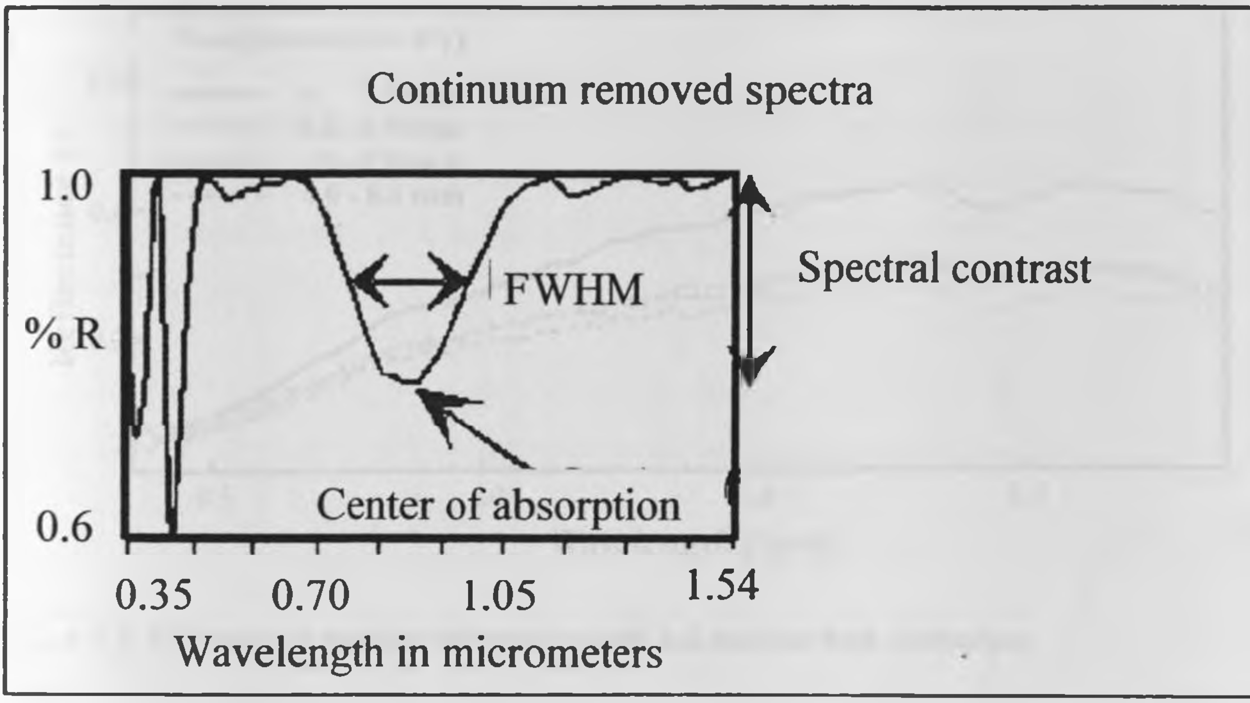

Figure 2.8. Features of absorption (Montero *et al.*, 2001)

2.5.3 Optical properties of soils

In soil science, pedologists have used colour to describe soils and to infer their characteristics. Soil constituents (such as soil organic matter, iron oxides and soil water) and roughness (such as particle and aggregate size) govern their spectral properties (Atzberger, 2002). Soil roughness is also important in determining the soil pore-spaces influencing soil-water movement. Generally, reflectance increases as particle or aggregate size decreases (Salisbury and Hunting, 1968). It has been shown that for a given a material, reflected light varies with the particle diameter (Figure 2.9) (Montgomery and Baumgardner, 1974).

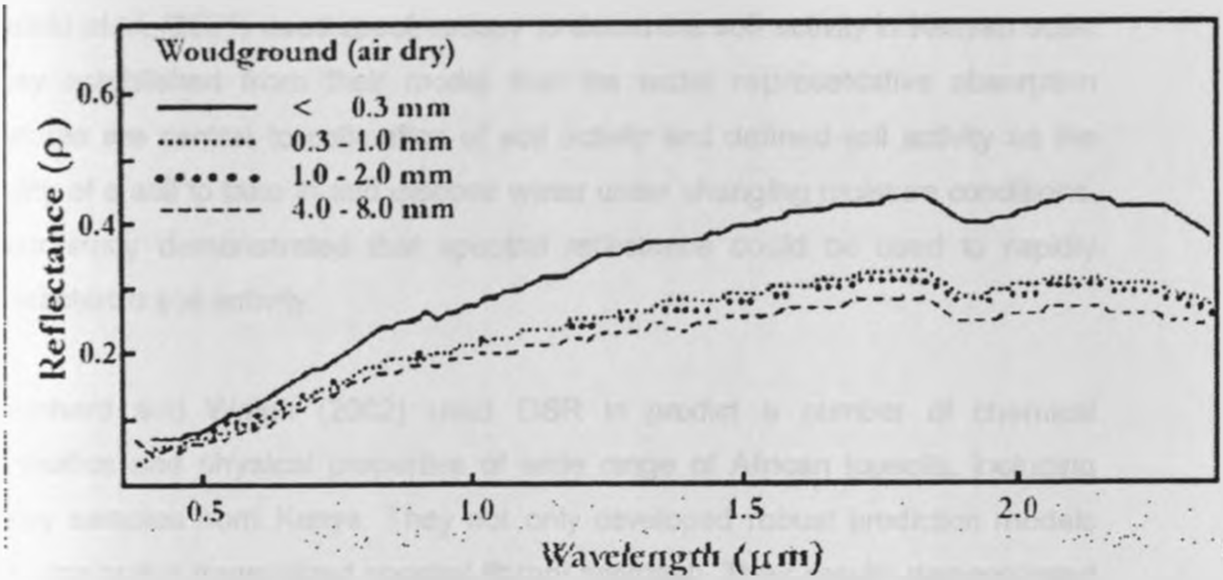

Figure 2.9. Variation of spectral reflectance with soil particle size (Atzberger, 2002)

Leger *et al.*, (1979) studied the effect of soil water, organic matter and iron oxides on soil spectra. They concluded that the interaction of the three components was much more important for understanding the soil spectra than considering them individually. Nevertheless, Da Costa (1979), working on sandy soils, observed significant changes on spectral curve shapes upon wetting of the soil. Da Costa suggested that this kind of change could be attributed to the spectral activity of water in the soils. Condit (1970) obtained a good correlation between particle distribution, water holding capacity and soil spectral reflectance.

2.5.4 Spectral reflectance studies in Kenya

Spectral reflectance studies have been going on in many parts of the world with applications significantly shifting from chemometrics to soil science (Ben-Dor *et al.*, 1999). Despite the relevance and opportunity that the spectral reflectance technique offers to soil science, little progress has been shown in its practical application for assessment of soil degradation.

Kariuki *et al.* (2001) used spectroscopy to determine soil activity in Kenyan soils. They established from their model that the water representative absorption features are central to estimation of soil activity and defined soil activity as the ability of a soil to take in and dispose water under changing moisture conditions. Their study demonstrated that spectral reflectance could be used to rapidly characterize soil activity.

Shepherd and Walsh (2002) used DSR to predict a number of chemical properties and physical properties of wide range of African topsoils, including many samples from Kenya. They not only developed robust prediction models but also built a generalized spectral library approach. Their results demonstrated the feasibility of using reflectance spectrometry for broad diagnosis of soil physical and chemical properties and have opened ways for mapping soil functional attributes across watersheds.

2.5.5 Potential of spectral reflectance in degradation assessments

Spectral reflectance is one of the soil properties that integrate many functional processes including the physical soil quality (Janik et al., 1998; Sanchez et al., 2003; Shepherd and Walsh, 2004). It is sensitive to iron oxide and soil carbon content that in turn influence aggregation and many other constituents that may relate to physical conditions (Baumgardner *et al.* 1985; West *et al.* 2004). Recently, Ben-Dor *et al.* (2003) and Eshel *et al.* (2004) used soil spectral reflectance to diagnose structural degradation. Thus, there is promise for use of spectral reflectance in physical degradation assessment.

In addition, Shepherd and Walsh (2004) have discussed the advantages of soil spectral reflectance in terms of relative costs, accuracy, and speed for wide-area characterization of many soil functional capacities. These advantages of spectral reflectance can enable high-density sampling over large areas. The difficulty of adequately sampling the variations in soil characteristics in a watershed has been identified as the major cause of failure of soil physical models to predict scenarios outside their calibration sites (Brus and De Gruijter 1997).

2.6 Applications of remote sensing in land degradation studies

2.6.1 Principles of remote sensing

In the context of land degradation, remote sensing is the collection of information about the Earth surface and atmosphere using electromagnetic radiation (Rees, 2001). One major classification of remote sensing is according to the source of the electromagnetic radiations, namely: natural (passive remote sensing) and artificially emitted radiation (active remote sensing) (Rees, 2001). According to Rees (2001), natural radiations originate from the sun, the atmosphere, and from the earth. These types of radiation can be classified as short-wave (0.25 - µm wavelength) or long-wave (4 – 100 µm wavelength) (Iqbal, 1984). They can be detected in space using specialized equipment on board aircraft or satellites. Figure 2.10 shows the simplified principle of remote sensing.

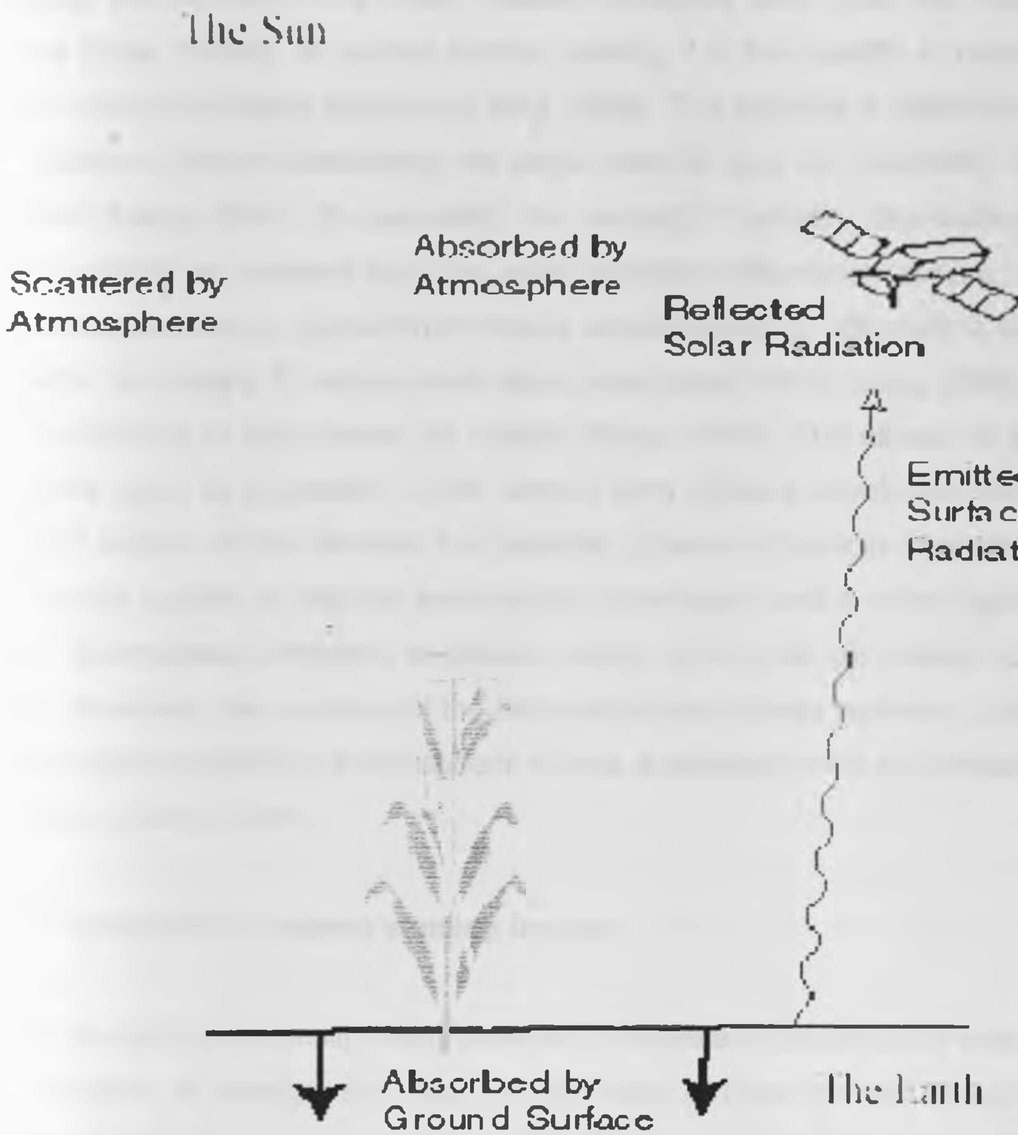

Figure 2.10. Principle of remote sensing of the Earth

Detection of the radiation by satellite sensors on-board aircrafts are restricted by the transparency of the earth's atmosphere (Rees, 2001). There are two main windows in the atmosphere: the first includes the visible and infrared parts between 0.25 and 14 μm while the second more or less corresponds to the microwave region (Iqbal, 19984). Through these windows, the sensors detects the electromagnetic radiation after it has interacted with or been emitted by the target material. There are essentially two variables to describe the radiation reaching the sensors: How much radiation detected and when the radiation arrives (Iqbal, 19984). In passive remote sensing, it is the quantity of radiations that is relevant in target detection (Liang, 2004). This quantity is determined by the radiation amount illuminating the target material and the reflectivity of the material (Liang, 2004). By assuming the amount of radiation illuminating the target material as constant (such as solar constant), information content of the target material can be inferred from remote sensing when its reflectivity is known and after accounting for atmospheric attenuation (Iqbal, 1984; Liang, 2004). The term reflectivity is also known as albedo (Rees, 2001). The albedo of target materials (such as vegetation or soil) sensed from different wavelength contains different aspects of the material. For example, albedos of soils or vegetation on the Earth's surface at different wavelengths have been used to infer vegetation vigour (Normalized difference vegetation index, NDVI) and soil salinity (Liang, 2004). However, the accuracy of the information about these materials depends on adequate accounting of atmospheric effects, a process known as atmospheric correction (Liang, 2004).

2.6.2 Correction of remote sensing images

Since the radiation intensity that is detected by satellites as continuous variables, the problem of storage and relay of the data is often solved through the conversion of the physical variables into digital numbers (DN) (Rees, 2001). Furthermore, data about Earth's surface is often mixed with unwanted atmospheric effects. Thus, images need to be corrected in order to obtain the physical variables of the earth's surface. This process involves radiometric, topographic, and atmospheric corrections (Liang, 2004). The radiometric corrections convert the DN to top-of-the-atmosphere (TOA) radiometers; topographic corrections resolve the radiances depending on topographic influence on solar illumination; and atmospheric corrections remove the effects of atmospheric attenuation (Liang, 2004). Laing (2004) has exhaustively discussed various methods that can be used to achieve these correction processes.

2.6.3 Examples of studies with remote sensing in land degradation

Innovations in remote sensing technology have provided new solutions to environmental problems in the earth sciences and in natural hazard monitoring such as for drought (Unganai and Kogan, 1998). Many studies have used Normalized Difference Vegetation Index (NDVI) for monitoring drought over large areas of land (see for example Park *et al.*, 2004). However, NDVI is not always an appropriate tool for real-time monitoring of drought since vegetation response to drought is not instantaneous (Unganai and Kogan, 1998).

There are many other remote sensing indicators with synchronous response with land degradation compared to NDVI. Recent applications combining LST and NDVI have shown promise in rapid mapping of land degradation (Unganai and Kogan, 1998; Park *et al.*, 2004). Land surface temperature (LST) is useful biophysical indicator because it is directly linked to the flux of net radiation and surface moisture conditions (Liang, 2004). Interacting with the soil–plant–air system, LST represents the instantaneous state of the energy flux for a land surface. By using thermal emission patterns in combination with meteorological observations, the relationship between surface temperature and the moisture regime on the ground can detect drought areas before biomass degradation occurs. With high radiometric and temporal resolution, thermal infrared data can allow more accurate inference of changes in surface thermal regimes and assist in improved detection of land degradation and drought.

2.6.4 Linking land surface temperature with soil degradation

Visible and thermal infrared sensors have been in orbit since the early 1970s (Liang, 2004). The principal advantages of these spectral measurements are accuracy, availability, and resolution. The methods used for retrieval of surface characteristics from thermal infrared measurements rely on the principle that the heat capacity and thermal conductivity of water are substantially greater than that of soil porous media (Campbell and Norman, 1998). Consequently, some signatures of the dynamics of ground temperature contain information on soil physical condition. The basis for this relationship may be illustrated using the following governing equation;

$$\rho_s C_s \frac{\partial T}{\partial t} = \frac{\partial}{\partial z}\left(\kappa_s \frac{\partial T}{\partial z}\right) \tag{2.8}$$

where κ_s is the thermal conductivity, $\rho_s C_s$ is the volumetric heat capacity (composed of the product of bulk density ρ_s and the specific heat capacity C_s). The sinusoidal variation of the LST about the mean value ⟨LST⟩ is given by the expression:

$$LST - \langle LST \rangle = \frac{A_G \sin(\omega t - 1/4\pi)}{\sqrt{\omega \rho_s C_s \kappa_s}} \tag{2.9}$$

where A_G is amplitude and ω is frequency. From equation (2.9), the amplitude of the periodic surface temperature oscillation is established to be:

$$\frac{1}{2}\Delta LST = \frac{A_G}{\mathrm{P}\sqrt{\omega}} \tag{2.10}$$

where $\mathrm{P} = \sqrt{\rho_s C_s \kappa_s}$ is the thermal inertia. Since P depends on the volumetric heat capacity, which in turn, is strongly affected by the soil physical degradation, equation (2.10) suggests that observations of the LST may be related to soil physical condition.

2.7 Conclusions on literature review

From the existing literature above, soil physical degradation is a significant contributor to poor environmental quality, food insecurity, and poor water quality. Although there are numerous ways that can be individually used to assess and monitor the degradation at various scales, effective control of the degradation needs accurate case-definition and subsequent early-detection routines. Especially in the tropics where the population is agrarian, rapid screening methods are needed for early detection of the degradation to permit timely prevention (Lal, 2000; Sanchez *et al.*, 2003). It is evident from the literature that there is promise in combining georeferenced point measurements of soil physical properties, soil DSR as a rapid integrating measurement of soil properties, and GIS and remote sensing for effective assessment and monitoring of physical degradation over large areas.

CHAPTER THREE

3. MATERIALS AND METHODS

3.1 Study area

This study was conducted in the Upper Athi river basin, in eastern Kenya (Figure 3.1). The basin was selected as the study area due to its high prevalence of soil physical degradation (Tiffen *et al.*, 1994). The basin which covers an area of 4,513 km^2, is gently sloping to almost flat in the central and southeastern parts (with altitudes less than 1000 m above sea level, a.s.l) and has steep slopes (> 20%) in the southern and northern parts (where altitudes are above 1500 m a.s.l). Most of the high altitude parts and much of the central regions of the watershed had either intact savannah vegetation or dense forest covers about five decades ago. However, much of these areas have now been converted to agricultural ecosystems. The average annual rainfall ranges from between 1100 to 800 mm in the high altitude zones and between 800 to 600 mm in the low altitude areas. Much of the rain occurs between late March and early June as long-rains whereas there are short-rains between September and October. However, for most times in the year the sky is clear of clouds especially in the February before the onset of the long rains. The soils are predominantly silty loam to sandy soils. According to FAO (1971-1981), much of the central part of the watershed is Utric Ferarsols while soils along the Athi River plain are largely dystic Cambisols. In the highland areas, soils are haplic Arenosols by majority (FAO, 1971-1981). These soils have low nutrient contents and are vulnerable to physical degradation (Tiffen *et al.*, 1994). In the presence of high evaporative demands and low rainfall in these soils, biomass production is sensitive to soil physical condition (Campbel and Norman, 1998). These characteristics make the area one of the worst and frequent famine-hit areas in Kenya (Tiffen *et al.*, 1994).

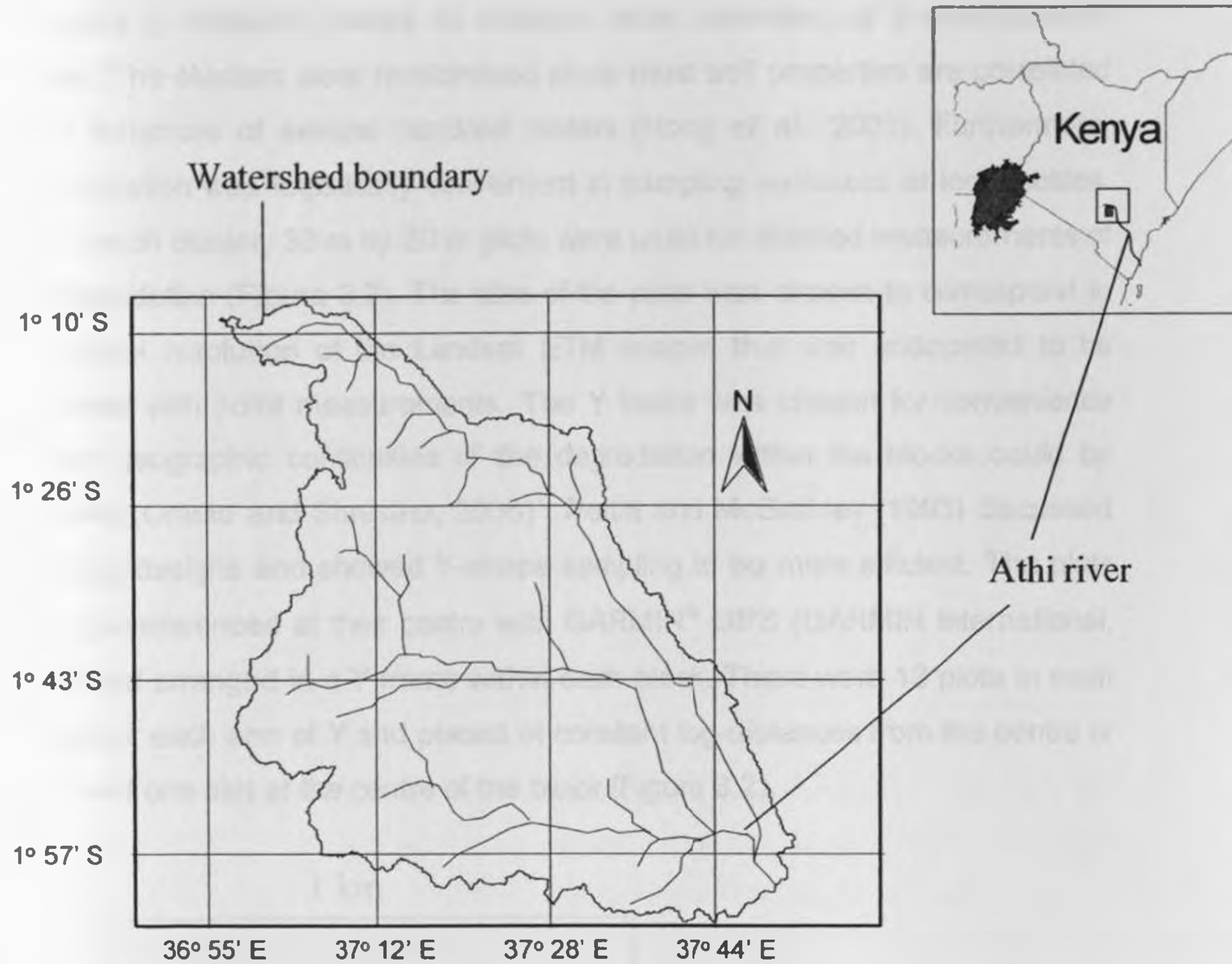

Figure 3.1. Location of the study area

3.2 Data collection

From the literature survey, the infiltration and water retention characteristics were identified as pertinent soil physical properties that are sensitive to physical degradation (Section 2.4). Therefore these characteristics were measured in the field.

3.2.1 Ground survey of physical degradation

Ground survey of soil physical degradation was carried out between December 2002 and March 2003. This entailed the assessment of physical degradation indicators in randomly-placed 45 clusters, each consisting of a one-kilometre square. The clusters were randomised since most soil properties are correlated within distances of several hundred meters (Hong *et al.*, 2005). Furthermore, randomisation was logistically convenient in sampling variances at local scales. Within each cluster, 30 m by 30 m plots were used for detailed measurements of the degradation (Figure 3.2). The size of the plots was chosen to correspond to the spatial resolution of the Landsat ETM images that was anticipated to be combined with point measurements. The Y frame was chosen for convenience so that geographic continuities of the degradation within the blocks could be captured (Omuto and Shrestha, 2006)[1]. Pettitt and McBratney (1993) discussed sampling designs and showed Y-shape sampling to be more efficient. The plots were georeferenced at their centre with GARMIN® GPS (GARMIN International, 2002) and arranged in a Y frame within each block. There were 13 plots in each Y: four for each arm of Y and placed at constant log-distances from the centre of the Y and one plot at the centre of the block (Figure 3.2).

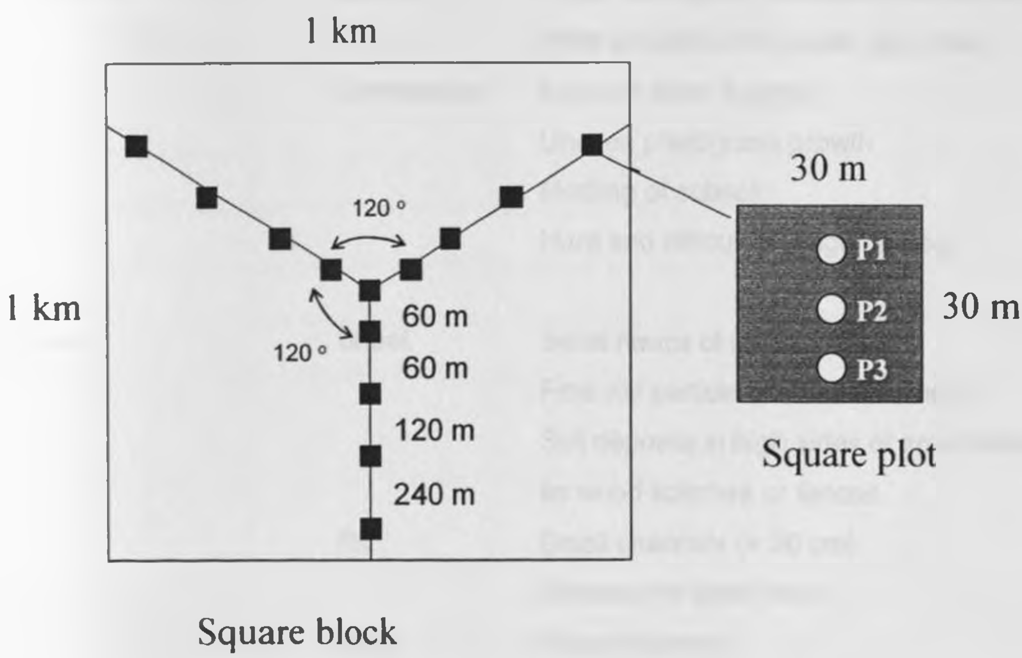

Figure 3.2. Y frame sampling protocol for soil physical degradation

[1] This paper has already been accepted by International Journal of Remote Sensing

Within each plot, measurements of soil physical properties, soil sampling for spectral reflectance, and observations of visible signs of physical degradation where made. Visible signs of degradation observed included: presence of signs of erosion (sheet, rill or gully erosion) and signs of structural deterioration (crusting, hardsetting, and compaction). These observations are listed in Table 3.1 and were used to classify the plots as follows: non-degraded (class E0) for sites without any observable sign, moderately degraded (class E1) for sites with signs of in-situ physical degradation, and severely degraded (class E2) for sites with multiple signs of degradation (that included in-situ physical degradation and/or erosion features). There were 26 cases of class E0 plots, 107 cases of class E1 plots, and 47 cases of class E2 plots.

Table 3.1. Field observations for the evidence of physical degradation

Form of degradation	Type	Observed signs
In-situ physical degradation	Crusting and sealing	Hard layers on soil surface
		Algae-strengthen pedestals in sheet eroded fields
		Hard and difficult-to-auger surfaces
	Compaction	Signs of water logging
		Uneven plant/grass growth
		Mottling of subsoil
		Hard and difficult-to-auger subsoil
Erosion	Sheet	Small heaps of washed sand
		Fine soil particle in small channels
		Soil deposits in high sides of small obstructions such as wood splinters or fences
	Rill	Small channels (< 30 cm)
		Exposure of plant roots
	Gully	Deep channels
		Exposure of lower soil depths

3.2.2 Measurement of soil physical properties

Measurement of soil physical properties consisted of infiltration tests and determination of water retention characteristics. Since these are tedious and time-consuming, they were surveyed on only four plots of each block. These plots included the centre-plot and the three outermost plots at the end of each arm of Y (Figure 3.2). In total, there were 180 plots surveyed for physical properties in the study area.

The infiltration measurements were made using single ring infiltrometers of 30 cm internal diameter. The infiltrometers were carefully inserted into pre-wetted soil surfaces (Dirksen, 1999) and infiltration rates determined using the falling-head approach (Elrick and Reynolds, 2002). Bulk density and water retention measurements were made in the laboratory on undisturbed soil samples taken from 0 – 20 cm of the soil profile. These samples were collected in the field using 100 cm^3 according to procedure reported in Dirksen (1999). Water retention characteristics were determined using sandbox apparatus (for $h > -1$ m) and a pressure chamber (for $h \leq -1.0$ m) (Figure 3.3 and appendix A4.1) while bulk density was determined on a dry basis from samples oven-dried at 105°C for 48 hours. The measurements for infiltration and sampling for retention were made on the topsoil (0 – 20 cm) at three positions within each plot (points P1, P2 and P3 in Figure 3.2). The positions were located along a slope directed gradient at 5, 15, and 25 m, respectively, from the plot edge.

3.2.3 Measurement of soil spectral reflectance

Soil samples for diffuse reflectance were taken using soil augers for topsoils (0 – 20 cm) and subsoils (20 – 50 cm) at the above three positions in each plot in the Y (Figure 3.2). The samples were then air-dried and gently crushed to pass through 2 mm sieve. Air-drying and crushing was done to minimize spectral variations among samples due to differences in moisture content and soil particle sizes (Shepherd and Walsh, 2002). The samples were then placed in Duran-glass Petri-dishes before scanning with a FieldSpec FR® spectroradiometer (Figure 3.3a) (Analytical Spectral Devices Inc., Boulder, Colorado) at wavelengths from 350 to 2500 nm and with spectral sampling resolution of 1 nm. The scanning was done from below the Petri dishes using a high-intensity light source probe as described by Shepherd *et al.* (2003).

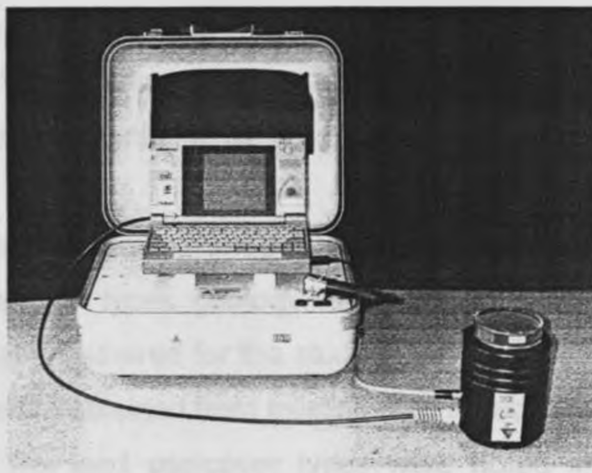

(a) Infrared Spectrometer

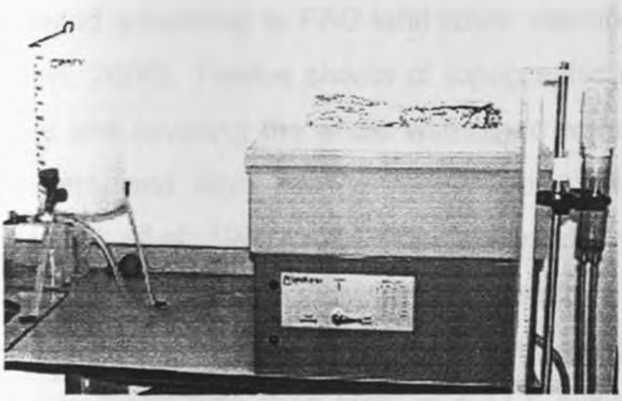

(b) Sandbox Apparatus

(c) Pressure Chamber

Figure 3.3. Laboratory equipment for soil analysis

3.2.4 Remote sensing and ancillary data

Landsat data were used to derive LST and NDVI for the study area for a long-term series. These data were obtained from the archives at the ITC, Netherlands and included six cloud-free scenes of Landsat TM (for the period between 1984 and 1998) and five scenes of Landsat ETM+ (between 1999 and 2003) all for path 168 and row 61. The month of February was chosen since it is the driest month when remote sensing scenes are clear of cloud contamination. These data were used to produce land surface temperature (60 m for ETM+) and high-resolution NDVI (spatial resolution of 30 m).

In addition to the remote sensing images, topographic maps, digital elevation (DEM) map, land use/cover types, geology, landscape slope, landscape position, and soil types were also gathered for the study area. Other than land use types, these ancillary data were obtained from existing map sources from GIS database at ICRAF, Nairobi. The land use/cover types were noted in the field during ground survey and grouped into: forest, woodlots, shrubland, cropland, and grassland according to FAO land cover classification procedures (Di Gregorio & Jansen, 2000). Twelve sheets of topographic maps each at 1:50, 000 nominal scales and covering the whole watershed were used. The geology and soil map were obtained from the georeferenced 1:1M maps of Kenya (Baker, 1952; Sombroek *et al*., 1982) while slope-zones map was developed from a 30-m DEM of the study area. The DEM was derived from digitized 1:50, 000 scale contour maps of the study area. The landscape positions were categorized as: lowland (for elevations less than 1000 m a.s.l.), midland (1000 ≤ elevation ≤ 1500 m a.s.l.), and uplands (elevation ≥ 1500 m a.s.l) while slope zones were categorized as: flat (slope ≤ 10%), gentle (10% ≤ slope ≤ 20%), and steep (slope ≥ 20%). These were chosen for convenience based on the data from DEM maps. Information from these ancillary data for the sampled plots were extracted from their respective maps using GIS Spatial Modeller in ERDAS IMAGINE® (ERDAS LLC, 2002).

3.3 Statistical analysis

3.3.1 Method for estimating physical properties

According to the theoretical approach for infiltration and water retention in Appendix A1, many data-fitting models can be used to predict the parameters of the infiltration and water retention characteristics. Since these models are nonlinear in their fitting parameters, a nonlinear regression approach was used to estimate the parameters from the experimental data. Thus, by considering the general form of the models as follows:

$$\mathbf{y} = \mathbf{f}(\Phi, \mathbf{x}) + \varepsilon \qquad (3.1)$$

where **y** is the vector of the measured moisture content, Φ is the vector of fitting parameters, **x** is the vector of suction pressure heads, and ε is the vector of error terms in fitting the models represented by the function **f** and is expected to be zero with constant variance σ^2 for all the observations. One of the popular methods for fitting Equation (3.1) is through the use of least squares (Leij et al., 1992). According to this strategy, Φ is determined to minimize the sum of squared error given by:

$$\mathrm{Sum}(\mathrm{error}^2) = \sum_{i=1}^{u} [\mathbf{y} - f(\Phi, \mathbf{x})]^2 \qquad (3.2)$$

where *u* is the number of observations. Equation (3.2) can also be obtained from the likelihood function of Equation (3.1) and which is given by:

$$L(\Phi, \sigma^2) = \frac{1}{(2\pi\sigma^2)^{u/2}} exp\left\{ -\frac{\sum [\mathbf{y} - f(\Phi, \mathbf{x})]^2}{2\sigma^2} \right\} \qquad (3.3)$$

The usual strategy for solving Equation (3.2) is either to aggregate data from different sources into one group and estimate their average parameters or to treat each group independently and estimate their parameters. Mixed effects modelling combine these two strategies in which average estimates (known as fixed effects) are obtained for aggregate group and individual group parameters. These are estimated simultaneously as random variations (known as random effects) around the fixed effects (Omuto *et al.*, 2006a)[2]. Thus, the parameters vector $\mathbf{\Phi}$ in Equation (3.2) can be re-written as:

$$\mathbf{y} = \mathbf{f}(\mathbf{\Phi}, \mathbf{x}) + \varepsilon$$
$$\mathbf{\Phi} = \mathbf{g}(\boldsymbol{\beta}, \mathbf{b}) \qquad (3.4)$$

where $\boldsymbol{\beta}$ is a p-dimensional vector of the population averages of fitting parameters and represents the fixed effects, **b** is a q-dimensional vector representing random effects and is assumed normally distributed with a unique variance-covariance matrix Ψ (Pinheiro and Bates, 2000). The evaluation of Equation (3.4) require the use of marginal densities in the likelihood estimations since the random effects are unobserved quantities in the experimental data. Accordingly, Lindstrom and Bates (1990) proposed an approximation that alternates between penalized non-linear least squares (PNLS) and linear mixed effects (LME) steps. In this method, the PNLS step begins with an initial estimate of the fixed effects from where the conditional modes of the *random effects* **b** are obtained by minimizing a penalized form of Equation (3.1) given by:

$$sum(error^2) = \sum_{i=1}^{n} \left[\| \mathbf{y}_i - f(\boldsymbol{\beta}, \mathbf{b}, \mathbf{x}_i) \|^2 + \| \mathbf{\Delta b} \|^2 \right] \qquad (3.5)$$

where the penalty $\mathbf{\Delta}$ is the precision factor to accelerate convergence. A first approximation of this penalty can be given by the ratios of standard residual error

[2] This paper has already been accepted in the Hydrology Journal

and the variances of the random effects (Thisted, 1988). In the PNLS step, the first approximation of Δ is held constant and Equation (3.3) minimized by approximating the conditional estimates of the population parameters and the conditional modes of the random effects. This can be done by converting Equation (3.3) into a simple nonlinear least squares in which the augmented response (now consisting of false additions of observations) and model function vectors are used (Pinheiro and Bates, 2000). Thus, Equation (3.3) becomes,

$$\text{sum}(\text{error}^2) = \sum_{i=1}^{n} \| \tilde{\mathbf{y}}_i - \tilde{f}(\boldsymbol{\beta}, \mathbf{b}, \mathbf{x}) \|^2 \qquad (3.6)$$

where $\tilde{\mathbf{y}}_i = \begin{bmatrix} \mathbf{y}_i \\ \mathbf{0} \end{bmatrix}$ and $\tilde{f}(\boldsymbol{\beta}, \mathbf{b}, \mathbf{x}) = \begin{bmatrix} f(\boldsymbol{\beta}, \mathbf{b}, \mathbf{x}) \\ \Delta \mathbf{b} \end{bmatrix}$. From Equation (3.6), the parameters $\boldsymbol{\beta}$ and $\mathbf{b}$ can be estimated using standard least squares estimation algorithms such as in Equation (3.2).

In order to update the estimates of Δ, the function f (Φ, $\mathbf{x}$) is linearized in the LME step using a first-order Taylor expansion around its current estimates of fixed effects ($\hat{\boldsymbol{\beta}}$) and the conditional modes of $\mathbf{b}$ ($\hat{\mathbf{b}}$)(Lindstrom & Bates, 1990). Thus, by letting $f'(\boldsymbol{\beta}, \mathbf{b}, \mathbf{x})$ be the partial derivatives of Equation (3.1) with respect to the fixed effects and random effects around the current estimates of $\hat{\boldsymbol{\beta}}$ and $\hat{\mathbf{b}}$ then the new estimate of Δ is obtained from approximate log-likelihood given

$$L(\boldsymbol{\beta}, \mathbf{b}, \Delta) = -0.5\left\{ u \log(2\pi\sigma^2) + \sum_{i=1}^{M} \left(\log | \boldsymbol{\Sigma}_i(\Delta) | \right) + \sigma^2 \mathbf{G} \right\} \qquad (3.7)$$

where M is the number of parameters in the Equation (3.1), Σ_i is the multivariate normal variance-covariance matrix, and **G** is the squared Euclidean distance for a multivariate response given by,

$$G = \left[\hat{w} - \beta f'(\beta, b, x)\Big|_{\hat{\beta}} \right]^T \Sigma^{-1}(\Delta) \left[\hat{w} - \beta f'(\beta, b, x)\Big|_{\hat{\beta}} \right] \quad (3.8)$$

in which $\hat{w} = y_i - f(\hat{\beta}, \hat{b}, x) + f'(\beta, b, x)\Big|_{\hat{\beta}, \hat{b}}$ according to the Taylor's first order expansion. The output of this LME steps is then fed back into the PNLS step and the iterative procedure is repeated until the convergence criterion is met. The random effects of the final output can be further modelled with external covariates such as land use and soil type to assess their effects on behaviour of unsaturated characteristics of the soils.

3.3.2 Choosing the best models to predict the experimental data

Table 3.2 shows the two physically based infiltration and the four water retention models tested for their ability to fit the measured data as well as predict the soil physical properties. These models were individually fitted to the measured data using nonlinear least squares regression of Equations (3.1), (3.2) and (3.3). For each model in Table 3.2, the likelihood function of Equation (3.3) was estimated and the Akaike Information Criteria (AIC) (Sakamoto *et al.*, 1986) determined as follows:

$$AIC = -2 * \log\{\text{likelihood}\} + 2 * \kappa \quad (3.9)$$

where κ is the number of fitting parameters in the model tested. In addition to AIC, residual standard error and coefficient of determination (r^2) (Kottegoda and Russo, 1997; Omuto, 2007a[3]) were also determined. These three statistics were used to select the best performing models in Table 3.2. The criterion for choosing the best performing model was based on the combination of low AIC, residual standard error, and high r^2.

[3] This paper has been submitted to Geoderma

Table 3.2. Hydraulic models tested for their ability to predict measured data

Model name	Model function	Parameters	Reference
Infiltration models			
Philip	$i(t) = \frac{S(\theta)}{2\sqrt{t}} + f_c$	S, f_c	Philip (1957)
Green and Ampt	$i(t) = KS/z + K$	K and S	Chow *et al.* (1988)
Water retention models			
Van Genuchten	$\theta(h) = \theta_r + (\theta_s - \theta_r)\left[1 + (\alpha h)^n\right]^{-m}$	θ_s, θ_r, α, n, m	Van Genuchten (1980)
Brooks-Corey	$\theta(h) = \theta_r + (\theta_s - \theta_r)(\alpha h)^{-\lambda}$	θ_s, θ_r, α, λ	Brooks and Corey (1964)
Campbell	$\theta(h) = \theta_s(\alpha h)^{-1/n}$	θ_s, α, n	Campbell (1972)

3.3.3 Strategies for prediction of physical properties

Three strategies were tried in fitting the best hydraulic model obtained in section 3.3.2 above. The first strategy was one in which each experimental unit was considered independently and parameters of the hydraulic functions obtained for every sample-point. This strategy was denoted as NLIS. The second strategy was one in which all data were pooled and treated as though coming from one experimental unit. Here the parameters estimates represented average values for the whole basin. This strategy was denoted as NLS. The last strategy was the nonlinear mixed effects (NLME) approach (Pinheiro and Bates, 2000). NLME is model-based fitting approaches that can permit accurate and reliable estimation of the required functional parameters and also to incorporate effects of covariates' during the analysis (Pinheiro and Bates, 2000; Lark and Cullis, 2004). It can allow variations in data to be explained by an appropriate functional model, by level-of-sample aggregation, and by significant covariates perceived to influence the parameter estimation (Draper, 1995; Pinheiro and Bates, 2000).

The computer codes for implementing these strategies are shown in Appendix (A2) while the strategies and procedures used in fitting them were those reported in Omuto (2007b[4]).

3.3.4 Case-definition of soil physical degradation

The set of seven soil physical properties (f_c, S, θ_s, θ_r, α, n, ρ_b) from section 3.3.3 above were used to derive a case definition of soil physical degradation. Since they encompass effects of many factors such as micropores, soil texture and structure, and relative soil compaction (Pagliai and Jones, 2002), their natural groupings were hypothesized to represent groups of soil physical condition. For example, the group of variables with low magnitudes of infiltration characteristics, pore-size distribution, and water holding capacity but with high bulk density could be considered to belong to the group of poor soil physical condition (Dexter, 2004). Cluster analysis of the physical properties was therefore used to determine these groups. An exploratory tree (Brieman *et al.*, 1984) was then used to interpret the physical properties of the final clusters and to define a case of physical degradation. Exploratory tree was developed using tree classification technique. In this approach, a vector of soil samples is recursively partitioned into binary homogeneous groups and then classes are assigned to the terminal branches (Brienman *et al.*, 1984). The method splits a learning sample set into two homogeneous groups known as child nodes. The two child nodes are further split into binary groups of increasing homogeneity until the terminal groups are pure enough to be assigned a particular class (Brieman *et al.*, 1984). The resulting impurity is error known as misclassification. The decision to split a node, the number of nodes, and class assignment all depend on classification rules as

[4] This software is available online from www.r-project.org

discussed in Brieman *et al.* (1984). In this study, a ten-fold cross-validation approach was used to explore the case-definition (Brieman *et al.*, 1984).

3.3.5 Screening of soils for physical degradation

The screening of soils for physical degradation was conceptualised using a decision tree approach (Figure 3.4). According to this approach, different evidences of degradation were used in successive order of testing to predict the likelihood of degradation at a particular site in the field. Thus, by beginning with a simple test involving observed features of degradation the screening tests identified all sites that had obvious signs of degradation as indicated in Table 3.1. The presence of features of degradation clearly separated the degraded sites from the non-degraded sites. However, for areas that had no clear signs of degradation subsequent tests were required to determine their true physical conditions. Soil spectral reflectance was used in this step since it is an integral indicator of many soil functional attributes and was also relatively easy to sample and estimate. The cases that were not properly diagnosed with spectral reflectance were further tested using measurements of selected soil physical properties.

In order to include the spatial correlation captured in the Y sampling frame in the screening tests, a generalized linear mixed effects logistic regression was used in each branch of Figure 3.3. The logistic regression model used is given by:

$$f[\gamma(\mathbf{X})] = \log\left\{\frac{[\gamma(\mathbf{X})]}{1-[\gamma(\mathbf{X})]}\right\} \qquad (3.12)$$

$$= \log\left\{\frac{[P(\mathbf{Y} \le y_i|\mathbf{X})]}{[P(\mathbf{Y} > y_i|\mathbf{X})]}\right\} = a + B\mathbf{X}, \quad i = 1, 2, ..., k\text{-}1$$

where *a* and *B* are regression coefficient to be estimated, *k* is the number of categories in the response variable, and $\gamma(\mathbf{X})$ is the response probability given the explanatory vector **X**.

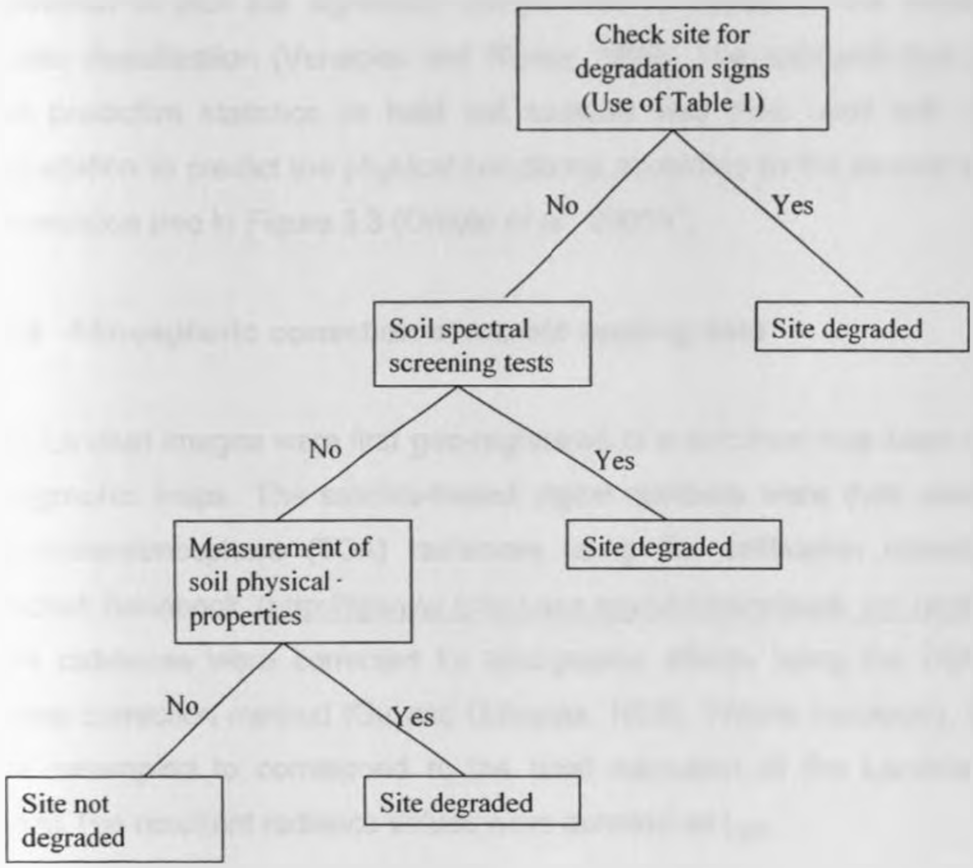

Figure 3.4. Concept of case-definition of soil physical degradation

According to Stern et al. (2004), the function $f[\gamma(\mathbf{X})]$ is the link that connects the systematic components ($a + B\mathbf{X}$) of the linear model. Equation (8) was applied on a random two-thirds of the Y clusters in the sampling design and predicted on the remaining one-third. Given the soil spectral reflectance spanned several wavebands thus giving more variables than total sample size, two approaches were tested for the inclusion of the spectra in the predictive model. The first approach involved the use of an exploratory classification tree between spectral wavebands and the cluster groups to determine the significant wavebands that correlated with the clusters. These wavebands were then used in the mixed effects logistic model to predict the soil physical conditions. The second approach involved the use of principal components of the spectral wavebands. In this case, all of the seven principal components were used in a stepwise regression to pick the significant components to include in the mixed effects logistic classification (Venebles and Ripley, 1999). The approach that gave the best predictive statistics on held out samples was then used with observed degradation to predict the physical conditions according to the second branch of the decision tree in Figure 3.3 (Omuto *et al.*, 2006b[5]).

3.3.6 Atmospheric correction of remote sensing data

The Landsat images were first geo-registered to a common map base using the topographic maps. The satellite-based digital numbers were then converted to top-of-the-atmosphere (TOA) radiances using the calibration models in the Landsat handbook (http://ltpwww.gsfc.nasa.gov/IAS/handbook_toc.html). These TOA radiances were corrected for topographic effects using the DEM with a cosine correction method (Gu and Gillepsie, 1998). Where necessary, the DEM was resampled to correspond to the pixel resolution of the Landsat thermal bands.The resultant radiance values were denoted as L_{sat}.

Since there were no reliable atmospheric profile data in the neighborhood of the study area for the periods before 1998, a uniform approach was used for approximate atmospheric corrections. The Chavez (1996) approach was used in which ground reflectance, r_g, for bands three and four were estimated by:

$$r_{band_i} = \frac{\pi(L_{sat} - L_p)d^2}{E_o \cos\phi_z \tau} \qquad (3.13)$$

where L_p is the atmospheric path radiance, d is the Earth-Sun distance at the time of satellite overpass, $\tau_{band\,i}$ is the atmospheric transmissivity of the solar band i, ϕ is the solar zenith angle, and E_o is the extraterrestrial solar irradiance corresponding to the Landsat band. The atmospheric path radiance is the

[5] This paper has been submitted to European Journal of Soil Science

upwelling radiance coming from zero-reflectance of the ground (Liang, 2004) and is obtained from:

$$L_p = L_{min} - 0.01\tau E_o \cos\phi(\pi d^2)^{-1} \quad (3.14)$$

where L_{min} is the radiance corresponding to digital number of a pixel for which the sum of all pixels with digital numbers lower or equal to L_{min} is one percent of the total sum of pixels in the scene under consideration (Sobrino *et al.*, 2004). Chavez (1996) has suggested conservative values of τ as 0.85 for band three and 0.91 for band four of Landsat images. The estimated values of values of L_{min} and L_p are shown in Table 3.3.

Table 3.3. Landsat solar bands for path 168 and row 61

Date	**Estimated parameters for the solar bands**			
	L_{min} (Watts m^{-2} $sr^{-1}\mu m^{-1}$)		L_p (Watts m^{-2} $sr^{-1}\mu m^{-1}$)	
	Band 3	Band 4	Band 3	Band 4
27 February 1984	14.26	6.55	10.88	3.01
10 February 1986	15.01	7.01	11.20	3.55
25 February 1987	14.97	5.99	10.93	3.23
17 February 1988	13.88	6.17	11.53	3.99
01 February 1995	14.22	6.89	11.11	3.78
22 February 1998	16.92	7.55	11.22	3.96
11 February 1999	15.88	7.89	11.04	3.90
21 February 2000	16.12	8.56	12.11	3.94
07 February 2001	16.22	7.99	12.03	4.15
10 February 2002	14.32	8.56	11.62	3.85
28 February 2003	14.90	8.11	11.71	3.86

From the calibrated and atmospherically corrected solar bands, NDVI for each scene were calculated using bands three (visible red) and four (infrared red) as follows:

$$\mathrm{NDVI} = \frac{r_{band4} - r_{band3}}{r_{band4} + r_{band3}} \quad (3.15)$$

For the thermal data, the radiative transfer equation applied was that given by (Liang, 2004):

$$B(\mathrm{LST}) = \frac{\left(L_{sat} - L_{atm}^{\uparrow}\right)}{\varepsilon \tau_{th}} - \frac{(1-\varepsilon)\mathrm{L}_{atm}^{\downarrow}}{\varepsilon} \quad (3.16)$$

where ε is the land surface emissivity, $L_{atm}^{\downarrow}$ is the down welling atmospheric radiance, $L_{atm}^{\uparrow}$ is the upwelling atmospheric radiance, τ_{th} is the atmospheric transmissivity of the thermal bands, and B(LST) is the blackbody radiance given by Plank's Law for the surface temperature, LST. The most important factors controlling $L_{atm}^{\uparrow}$, $L_{atm}^{\downarrow}$, τ_{th}, are the vertical distributions of water vapour, ozone, and aerosols that need to be determine at the time of satellite overpass (Liang, 2004). The task of atmospheric correction is to estimate the three quantities: $L_{atm}^{\uparrow}$, $L_{atm}^{\downarrow}$, τ_{th} on image basis (or pixel basis). However, due to the difficulties in getting atmospheric profile data the ancillary information from neighbouring weather stations can be the best alternative (Schadlich *et al*., 2001). In this study, atmospheric profiles were those provided by SHADOZ at Nairobi station (1.27° S, 36.8° N) within 4-6 hours of the satellite overpass (Thompson *et al*., 2003). These data were run in PcModWin© 4.0 (Ontar Corp., 2002) on image basis with default aerosol profile for rural model. The default value was used due to lack of data for aerosol estimates. Many researchers have used this procedure whenever they do not have measured data (Schadlich *et al*., 2001; Omuto and Shrestha, 2006). The estimated parameters for the thermal bands are shown in Table 3.4.

Table 3.4. Landsat ETM+ thermal data for path 168 and row 61

Date	Thermal band (high gain) and estimated parameters		
	$L_{atm}^{\downarrow}$ (Watts m^{-2} sr^{-1} μm^{-1})	$L_{atm}^{\uparrow}$ (Watts m^{-2} sr^{-1} μm^{-1})	τ_{th}
11 February 1999	3.66	3.54	0.71
21 February 2000	3.45	2.55	0.73
07 February 2001	3.77	3.01	0.75
10 February 2002	4.01	2.88	0.68
28 February 2003	3.89	3.45	0.75

This relationship was utilized to derive the emissivity in Equation (3.17) as follows:

$$f_v = 1 - \left(\frac{NDVI_{max} - NDVI}{NDVI_{max} - NDVI_{min}} \right)^a \qquad (3.18)$$

where a is a coefficient for leaf orientation distribution ($0.6 \leq a \leq 1.25$), $NDVI_{min}$ is the NDVI for bare soil, and $NDVI_{max}$ is the NDVI for complete vegetation cover. After assessing pixels in complete forest cover and bare ground for all the scenes, $NDVI_{min}$ was assigned 0.01 while $NDVI_{max}$ was assigned 0.96. An average value for a was chosen as 0.93 to represent a mix among the canopy types in the study area.

Using the estimated land surface emissivity, atmospheric transmissivity, and upwelling and down welling radiances, Equation (3.16) was then inverted to derive LST using the Landsat constants provided in the online Landsat 7 data users handbook. Thus, LST in Kelvin for each scene was calculated as follows:

$$LST = 1282.71 / \ln[\{666.09 / B(LST)\} + 1] \qquad (3.19)$$

3.3.7 Calibration of soil physical degradation with remote sensing

The deviations of LST and NDVI from long-term averages were hypothesized to be due to cumulative effects of soil physical degradation. The basis for this assumption was derived from the basic equation relating soil thermal characteristics and physical properties and which is given by Equation (2.10). The term $\rho_b C_s$ in Equation (2.10) is the volumetric heat capacity that is governed by soil porosity, soil texture, and organic content (Marshall *et al.*, 1996; Campbell and Norman, 1998). Volumetric heat capacity and thermal conductivity combine to form soil's thermal admittance that controls heat dissipation at the soil surface. When soil physical properties are adversely affected and thermal admittance raised, much of the surface heat goes to heating the soil and consequently raising LST (Campbell and Norman, 1998). Therefore, land areas experiencing physical degradation may show positive departures of LST from the long-term average. However, since soil physical degradation also affects biomass production (Wright *et al.*, 1990), negative departures of NDVI from long-term average may also be used alongside LST deviations to delineate degraded pixels. In order to remove the effects of geographic resources (such as climate, vegetation type, and soil types) standardized deviation was used (Farrar *et al.*, 1994; Unganai and Kogan, 1998). Thus, the remote sensing indicators of degradation were estimated from the expression:

$$\text{degradation indicator} = \begin{cases} \dfrac{\text{NDVI}_{2003} - \text{NDVI}_{\text{long-term}}}{\text{NDVI}_{2003} + \text{NDVI}_{\text{long-term}}} & < 0 \\ \\ \dfrac{\text{LST}_{2003} - \text{LST}_{\text{mean}}}{\text{LST}_{2003} + \text{LST}_{\text{mean}}} & > 0 \end{cases} \tag{3.20}$$

where NDVI_{mean} was the eleven-year average of the NDVI of each Landsat scene and LST_{mean} was the five-year average of LST values. These image indicators were extracted for all surveyed plots and assessed for their association with the physical degradation classes so that a general relationship could be established to map out the degradation in the whole scene (Omuto and Shrestha, 2006).

CHAPTER FOUR

4. RESULTS AND DISCUSSION

4.1 Soil properties that index physical degradation

From the literature survey, it emerged that soil properties that are significantly affected by physical degradation are the water infiltration and retention characteristics. Theoretical considerations of the water flow and retention characteristics in Appendix (A1 and A2) and literature survey suggested the following to be the physical properties that can index physical degradation: f_c, S, θ_s, θ_r, θ_i, n, α, and ρ_b.

The infiltration characteristics (f_c and S) are sensitive to soil physical degradation because they are affected by changes in both the magnitude and shape of soil pores (Lilly, 2000). Infiltration, which is the entry and movement of water in soil, is governed by both the path connectedness and volume of the conducting pores while water retention's θ_s and α are largely dependent on the volume and pressure of the pores (Marshall *et al.*, 1996; Brady and Weill, 2002). When physical degradation obliterates the pore connectedness and also negatively affects the pore volume, the infiltration characteristics are most influenced.

The water retention's n, ρ_b and α are indicative of the soil's textural characteristics. Since the changes in these properties denote changes in textural composition, the increase in the magnitude of n, ρ_b and α *can* be associated with the transfer soil particles that occurs during physical degradation (Reynolds and Elrick, 1990; Cresswell *et al.*, 1992). For example, some studies have shown the increase in fine particles to be associated with severe physical degradation (Richard *et al.*, 2001). The soil pore-size distribution index n represents the range of sizes of soil pores: being small for a wide range of pore sizes and large for nearly uniform distribution of soil pores (Brooks and Corey, 1964).

4.1.1 Estimation of physical properties from measured data

Table 4.1 shows the results of comparison of different models cited in the literature in predicting the measured infiltration and water retention characteristics. It was evident that the Philip's infiltration model and the van Genuchten model gave the best fit to the data.

Table 4.1. Comparison of alternative model fits to measured infiltration and water retention characteristics

Model	Number of parameters	AIC	Standard residual error	Coefficient of determination, r^2
Infiltration models				
Philip	2	21875	0.422	0.88
Green and Ampt	2	23584	0.507	0.86
Water retention models				
Brooks-Corey	4	-19452	0.0435	0.92
Van Genuchten	4	-21712	0.0321	0.96
Campbell	3	-20568	0.0361	0.94

These two models were then used to predict the parameters (also known as physical properties) in the infiltration and water retention functions from the experimental data according to the three parameter estimation strategies: NLS, NLIS, and NLME. The NLS strategy gave a residual standard error (RSE) of 0.561 cm $minute^{-1}$ for infiltration and 0.078 cm^3 cm^{-3} for water retention function (Table 4.2). Although different models can result in different RSE values, fitting a single hydraulic function for all samples drawn from different parts of a watershed could mask the possibility of knowing individual characteristics of these parts of the watershed. Like in the case of NLS, the individual sample differences were incorporated in the residuals hence the large magnitudes of the RSE. This resulted into poor fits such as is illustrated in Figure 4.1. Similar poor fit was also observed with the infiltration data.

Table 4.2. Model fit information for NLS strategy

Infiltration function			Water retention function		
Parameter	Minimum	Maximum	Parameter	Minimum	Maximum
S (cm minute$^{-0.5}$)	0.45 (0.73[a])	30.7 (7.4)	θ_s (cm^3 cm^{-3})	0.13 (0.19)	0.60 (0.51)
f_c (cm hour^{-1})	0.01 (0.23)	1.31 (0.11)	θ_r (cm^3 cm^{-3})	0.00 (0.20)	0.36 (0.22)
			α (m^{-1})	0.1 (0.1)	0.89 (0.22)
			n	1.03 (0.14)	1.97 (0.16)
Residual standard error = 0.422(df = 16128)			Residual standard error = 0.015(df = 2171)		

[a]Standard errors

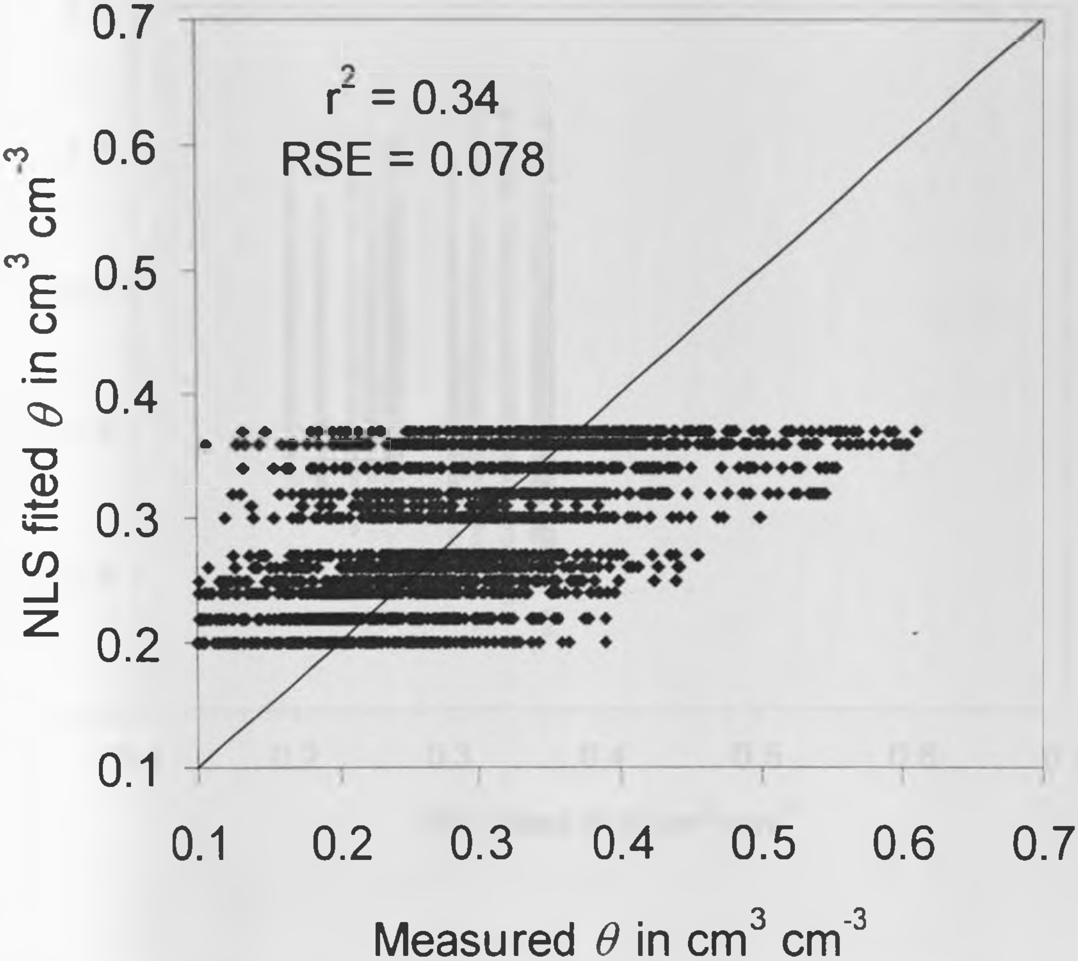

Figure 4.1. Measured versus NLS fitted moisture contents

A plot of the standardized residuals versus the NLS fitted moisture contents showed a pattern of residuals systematically increasing with predicted values thus indicating violation of the assumption of constant residual errors. For example, Figure 4.2 shows the case with water retention characteristics. Further analysis of the residuals revealed strong spatial correlation among observations. Figure 4.3 shows example with water retention characteristics. These plots and the low coefficient of determination demonstrated the inadequacy of the NLS strategy in accurate prediction of soil hydraulic parameters.

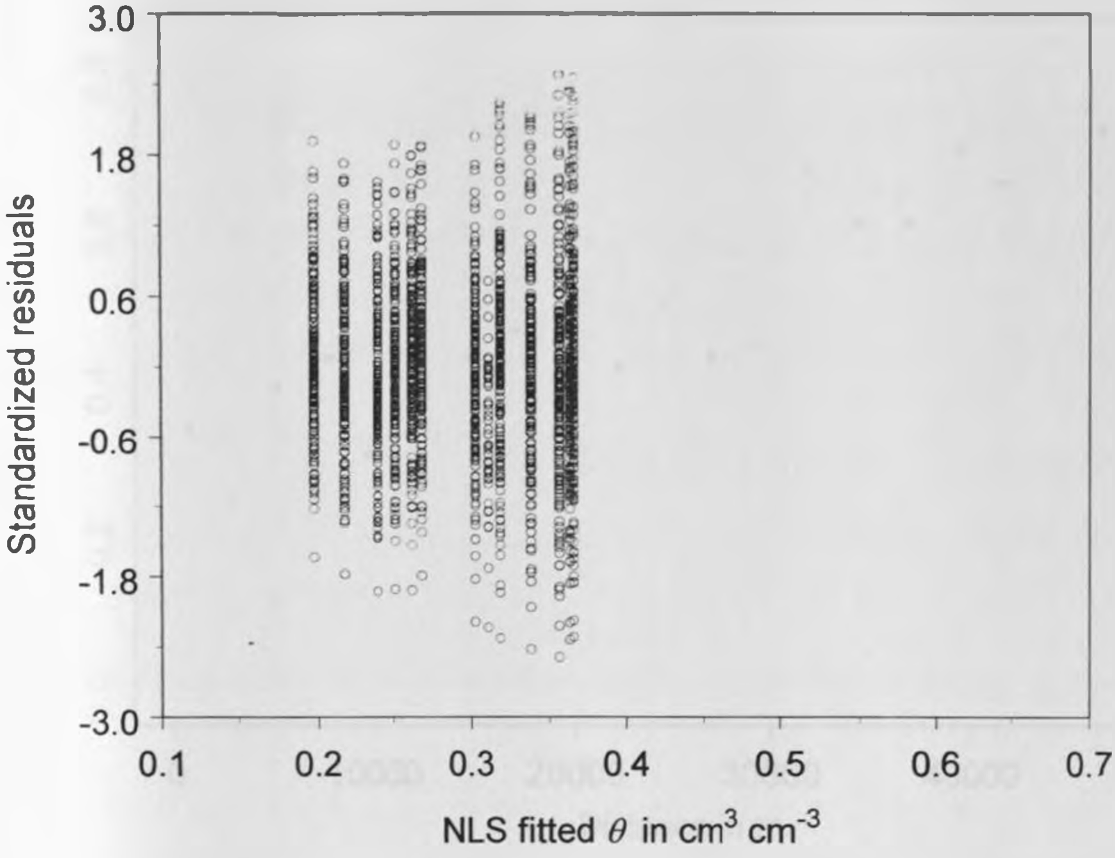

Figure 4.2. Scatter plot of standardized residuals versus NLS fit of the van Genuchten model.

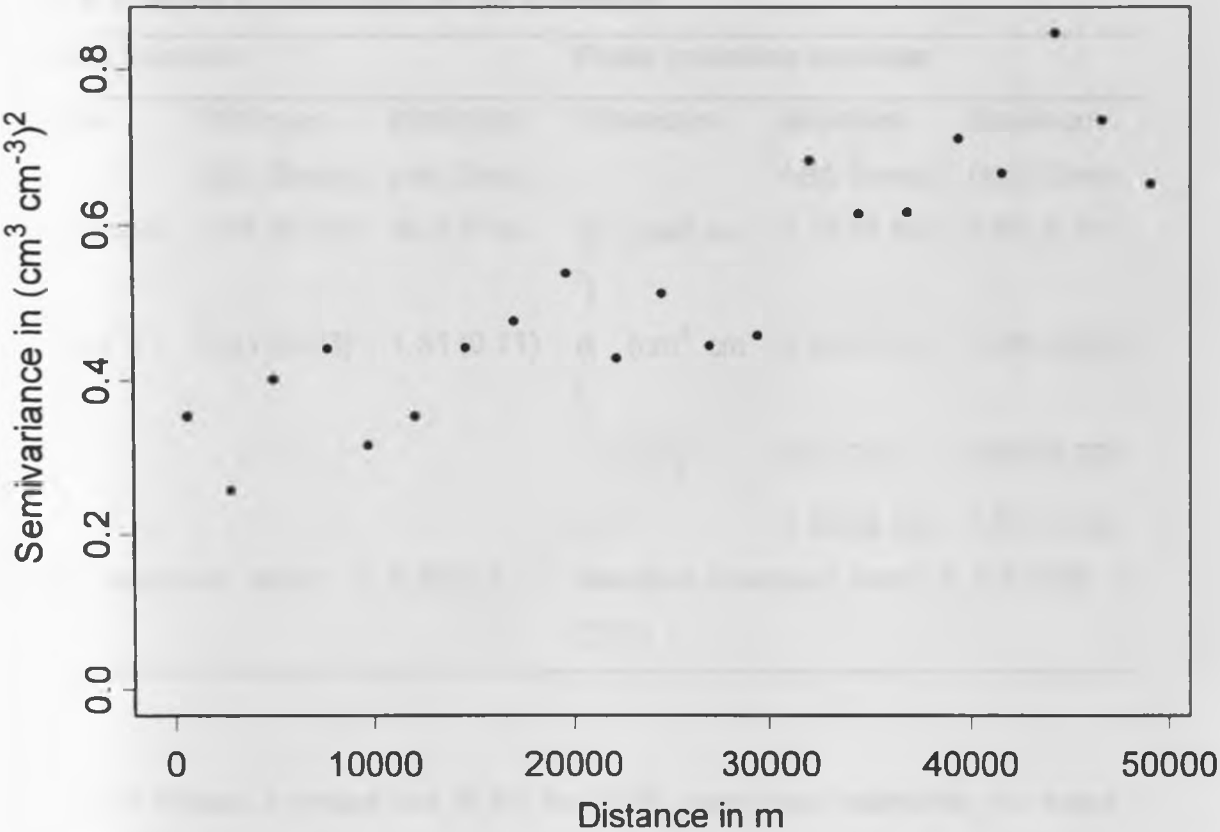

Figure 4.3. Semivariogram of the NLS regression residuals

The NLIS strategy tried to remove part of the statistical deficiencies in the NLS method by recognizing the individual differences in soil characteristics. Here, the standard error of the residuals was 0.422 cm minute^{-1} for the infiltration function and 0.015 cm^3 cm^{-3} for the water retention function (Table 4.3). These standard errors of residuals represented a 25% reduction in the infiltration and 80% reduction in the water retention functions compared with those of the NLS strategy.

Table 4.3. Model fit information for NLIS method

Infiltration function			**Water retention function**		
Parameter	Minimum (std. Error)	Maximum (std. Error)	Parameter	Minimum (std. Error)	Maximum (std. Error)
S (cm minute$^{-0.5}$)	0.45 (0.73)	30.7 (7.4)	θ_s (cm^3 cm^{-3})	0.13 (0.19)	0.60 (0.51)
f_c (cm hour^{-1})	0.01 (0.23)	1.31 (0.11)	θ_r (cm^3 cm^{-3})	0.00 (0.20)	0.36 (0.22)
			α (m^{-1})	0.1 (0.1)	0.89 (0.22)
			n	1.03 (0.14)	1.97 (0.16)
Residual standard error = 0.422(df = 16128)			Residual standard error = 0.015(df = 2171)		

Figure 4.4 shows a typical the fit for the NLIS parameter estimation for water retention. This method is therefore useful when the interest is in modelling the behaviour of a particular fixed set of individuals.

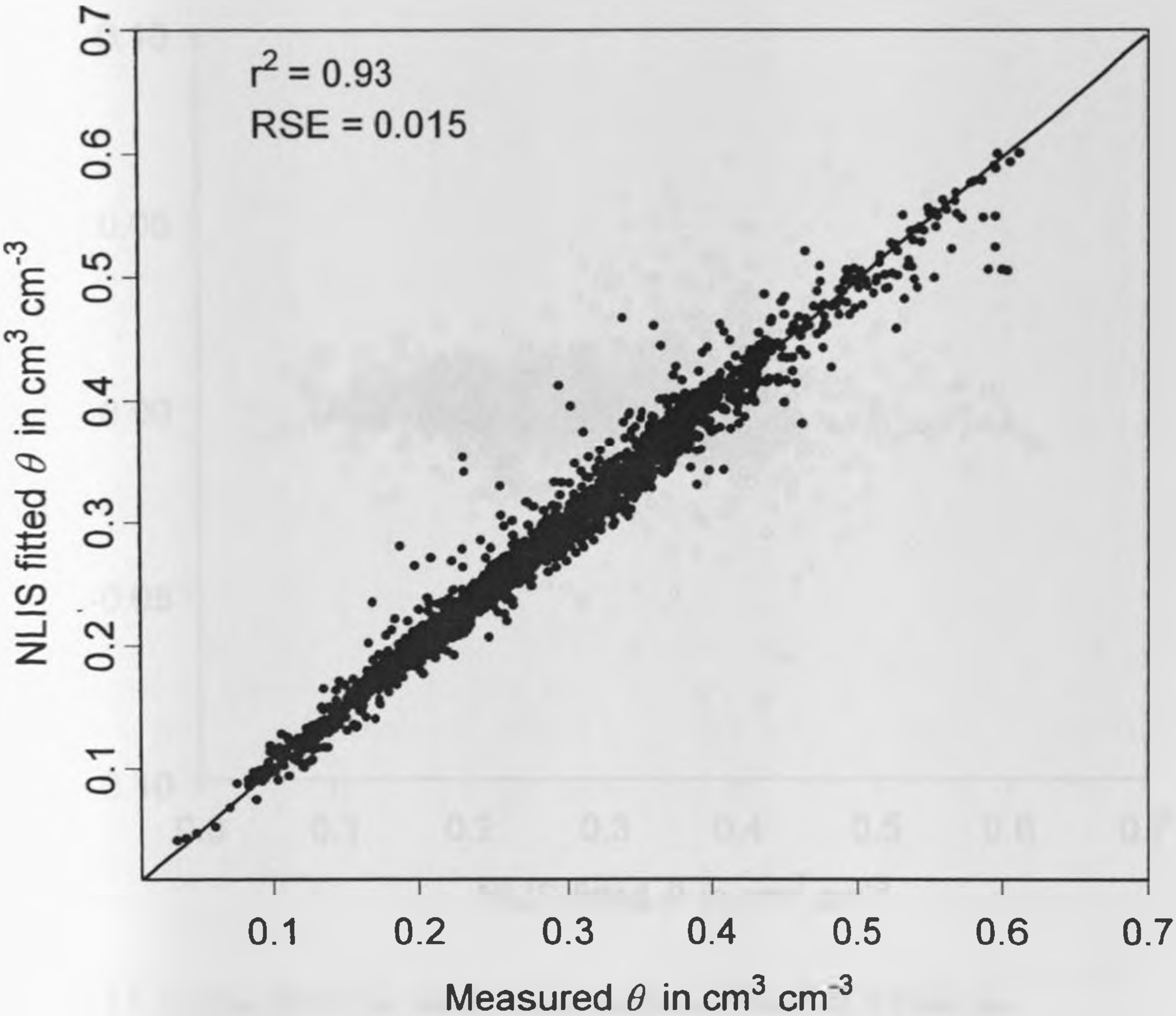

Figure 4.4. Measured versus NLIS fitted moisture contents

Unlike the case with the NLS method, the assumption of the constant variance of the residuals was not violated: there was little evidence for residuals increasing with the fitted values (Figure 4.5). No spatial correlation was evident with this method since the nugget was almost equivalent to sill of the semivariogram of regression errors (Figure 4.6).

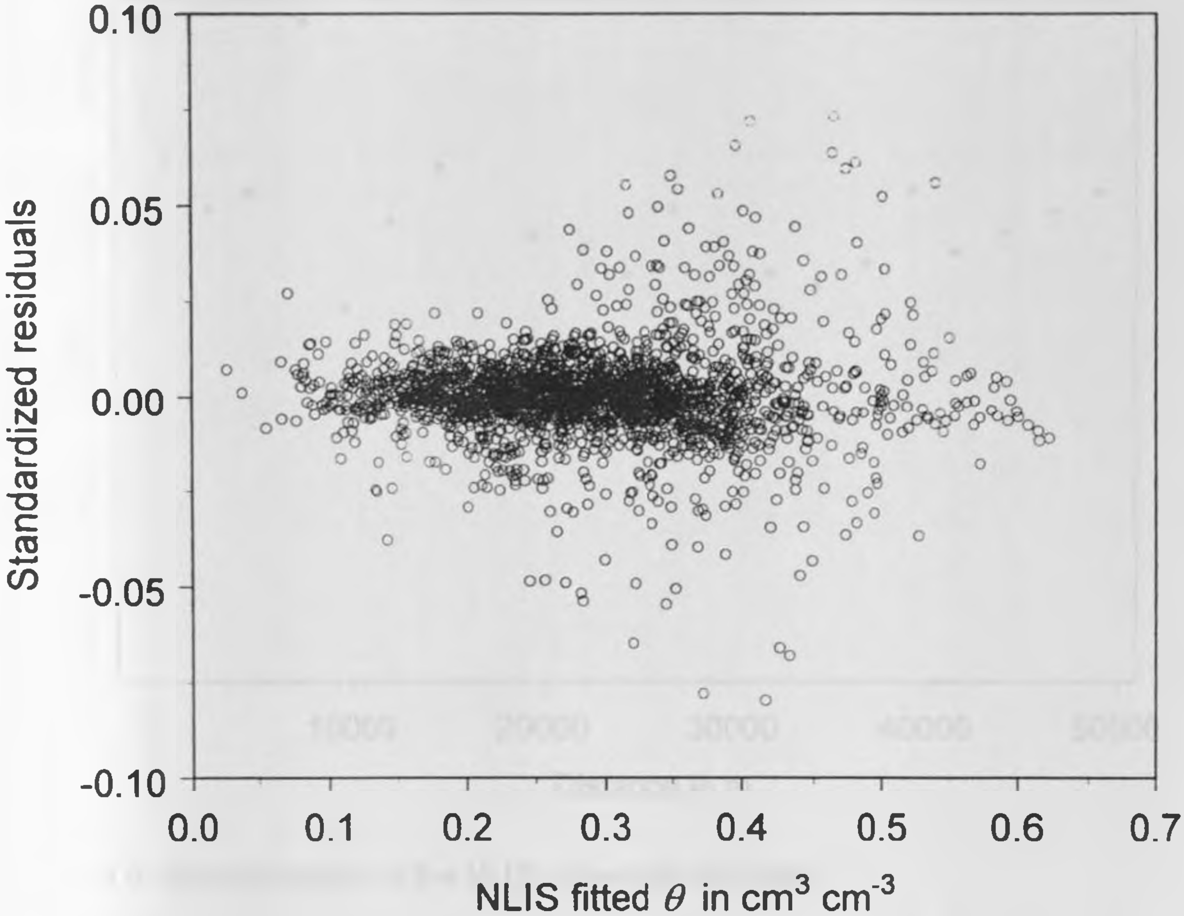

Figure 4.5. Scatter plot of the standardized residuals versus NLIS fitted van Genuchten model

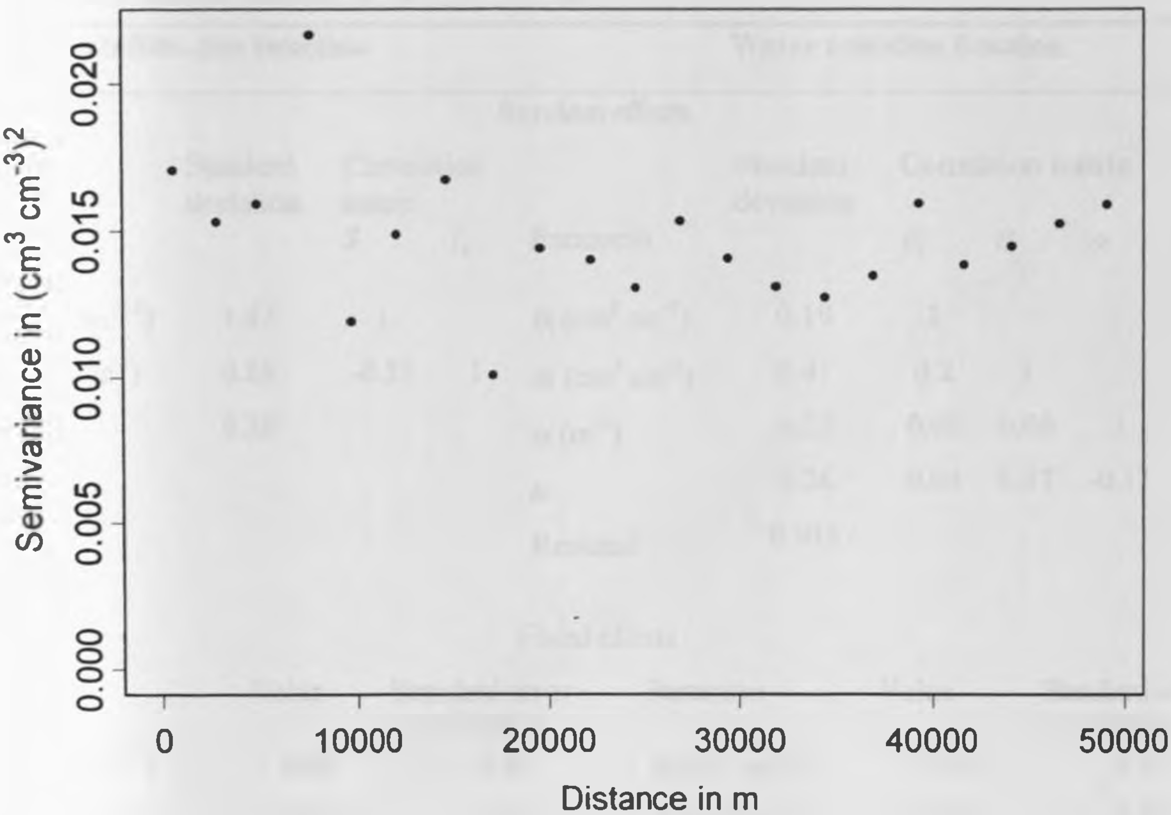

Figure 4.6. Semivariogram of the NLIS regression residuals

Although the NLIS method showed individual variability in parameter estimates, the method was not adequate in description especially where individual point-measurements were treated as samples from a large population of similar characteristics. Often, the essence of hydraulic parameter estimation is to study the average hydrologic behaviour of a watershed as well as the effects of the variability among and within plots in the watershed. The NLME method offered this opportunity by estimating whole watershed average values of the hydraulic parameters (as fixed effects) as well as estimating the random variations of individual point-measurements in the watershed as random effects (Table 4.4). The standard error of the residuals was reduced further by 10% in infiltration and 13% in water retention functions compared to NLIS.

Table 4.4. Model output for NLME method

Infiltration function				**Water retention function**					
				Random effects					
Parameter	Standard deviation	Correlation matrix S	f_c	Parameter	Standard deviation	Correlation matrix θ_s	θ_r	α	n
S (cm minute$^{-0.5}$)	1.42	1		θ_s (cm^3 cm^{-3})	0.19	1			
f_c (cm minute^{-1})	0.88	-0.55	1	θ_r (cm^3 cm^{-3})	0.41	0.2	1		
Residual	0.38			α (m^{-1})	0.35	0.02	0.06	1	
				n	0.26	0.04	0.47	-0.17	1
				Residual	0.013				
				Fixed effects					
Parameter	Value	Standard error (df =15592)		Parameter	Value	Standard error (df =2166)			
S (cm minute$^{-0.5}$)	4.00	0.51		θ_s (cm^3 cm^{-3})	0.36	0.27			
f_c (cm minute^{-1})	0.22	0.33		θ_r (cm^3 cm^{-3})	0.00	0.23			
				α (m^{-1})	11	0.41			
				n	1.15	0.30			

The low residuals indicated improvement in the accuracy in parameter estimation (Figure 4.7).

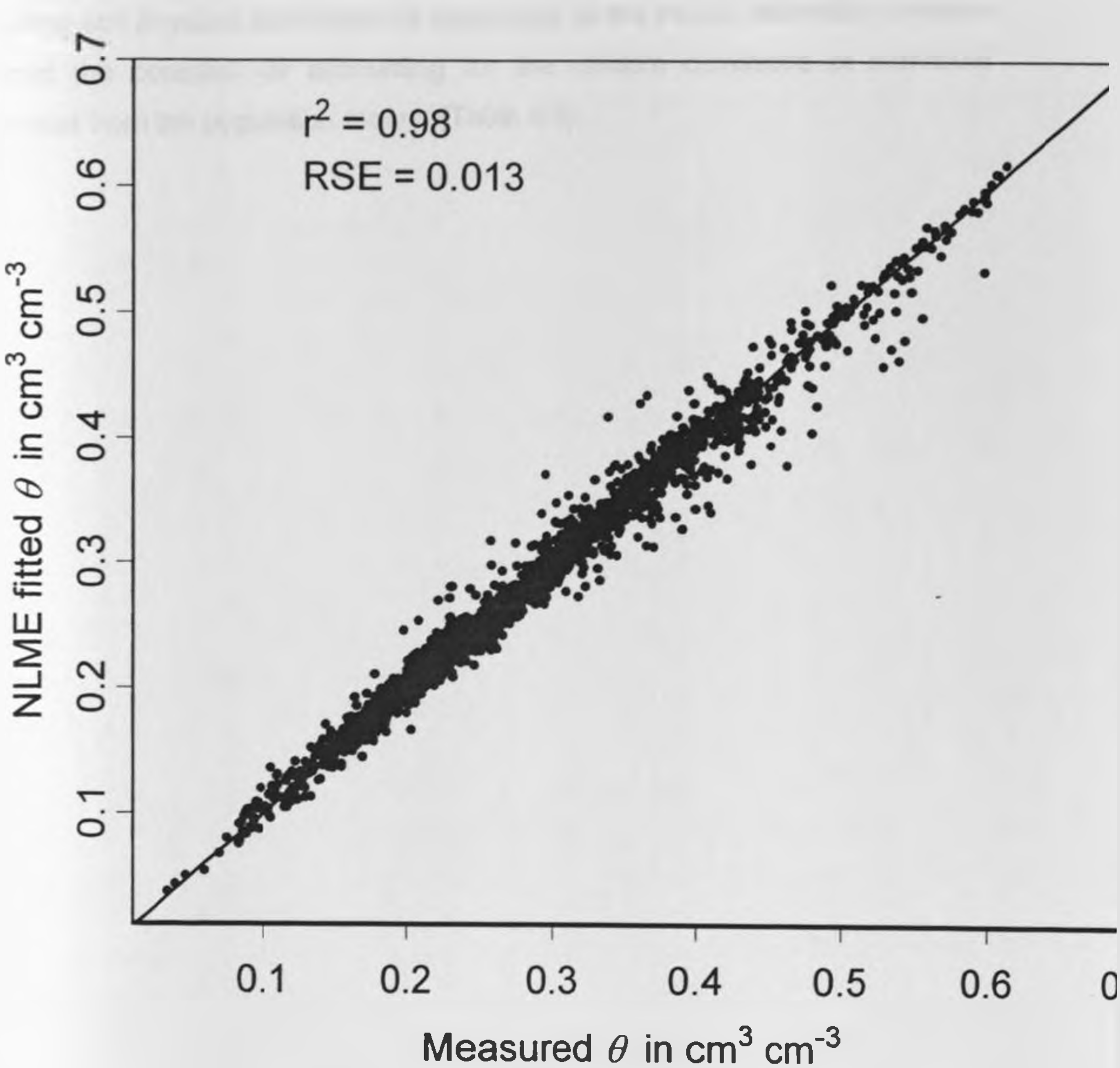

Figure 4.7. Measured versus NLME fitted moisture content

In Figure 4.8, the residuals were not only lower than those of NLIS (Figure 4.5), but also clustered around zero showing lack of bias, and confirming the validity of the assumption of constant residual variance. Furthermore, assessment using the semivariogram also revealed no apparent spatial correlation of the residuals (Figure 4.9 for the case of water retention). Further improvement in NLME models can be achieved by using covariates condition on the random effects.

Including soil physical conditions as covariates in the model estimation process showed the potential for accounting for the random deviations of individual estimates from the population means (Table 4.5).

Table 4.5. NLME with covariate modelling

Infiltration function				Water retention function					
		Random effects							
	Standard deviation	Correlation matrix			Standard deviation	Correlation matrix			
Parameter		S	f_c	Parameter		θ_s	θ_r	α	n
S (cm minute$^{-0.5}$)	1.36	1		θ_s (cm^3 cm^{-3})	0.09	1			
f_c (cm minute^{-1})	0.73	-0.49	1	θ_r (cm^3 cm^{-3})	0.12	0.2	1		
Residual	0.38			α (m^{-1})	0.15	0.02	0.06	1	
				n	0.26	0.04	0.47	-0.17	1
				Residual	0.013				

Fixed effects

	Value	Standard error (df=15590)		Value	Standard error (df=2164)
Non-degraded					
S (cm minute$^{-0.5}$)	5.37	0.57	θ_s (cm^3 cm^{-3})	0.40	0.02
f_c (cm minute^{-1})	0.47	0.03	θ_r (cm^3 cm^{-3})	0.09	0.02
			α (m^{-1})	17	0.4
			n	1.69	0.30
Moderately degraded					
S (cm minute$^{-0.5}$)	2.48	0.18	θ_s (cm^3 cm^{-3})	0.37	0.01
f_c (cm minute^{-1})	0.21	0.01	θ_r (cm^3 cm^{-3})	0.09	0.01
			α (m^{-1})	7	0.7
			n	1.35	0.06
Severely degraded					
S (cm minute$^{-0.5}$)	1.23	0.13	θ_s (cm^3 cm^{-3})	0.33	0.01
f_c (cm minute^{-1})	0.10	0.01	θ_r (cm^3 cm^{-3})	0.06	0.02
			α (m^{-1})	4	0.1
			n	1.23	0.05

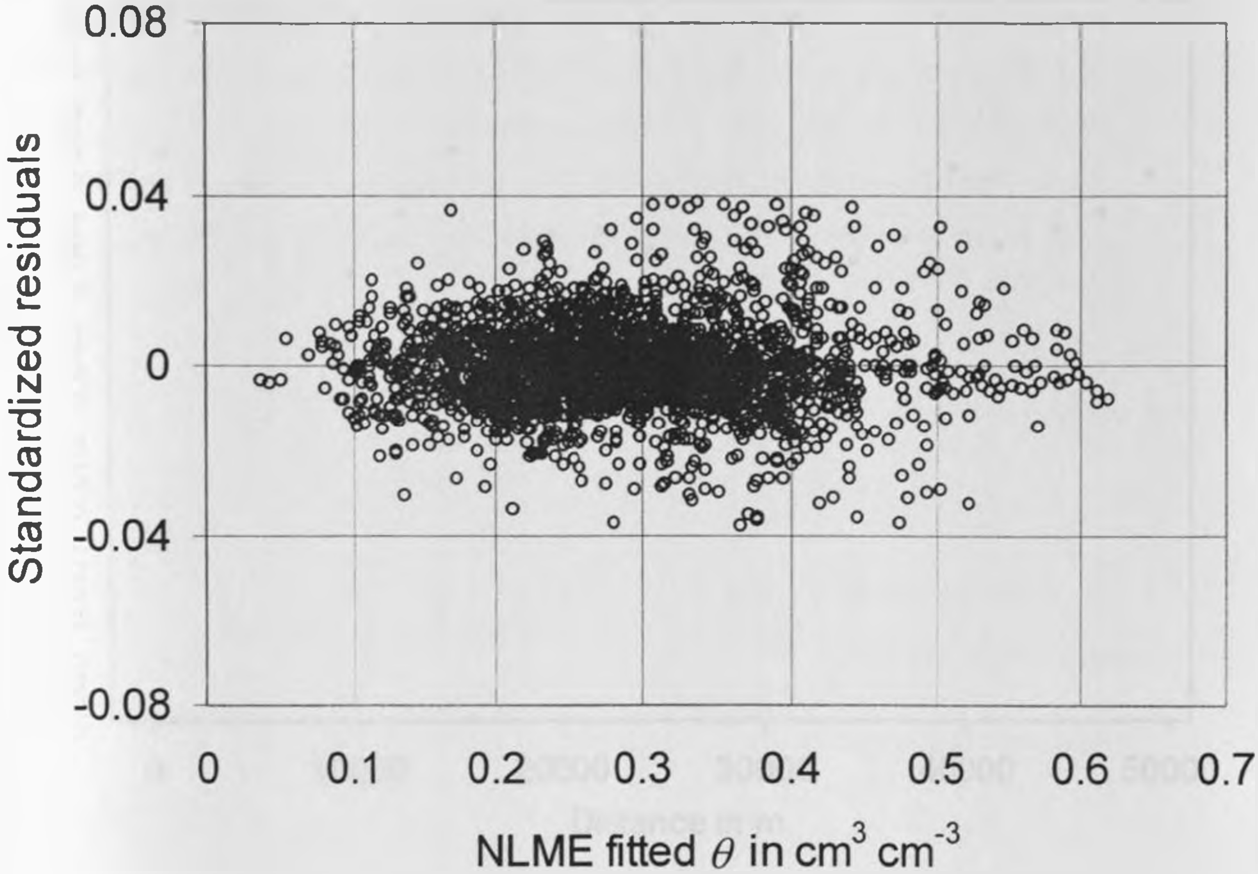

Figure 4.8. Scatter plot of the standardized residuals versus the NLME fit of the van Genuchten model

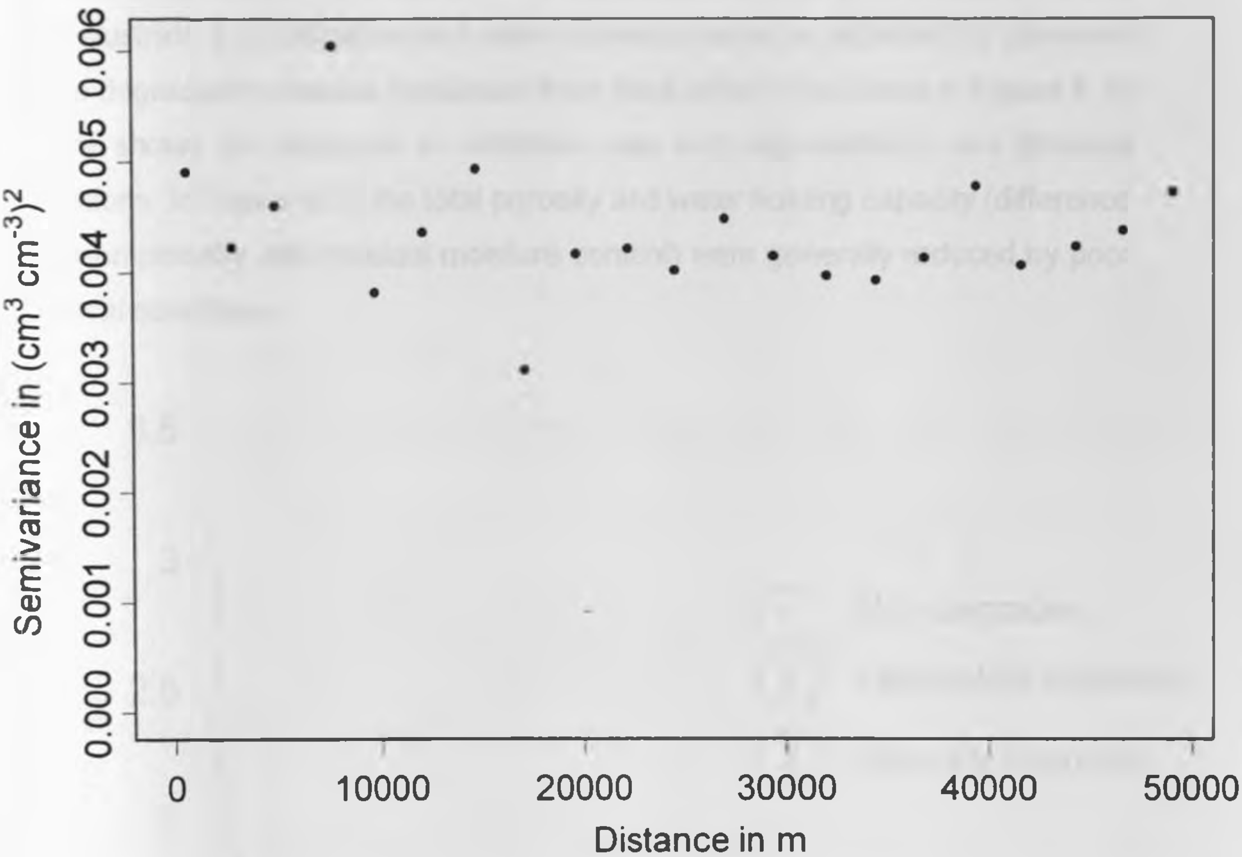

Figure 4.9. Spatial correlation of the NLME residuals

4.1.2 Adding visual physical degradation classes as covariate

Adding visual soil physical degradation classes as a covariate did not reduce the magnitude of the residuals compared with Table 4.4, but substantially reduced the standard error of residuals. This indicates that additional between-sample variability in soil physical properties was accounted for by the soil degradation classes. Further analysis of variance of the final NLME output showed that all of the estimated hydraulic parameters were significantly affected by visual degradation classes (at 5% significance level) except for the residual moisture content θ_r. The effect of the physical condition on pore-size distribution index *n* was marginal (p=0.057) at this level of significance (Table 4.5). Figure 4.10 and 4.11 illustrate the infiltration and water retention curve as affected by observed visual degradation classes (predicted from fixed effect). The curve in Figure 4.10 clearly shows the reduction in infiltration rate with degradation in soil physical conditions. In Figure 4.11 the total porosity and water holding capacity (difference between porosity and residual moisture content) were generally reduced by poor physical conditions.

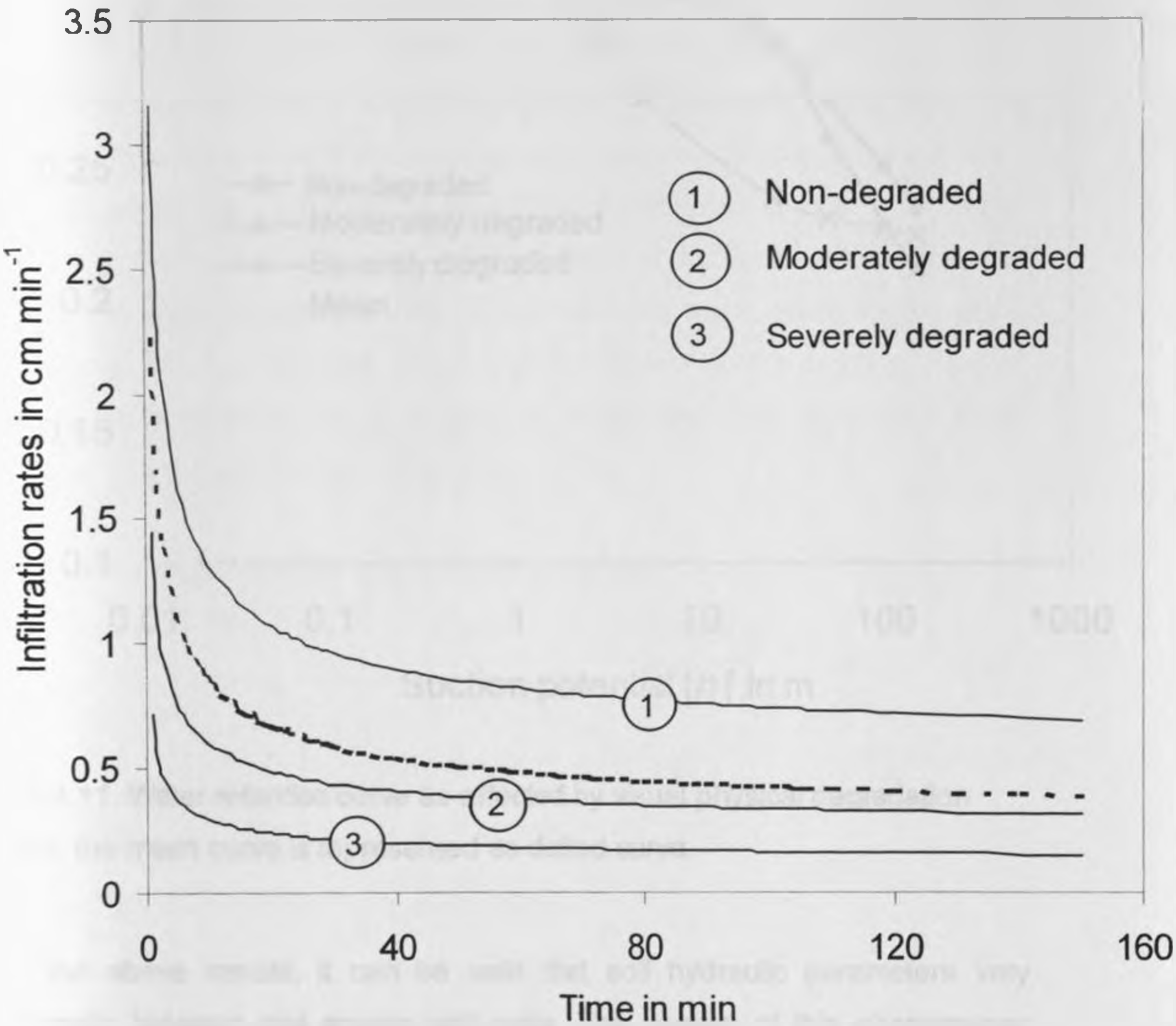

Figure 4.10. Infiltration rate as affected by observed soil degradation classes, the mean curve is represented as dotted curve.

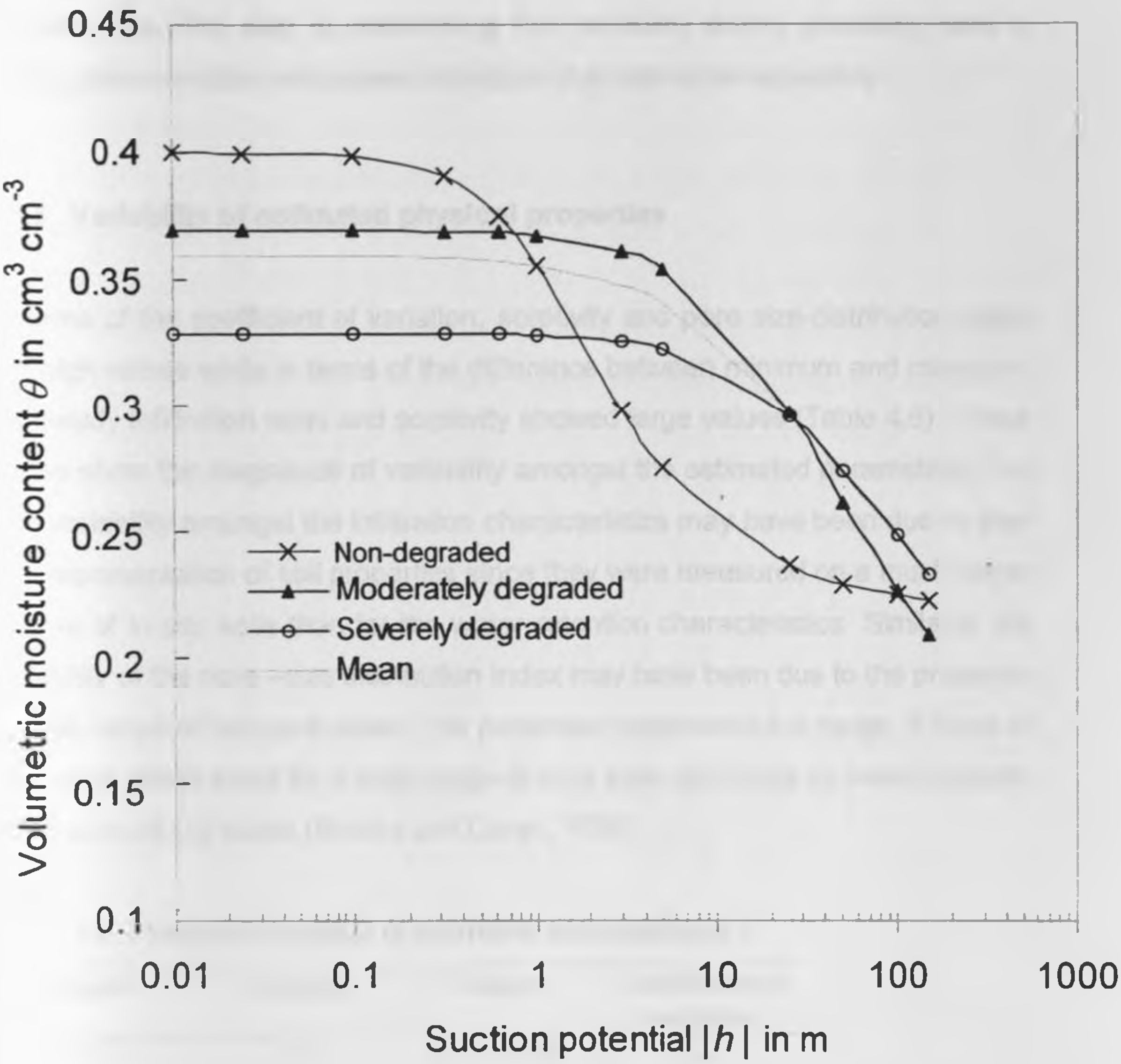

Figure 4.11. Water retention curve as affected by visual physical degradation classes, the mean curve is represented as dotted curve.

From the above results, it can be said that soil hydraulic parameters vary significantly between and among soil units. The neglect of this phenomenon during modelling of the functional soil processes can lead to serious errors as seen with the case of NLS hydraulic parameter estimation in this study. A large part of the inflated unidentified variability in the parameter estimation with NLS strategy was due to the inclusion of individual differences in the estimation process. One first step in overcoming this variability during modelling was to stratify point samples and assess individual characteristics separately.

4.1.3 Variability of estimated physical properties

In terms of the coefficient of variation, sorptivity and pore size-distribution index had high values while in terms of the difference between minimum and maximum the steady infiltration rates and sorptivity showed large values (Table 4.6). These values show the magnitude of variability amongst the estimated parameters. The high variability amongst the infiltration characteristics may have been due to their bulk representation of soil properties since they were measured on a much larger volume of in-situ soils than for the water retention characteristics. Similarly, the variability of the pore –size distribution index may have been due to the presence of wide range of soil pore sizes. This parameter represents the range of sizes of soil pores: being small for a wide range of pore sizes and large for nearly uniform distribution of soil pores (Brooks and Corey, 1964)

Table 4.6. Plot-level averages of estimated soil properties

Parameter	Average	Range	Coefficient of variation
f_c (cm hr^{-1})	4.1	21.3 – 0.40	5.1
S (cm hr$^{-0.5}$)	6.6	20.7 – 4.0	42
θ_s (cm^3 cm^{-3})	0.36	0.57 – 0.14	25
θ_r (cm^3 cm^{-3})	0.16	0.1 – 0.06	37
α (m^{-1})	2.41	0.8 – 0.003	28
ρ (g cm^{-3})	1.29	1.71 – 0.86	17
n	1.39	1.96 – 1.03	84

4.1.4 Soil spectral reflectance

Soils in the study area had similar spectral characteristics to those reported by other researchers (Shepherd *et al.*, 2003): low reflectance in the visible range (350-700 nm), high reflectance around 1800 nm, and three significant absorption features at 1420 nm, 1920 nm, and 2210 nm (Figure 4.10). In addition, most soils displayed a duplet feature at the 1420 nm and 2210 nm with asymmetric left shift (Figure 4.12). The 2210 nm duplet is characteristic of kaolinitic clays (Raggatt et al., 2004). Weathered soils have been shown to have a relatively stable soil physical structure and strong micro-aggregation due to binding from iron oxides (West *et al.*, 2004).

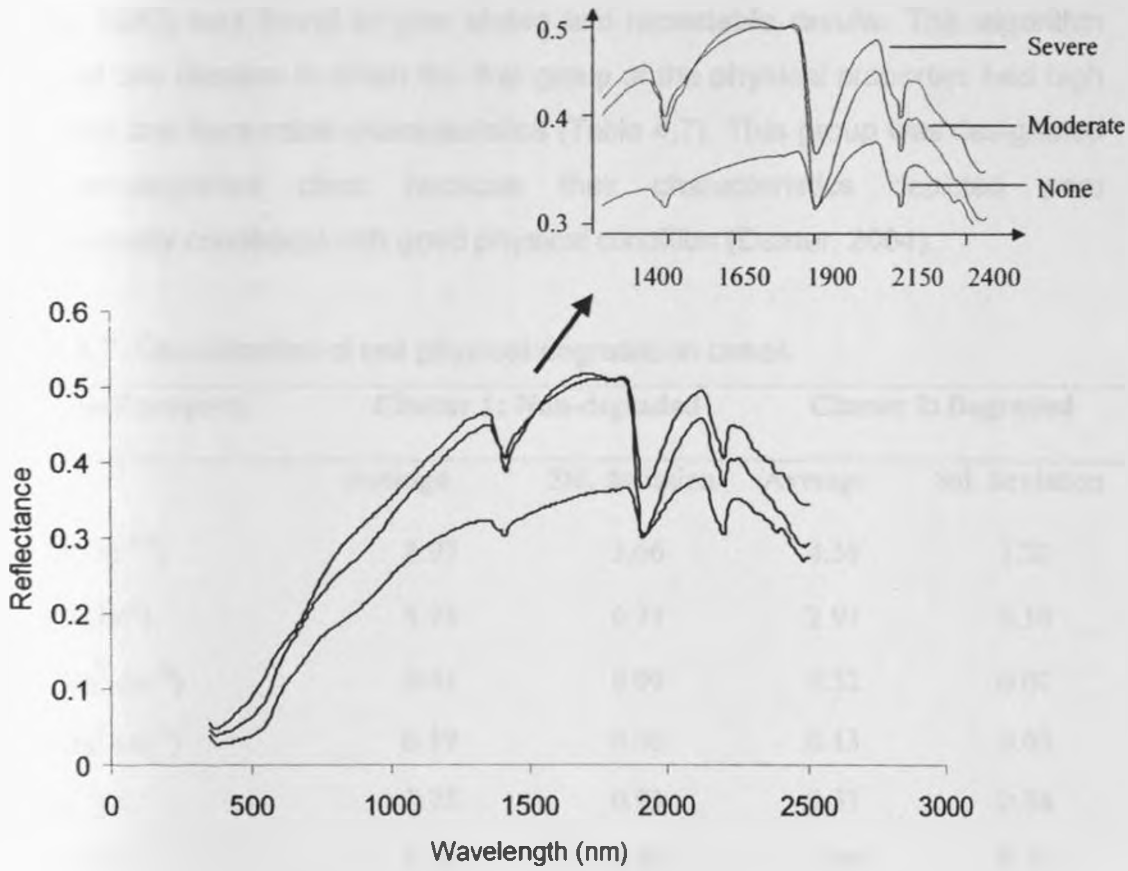

Figure 4.12. Average soil spectral reflectance for the visual physical degradation classes

4.2 Case-definition of soil physical degradation

The marginal distributions of the standardized physical properties appeared normal with the possible exception of three sampling plots. These plots were treated as multivariate outliers since their $\chi^2_7(0.005)$ were greater than 20.28; yet all other individual measurements were well within their respective univariate scatters. Further examination of these three plots showed they came from shallow soils with variable depths. They had the highest infiltration characteristics while samples for water retention characteristics revealed presence of stones. Therefore they were omitted from the analysis.

After testing numerous algorithms, the fuzzy cluster algorithm (Venebles & Ripley, 1992) was found to give stable and repeatable results. This algorithm revealed two clusters in which the first group of the physical properties had high variability and favourable characteristics (Table 4.7). This group was designated the non-degraded class because their characteristics depicted pore heterogeneity consistent with good physical condition (Dexter, 2004).

Table 4.7. Classification of soil physical degradation cases

Soil property	Cluster 1: Non-degraded		Cluster 2: Degraded	
	Average	Std. deviation	Average	Std. deviation
S (cm hr$^{-0.5}$)	8.97	3.66	4.58	1.20
f_c (cm hr^{-1})	5.74	0.27	2.97	0.10
θ_s (cm^3 cm^{-3})	0.41	0.09	0.32	0.07
θ_r (cm^3 cm^{-3})	0.19	0.06	0.13	0.03
α (m^{-1})	2.25	0.93	2.53	0.36
ρ (g cm^{-3})	1.30	0.20	1.46	0.12
n	1.42	1.26	1.18	0.07

A ten-fold cross-validated exploratory tree analysis of the soil physical degradation clusters with soil physical properties showed that pore-size distribution index was the most significant variable during the clustering (Figure 4.13). This parameter is important since it represents the range of pores that provide key pathways for exchange of water and gases in the soil. A high value of pore-size distribution index is an indication of poor physical condition while low values indicate good physical condition. Therefore, in diagnosing soil physical degradation, pore-size distribution index higher than a certain value (for example, 1.31 in upper Athi watershed) could signify degraded soils. However, when the value is higher than this limit the possibility of degradation could be discerned by testing for infiltration characteristics and water holding capacity (θ_s and θ_r). The steady infiltration rate f_c appears to be the ultimate discriminator of degraded from non-degraded soils since it is invariably the parameter that separates the groups in the terminal nodes (Figure 4.13).

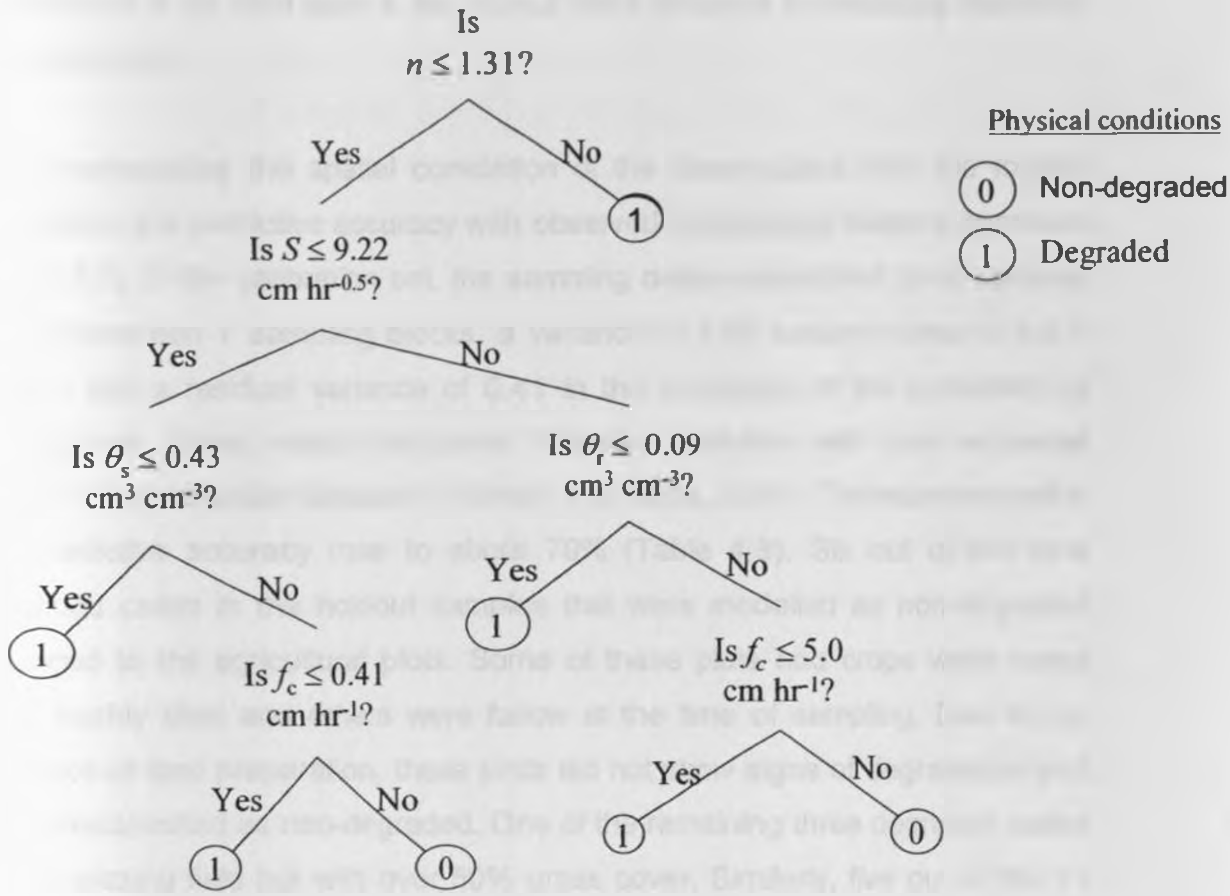

Figure 4.13. Exploratory tree of the physical properties for case-definition of degradation

4.3 Screening soils for physical degradation

The comparison of cluster groups based on physical properties with the groups from visible features revealed that of the 81 cases grouped by cluster analysis as non-degraded 27 cases were in class E0, 48 cases in class E1, and six cases in class E2 while of the 99 degraded cases 14 cases in class were E0, 59 cases in class E1, and 26 cases in class E2. This simple comparison gave 33% sensitivity and 27% specificity of observable features in predicting soil physical conditions. Thus, without considering spatial correlations the observed features of degradation in the field gave a low (about 30%) accuracy in predicting likelihood of degradation.

After incorporating the spatial correlation of the observations from the logistic regression, the predictive accuracy with observed degradation features improved (Table 4.8). In the calibration set, the sampling design accounted for a variance of 1.97 between Y sampling blocks, a variance of 1.87 between plots in the Y blocks, and a residual variance of 0.41 in the prediction of the probability of degradation. These spatial structures however modelled with zero expected values in the validation datasets (Pinheiro and Bates, 2000). The improvement in the predictive accuracy rose to about 70% (Table 4.8). Six out of the nine degraded cases in the holdout samples that were modelled as non-degraded belonged to the agricultural plots. Some of these plots had crops while some were freshly tilled and others were fallow at the time of sampling. Due to the influence of land preparation, these plots did not show signs of degradation and were misclassified as non-degraded. One of the remaining three degraded cases was a grazing field but with over 50% grass cover. Similarly, five out of the 11 non-degraded cases that were modelled as degraded belonged to the shrubland of the savannah type of vegetation. These plots seemed degraded due to their scanty vegetation cover. Two plots of the remaining six cases non-degraded cases came from low-lying plains with predominant clayey soils.

Table 4.8. Confusion matrix with observed degradation features

	Calibration set				**Validation set**		
	Model predictions				Model predictions		
Observed clusters	Non-degraded	Degraded	Total	Observed clusters	Non-degraded	Degraded	Total
Non-degraded	36	14	50	Non-degraded	19	12	31
Degraded	19	51	70	Degraded	9	20	29
Sensitivity = 73% and specificity =72%				Sensitivity = 69% and specificity =61%			

The exploratory analysis of the spectral reflectance showed the following wavebands to be significantly correlated with degradation classes, in order of importance: 2320, 950, 1020, 1010, 2400, 1000, 2310, 2090, 2110, 2100, 1030 nm. The mixed effects logistic model developed with these wavebands correctly classified 23 cases out of the 31 non-degraded case in the holdout samples and also correctly classified 19 out of the 29 degraded cases. Similarly, out of the seven principal components from the spectra model developed, only four were found to be significantly correlated with degradation classes and included: the first component (explaining 53% in spectral variation), second component (27%), fifth (4%), and seventh component (explaining 1%). The model developed with the principal components did not correctly classify any non-degraded samples while it correctly classified 27 cases out of the 29 degraded cases of the holdout samples. From these analyses, the selected spectral wavebands performed better than the principal components and were included in the mixed effects model. The model gave an overall accuracy of about 94% (Table 4.9). The variance between Y blocks reduced to 1.38, between plots in the blocks had variance of 1.03, and the residual variance in the estimation of probability of degradation was 0.01.

Table 4.9. Confusion matrix of the classification model with spectra and observed degradation features

Calibration set				**Validation set**			
	Model predictions				Model predictions		
Observed clusters	Non-degraded	Degraded	Total	Observed clusters	Non-degraded	Degraded	Total
Non-degraded	47	3	50	Non-degraded	28	3	31
Degraded	2	68	70	Degraded	2	27	29
Sensitivity = 97% and specificity =94%				Sensitivity = 93% and specificity =90%			

The incorporation of soil spectra into the predictive model helped to identify the seven plots that were previously misclassified as non-degraded. Although these plots did not have observable degradation features, they were identified by the spectra as degraded. Therefore, they could be regarded as coming from sites with emerging signs of degradation. In this respect, the spectral reflectance acted as an early-warning indicator of degradation that would otherwise not have been apparent from visual observations above. Similarly, the inclusion of soil spectral reflectance in the predictive model resolved the eight non-degraded cases that were visibly classified as degraded thereby increasing the predictive accuracy by over 20%. There would be no need to continue to the final step of using measured soil physical properties to assign a site to a degradation case or reference (see Figure 3.4).

4.4 Spatial interpolation of probability of physical degradation

The soil spectral reflectance for other plots (without measured physical properties) was then run down the tree model to predict their degradation characteristics. Both the topsoil and subsoil spectra were used to predict their physical degradation cases as either being non-degraded or moderately degraded or severely degraded. Figure 4.14 shows the spatial variation of the interpolated probabilities of soil physical degradation at 1 km-resolution using inverse weighted average (ERDAS, LLC, 2002). Much of the northern parts of the study area showed sever degradation in both the topsoil and subsoil while the southern and western parts showed severe degradation in the topsoil only.

An overlay of Figure 4.14 with soil types indicated soils in the western parts to be predominantly developed from silt-rich schist with saline phase Vertisols. According to Valentine and Bresson (1992), silty soils developed from schists generally presents severe problems of crusting especially with low pH content. Therefore, the pattern shown in the western parts of the study area could be attributed to surface crusting. Previous study in selected points in these areas show that the soils have high silt and sand content, very low soil carbon, and high exchangeable potassium ions in the topsoils (Ellenkamp, 2004).

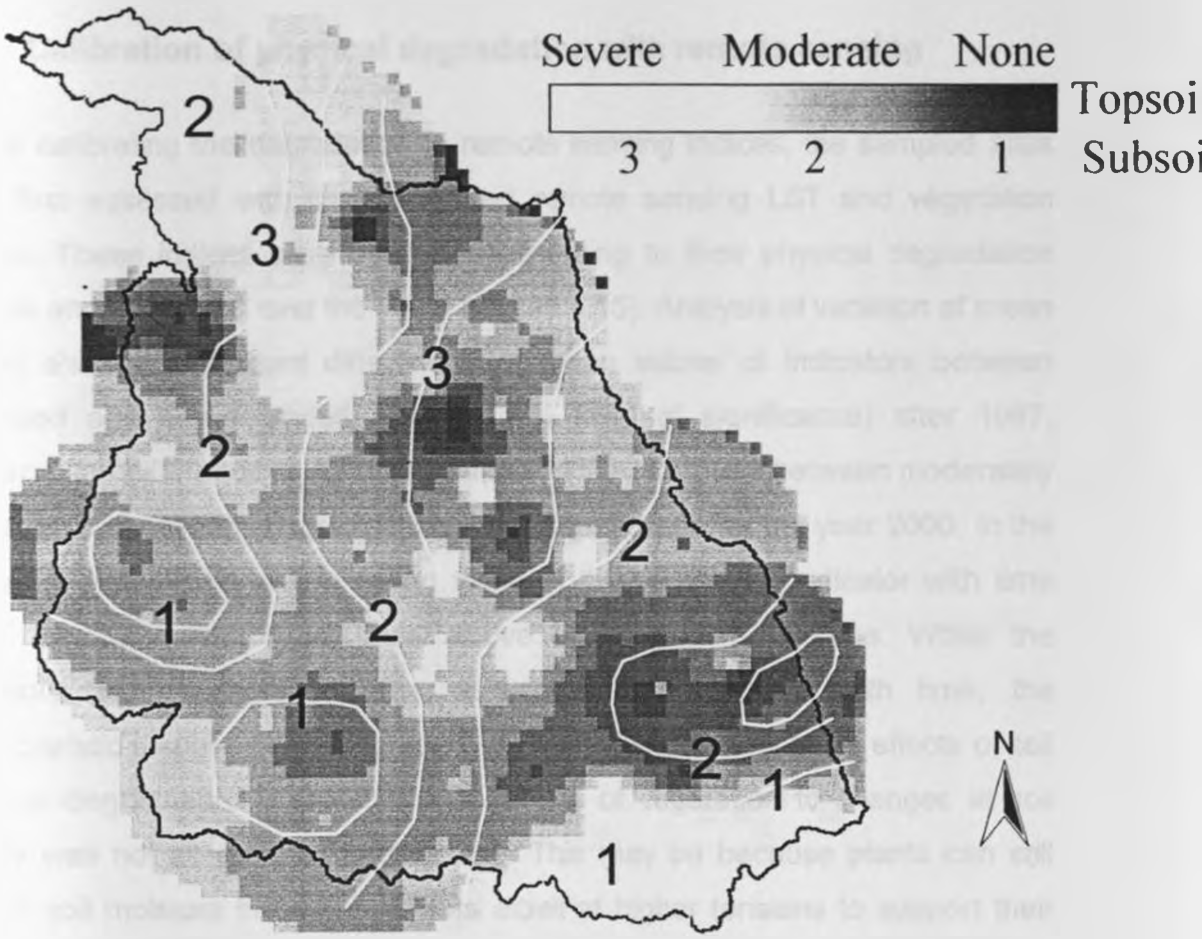

Figure 4.14. Variation of soil physical degradation in the study area. Contour lines show probability of degradation in the subsoil in which 1 : < 0.25, 2: 0.25-0.75, and 3: > 0.75.

In the south-eastern parts, much of the degradation in the subsoils was associated with sedimentation since it is where most of the rivers from the study area converge. The overburden and repacking of sediments from uplands could undermine the physical characteristics of the soils (Horn *et al.* 1995). In the central part of the study area, soils that showed degradation in the subsoils only were mainly associated with agricultural plots. The fertilization of these plots with potassium and effects of cultivation could have caused compaction in the subsoils (Auerswald *et al.* 1996).

4.5 Calibration of physical degradation with remote sensing

Before calibrating the degradation to remote sensing indices, the sampled sites were first assessed with time-integrated remote sensing LST and vegetation indices. These indices were averaged according to their physical degradation classes and compared over the years (Figure 4.15). Analysis of variation of mean values showed significant differences of mean values of indicators between degraded and non-degraded sites (at 5% level of significance) after 1987. Similarly, the difference of the mean values of the indicators between moderately degraded and severely degraded sites was significant after the year 2000. In the degraded sites, there was a falling trend of the vegetation indicator with time while thermal indicator oscillated above the long-term average. While the variations in non-degraded sites remained fairly constant with time, the characteristic response from degraded sites showed the cumulative effects of soil physical degradation. However, the response of vegetation to changes in soil quality was not as rapid as that of LST. This may be because plants can still extract soil moisture in degraded plots albeit at higher tensions to support their development.

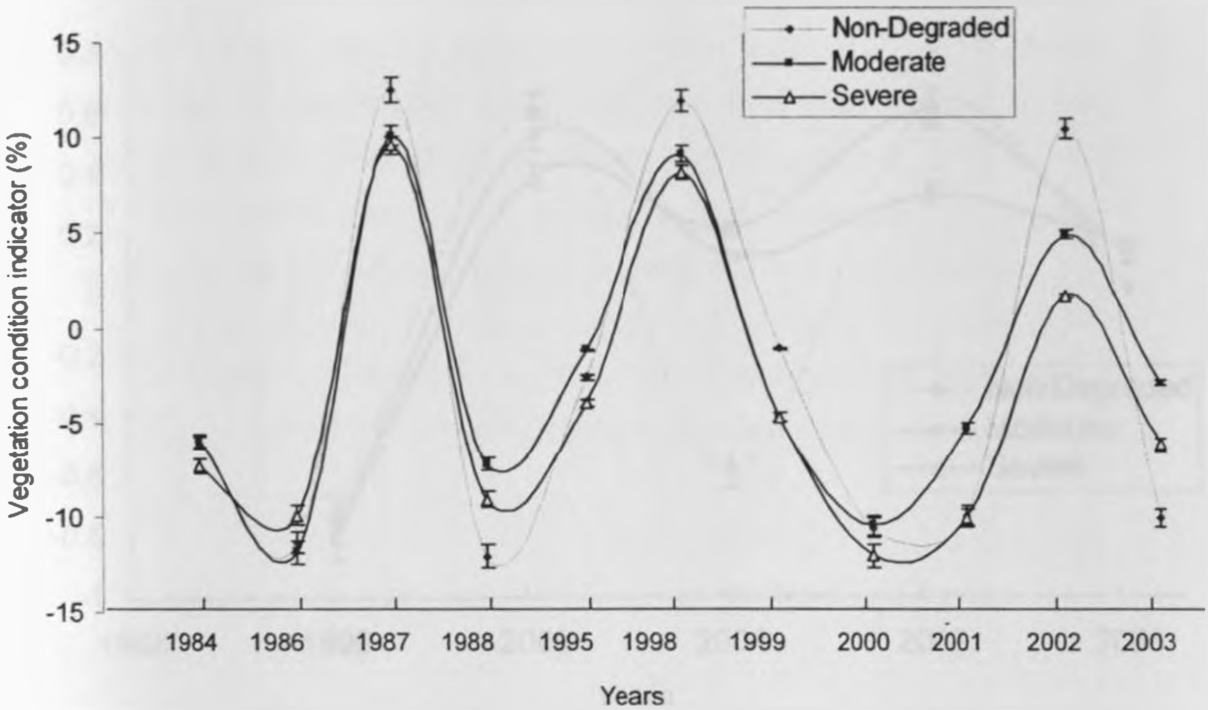

Figure 4.15a. Historic changes in vegetation condition at sampled sites, vertical bars shows standard error of means

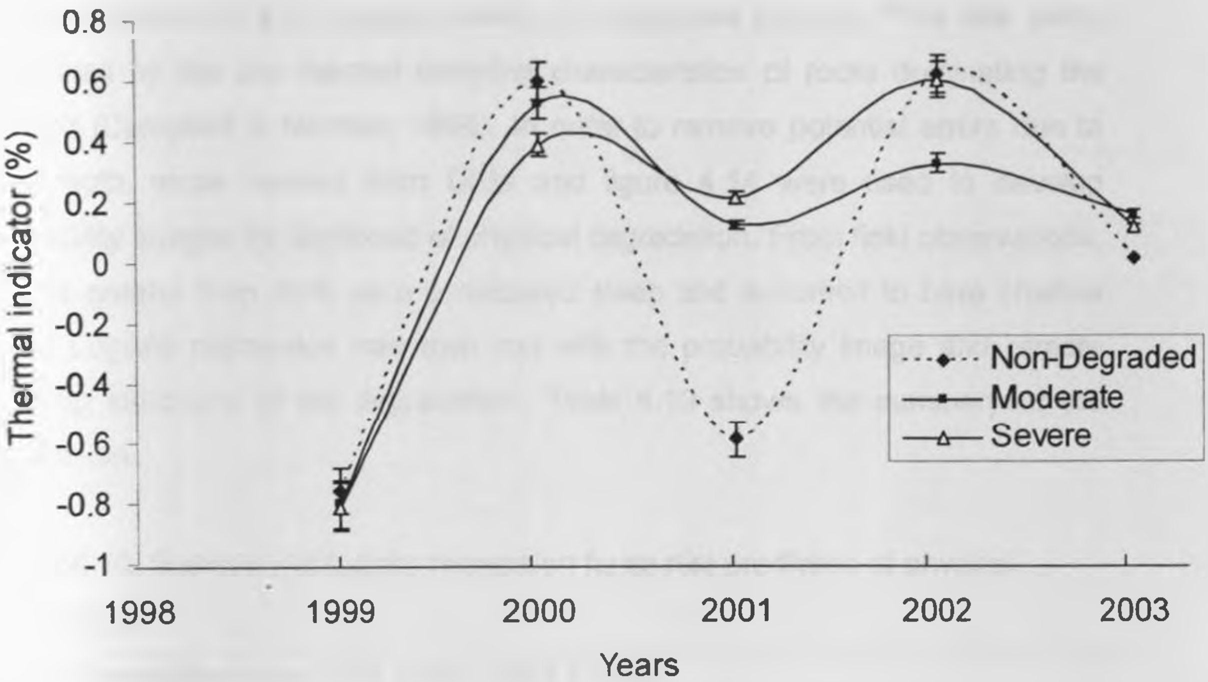

Figure 4.15b. Historic changes in LST at sampled sites, vertical bars shows standard error of means

Further analysis of each case showed the degraded sites had large deviations from mean values with largest amplitude amongst cases of severe degradation in the profile and least deviations amongst cases of severe degradation in the topsoil only. Although there were no clear records for particular times at which land use patterns changed, the majority of the cases with large deviations were reported to have undergone multiple changes in land use in the last decades (Tiffen *et al.*, 1994). From Figure 4.15, around the 2001 and 2002, remarkable changes started emerging between sites according to their soil physical conditions. If land use changes occurred a few years before these times, then it could be said that unsustainable land use changes triggered soil physical degradation.

A few places that had shallow soils (especially in steep slopes) also showed very large deviations of LST despite having non-degraded topsoils. This was partly explained by the low thermal damping characteristics of rocks dominating the subsoil (Campbell & Norman, 1998). In order to remove potential errors due to soil depth, slope derived from DEM and figure 4.14 were used to develop probability images for likelihood of physical degradation. From field observations, slopes greater than 20% were considered steep and assumed to have shallow soils. Logistic regression was then run with the probability image and remote sensing indicators of the degradation. Table 4.10 shows the summary of the regression.

Table 4.10. Summary of logistic regression for spatial prediction of physical degradation

Logit(degradation)=a + bP1 + cP2+ dP3 + error		
Variable	**Estimated coefficient**	**t –test (d.f =103891)**
	Intercept, a = -1.0568	-1025
Probability image, P1	b = 0.015	70.52
Vegetation indicator, P2	c = -0.016	4.12
Thermal indicator, P3	d = 0.125	3.98
Apparent R = 0.82 and apparent R squared = 0.67		
Adjusted R = 0.75 and adjusted R squared = 0.56		

Since the logit transformation linearizes the model so that the dependent variable of the regression is continuous in the range of 0 and 1, the equation and the summary statistics relate to the transformed linear regression. Furthermore, when images are regressed, there is need to note that spatial correlation exists between neighbouring pixels so that the valid sample size and degrees of freedom are not realistic. Therefore, the summary statistics in table 4.10 are not very good indicators of goodness of fit (ERDAS, LLC, 2002). The appropriate statistics can therefore be developed from ground truthing using classification matrix. Figure 4.16 shows the resultant combination of the output of each logistic regression for the three degradation classes.

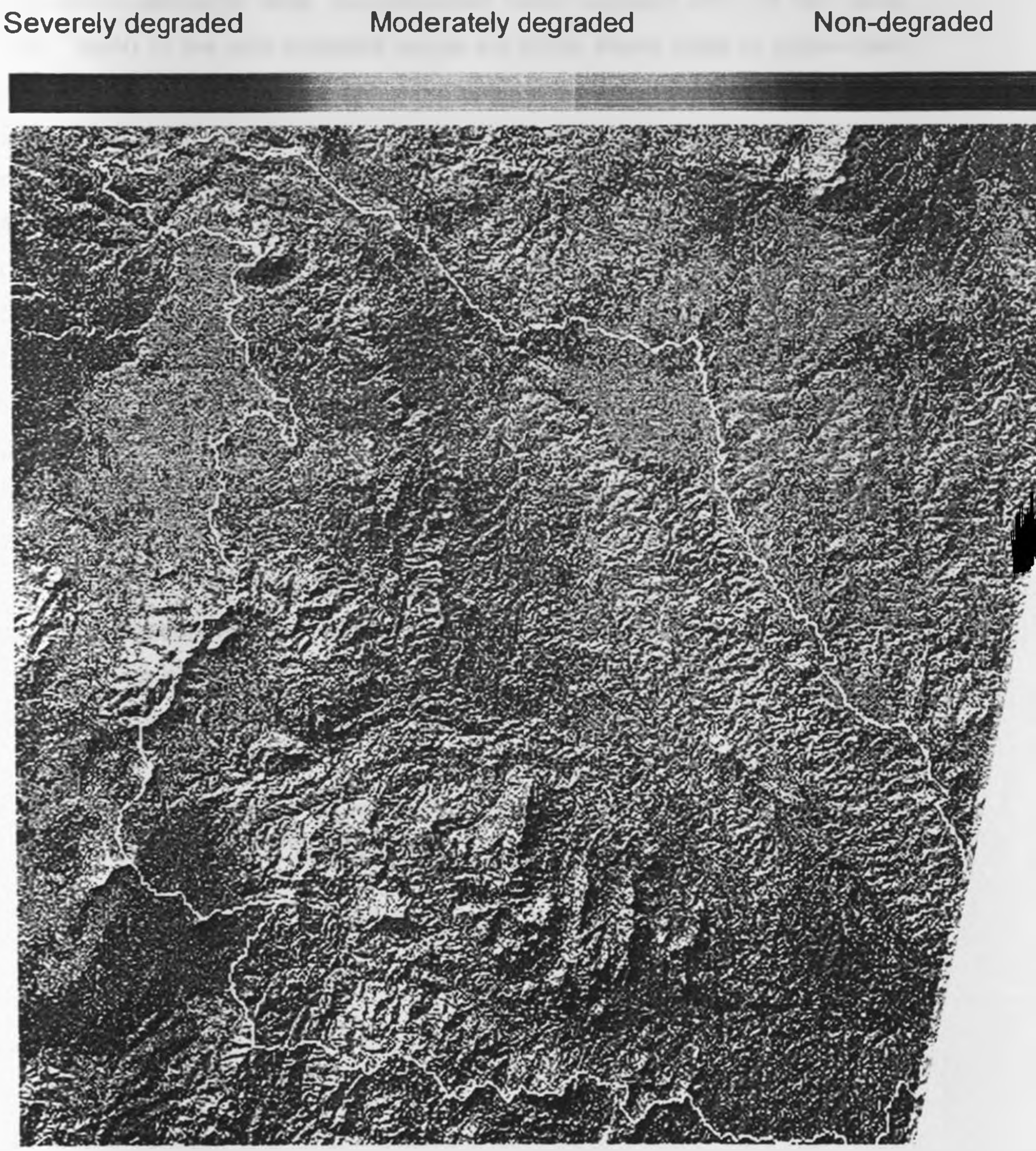

Figure 4.16. Spatial prediction of soil physical degradation

In the whole scene in Figure 4.16, 28% of the total area were had severe degradation with majority of the cases in fragile soils prone to crusting and hardsetting soils. Moderately degraded areas dominate the scene with 58% of total scene coverage while non-degraded sites occupied 20% of the whole scene. Much of the non-degraded areas are within intact forest or government protected woodlots, however with increasing population pressure (Tiffen *et al.* 1994) these areas may soon be converted to other unsustainable land use types and contributing to the problems of soil physical degradation. The predicted degradation cases of Figure 4.16 at 30 points randomly selected within the study area were checked with ground references to determine the predictive accuracy of the remote sensing approach (Table 4.11). The overall predictive accuracy of 80% achieved with remote sensing was considered very good even though lower than that of diffuse spectral reflectance. The loss of predictive accuracy compared to DSR was attributed to the lower spatial resolution. Ground sampling was done at 30-m resolution while remote sensing data were at 60-m. In addition, there was lack of complete unmixing of vegetation from soil background in the thermal remote sensing. Despite the limitations, the overall predictive accuracy was believed to be sufficient for large-area assessment protocols. The relatively high producer accuracy for moderately degraded sites is encouraging for early warning of soil physical degradation.

Table 4.11. Error matrix for the remotely predicted soil physical degradation

Group by classified by soil physical properties	Group predicted by remote sensing			Row total	User accuracy (%)
	None	Moderate	Severe		
Non-degraded	6	0	2	8	75
Moderately degraded	1	11	0	12	92
Severely degraded	0	3	7	10	70
Column total	7	14	9		
Producer accuracy (%)	86	79	78		

CHAPTER FIVE

5. CONCLUSIONS AND RECOMMENDATIONS

5.1 Conclusions

The broad objective of this study was to develop a rapid protocol for assessing soil physical degradation in the large areas of arid and semi-arid land with specific applications in Eastern Kenya. This study has shown the promise in using a combined application of visual assessment of the degradation features, soil physical properties, soil diffuse spectral reflectance, and GIS and remote sensing for rapid characterization of the degradation in a large watershed. A major contribution of this study was the use of appropriate soil physical properties to derive a case-definition of physical degradation and subsequent use of the case-definitions to diagnose the degradation. Rapid large-are screening was made possible through the use of DSR, GIS, and remote sensing. The main conclusions are summarized in this chapter.

5.1.1 Soil properties that index physical degradation

Soil physical degradation adversely affects both the structural and textural pore characteristics. Since these characteristics are directly related to physical quality such as infiltration and water retention, the infiltration and water retention characteristics were used to index soil degradation. Specifically, these soil properties were found to be able to distinguish between soils with different visible signs of physical degradation and included that include f_c, S, θ_{s1}, θ_{s2}, θ_r, α_1, α_2, ρ_b. Among these properties, infiltration characteristics (f_c and S) were found to provide the most indicative indices for differentiating non-degraded soils from soils with visual signs of degradation and to be sensitive enough to be useful in assessing early development of physical degradation. Some of the water retention characteristics, such as the pore-distribution index and alpha parameter, were also found to be important in assessing severe degradation from moderately degraded soils. These properties are indicative of the increase in soil textural pore spaces that occurs when severe degradation develops into erosion.

The soil physical properties above can be accurately established from water retention and infiltration tests by using nonlinear mixed effects modelling of infiltration and retention functions commonly reported in literature. When based on well-designed ground survey to capture the main variability in soil characteristics in an area, NLME was shown to provide a reliable approach for parameter estimation in which important covariates and geographic continuities could be included to improve the estimation process. This study showed that a combination of spatially explicit ground survey including simple infiltration and water retention tests at spatially and randomly stratified sites, NLME and cluster analysis of NLME estimates can be used to define cases of soil physical degradation.

5.1.2 Case-definition and screening of soil physical degradation

A case-definition protocol was developed that takes evidence of degradation from visible assessment, simple tests based on soil spectral reflectance, and more elaborate and expensive tests based on soil physical properties. The protocol proposed the use of visible assessments to identify obvious degradation cases in the field. However, cases that were not obvious were further screened using rapid and simple methods based on soil spectral reflectance. Soil spectral reflectance, which integrates information on many soil properties, facilitated early identification of cases of soil physical degradation and provided a powerful tool for early interventions and targeting interventions. Soil reflectance, which is cheap and easy to measure and therefore permits high sampling densities over large areas, can allow rapid screening of whole-basins and aid decision-making on soil management. The accuracy of the sequential screening of visual followed by spectral tests was very high (sensitivity of 93% and specificity of 90% on holdout samples) so that further screening using measured soil physical properties may not be needed.

5.1.3 Calibration of physical degradation to remote sensing indices

Soil physical degradation is a gradual process that may not be visibly detected in the field for a number of years. However, during its development it negatively influences land surface temperature and vegetation growth conditions. The standardized deviations of land surface temperature (LST) and NDVI from long-term Landsat scenes were used to study the thermal and vegetation conditions of the degradation at sampled points. It was shown that progressive decline in vegetation vigour and simultaneous increase in land surface temperature could be linked to soil physical degradation. These time-integrated indices effectively predicted the likelihood of the degradation at other places (with an average accuracy of 80%). This approach showed promising opportunity for spatial prediction of physical degradation at high spatial resolutions (30 m).

The approach of combining point-measurements with spectral reflectance and remote sensing has the important implication of early detection of soil physical degradation at high spatial and temporal resolution in a way that can expedite effective monitoring and prevention of degradation. Especially if used with high temporal resolution imagery, the approach demonstrated in this study can be used to guide policy decisions for sustainable management of the environment.

5.2 Recommendations

5.2.1 Recommendations from the study

It is recommended that the methods developed from this study be tested in other parts of Kenya to confirm and extend the models developed.
Since some of the major beneficiaries of the outputs of this study may be policy decision-making on land use, it is recommended that the outputs in this study be used in scenario developments for finding the best alternatives for land management.

5.2.2 Recommendations for further research

Although soil degradation considered in this study had bias towards physical degradation, a more holistic approach considering physical, chemical, and biological degradation is needed since they are often interrelated and together determine soil production and environmental functions. In addition, some other recommendations for further research are needed as suggested below.

5.2.3 Soil properties for defining physical degradation cases

Although soil infiltration and retention characteristics are good indicators of physical degradation, other properties that also link chemical properties like sodium absorption ratio, stable aggregates, and electrical conductivity should be tested for their usefulness in providing case-definitions of physical degradation.
The soil properties were estimated from the two parameter infiltration function proposed by Philip's and the water retention function proposed by van Genuchten. However, other simpler functions have been found to perform equally well in fitting to experimental data and alternative functions should be tested for any improvement.

5.2.4 Soil spectral reflectance and calibration with degradation cases

The soil spectral reflectance range tested in this study was the visible-near infrared region (350 nm to 2500 nm). However, recent developments in soil spectroscopy have shown more stable in soil spectral calibrations across sites with mid-infrared spectral reflectance and is alternative could be tested.

The direct calibration of spectral reflectance with soil physical properties was not tested. There are other calibration methods that can optimize calibrations between spectral reflectance and soil properties in a way that can expedite co-kriging of physical degradation in small watersheds.

Soil spectra differ with regions and geological settings and so the methods developed here should be tested in other watersheds to ensure that they are equally useful on other soil types.

5.2.5 Remote sensing applications

The methods used for processing remote sensing images in this study were approximations and other methods could be tried with combination of high temporal resolution and high spatial resolution images for near-real time monitoring of degradation.

The alternatives of calibrating soil physical degradation directly to Landsat spectral bands as opposed to use of NDVI and LST should be tested.

The synergistic use of high temporal but low spatial resolution imagery and low temporal and high spatial resolution imagery has gained popularity in remote sensing applications. Sampling strategies combining both types of imagery should be developed.

REFERENCES

Agassi, M., Shainberg, I., Morin, J., 1981. Infiltration and runoff in wheat fields in the semi-arid regions of Israel. *Geoderma, 36*, 263-276.

Alegre, J.C., Cassel, D.K., 1986. Effect of land clearing methods and postclearing management on aggregate stability and organic carbon content of a soil in the humid tropics. *Soil Science, 142*, 289-295.

Analytical Spectral Devices Inc. 1997. *FieldSpec™ user's guide*, Boulder, CO, Analytical Spectral Devices Inc.

Atzberger, C., 2002. *Soil optical properties – A Review*. Remote Sensing Report, D-54286 Tier, Germany.

Auerswald, K., Kainz, M., Angermuller, S., Steindl, H., 1996. Influence of exchangeable potassium on soil erodibility. *Soil Use and Management, 12*, 117-121.

Ayers, R.S., Westcot, D.W., 1985. *Water quality for agriculture*. FAO Irrigation and Drainage, Paper 29, Rome, Italy.

Baker, B.H., 1952. *Geology of the Southern Machakos District (degree sheet 52 S.W.)*, Geological Survey of Kenya, Ministry of Natural Resources, Government of Kenya.

Ball, B.C., Campbell, D.J., Douglas, J.T., Henshall, J.K., O'Sullivan, M.F., 1997. Soil structural quality, compaction and land management. *European Journal of Soil Science, 48*, 593-601.

Baumgardner, M.F., Silva, L.F., Biehl, L.L., Stoner, E.R., 1985. Reflectance properties of soils. *Advances in Agronomy, 38*, 1-44.

Bazzofi, P., 2002. *Impacts of human activities on soil loss: direct and indirect evaluation*. In: Pagliai, M., Jones, R. (Eds), Sustainable Land Management-Environmental Protection- A soil Physical Approach. Advances in AgroEcology, vol 35. Catena-Verlag, Reiskirchen, pp. 429-442. 598 pp.

Ben-Dor, E., Goldlshleger, N., Benyamini, Y., Agassi, M., Blumberg, D.G., 2003. The spectral reflectance properties of soil structural crusts in the 1.2- to 2.5μm spectral region. *Soil Science Society of America Journal, 67*, 289-299.

Ben-Dor, E., Irons, J.R., Epema, G.F., 1999. *Soil reflectance*. In N. Rencz (Ed.), Remote sensing for the earth sciences: Manual of remote sensing. Vol. 3. (pp. 111-118), John Wiley and Sons, New York.

Ben-Dor E., Benin, A. 1990. Diffuse reflectance spectra of smectite minerals in the near infrared and their relation to chemical composition. *Science of Geology Bulletin, 43(2-4)*, 117-128.

Blum, H.P., Eger, H., Fleischhauer, E., Hebel, A., Reij, C., Steiner, K.G., 1998. *Towards sustainable land use: Furthering cooperation between people and institutions*. Advances in AgroEcology, vol. 31. Catena-Verlag, Reiskirchen.

Blume, E. H. W., 1998. *Basic concepts: Degradation, resilience, and rehabilitation*. In Lal, R., Blume, W.H, Valentine, C. and Stewart, B.A. (Eds). methods for assessment of soil degradation, CRC.

Brady, N.C., Weill, P.R., 2002. *The nature and properties of soils*, (pp. 206 – 210). Prentice-Hall, Upper Saddle River.

Breuer, J., Schwertman, U., 1999. Changes to hardsetting properties of soil by addition of metal hydroxides. *European Journal of Soil Science, 50*, 657-664.

Brieman, L.J., Friedman, J., Stone, C.J., Olshen, R.A.,. 1984. *Classification and regression trees*. (pp. 358), Boca Raton, FL: CRC Press.

Brooks, R.H. and Corey, A.T. (1964). Hydraulic properties of porous medium. Colorado State University (Fort Collins), Hydrology paper, Nr. 3. March.

Brus, D.J. and DE Gruijter, J.J. (1997). Random sampling or geostatistical modeling? Choosing between design-based and model-based sampling strategies for soil (With discussions). *Geoderma*, *80*, 1-44.

Campbell, G. S., Norman, J.M., 1998. *An introduction to environmental biophysics*. (pp. 286). Springer, New York.

Campbell, G.S. (1974). A simple method for determining unsaturated conductivity from moisture retention data. *Soil Science, 117*, 311-314.

Chang, C., Laird, D.A., Mausbach, M.J., Hurburgh, C.R., 2001. Near-infrared spectroscopy-Principal component regression analysis of soil properties. *Soil Science Society of America Journal, 65*, 480-490.

Chatres, C. 1987. *Australia's land resources at risk.* University of Cambridge, Melbourne.

Chartres, C.J., Kirby, M.J., Raupach, M., 1990. Poorly ordered silica and aluminosilicates as temporary cementing agents in hardsetting soils. *Soil Science Society of America Journal, 51,* 819-824.

Chavez, P.S., 1996. Image-based atmospheric correction –revisited and improved. *Photogrammetric Engineering and Remote Sensing, 62(9),* 1025-1036.

Chow, V.T., Maidment, D.R. and Mays, L/W. (1988). *Applied hydrology.* USA, McGraw Hill.

Chen, Y., Tarchitzy, J., Brouwer., J., Morin., J., Banin, A., 1980. Scanning electron microscope observations on soil crusts and their formation. *Soil Science, 130,* 49-55.

Choudhury, B.J., Ahmed, N.U., Idso, S.B., Reginato, R.J., Daughtry, C.S.T., 1994. Relations between evaporation coefficient and vegetation indices studied by model simulation. *Remote Sensing of Environment, 50,* 1-17.

Clapp, R.B. and Hornberger, G.M. (1978). Empirical equations for some soil hydraulic properties. *Water Resources Research, 14,* 601-604.

Clark R.N., Roush L.T., 1984. Reflectance spectroscopy: quantitative analysis techniques for remote sensing applications. *Journal of Geophysical Research, 89,* 6329-6340.

Collis-George, N. (1977). Infiltration equations for simple soil system. *Water Resources Research, 2,* 729-738.

Condit H.R., 1970. The spectral reflectance of American soils, *Photogrammetric Engineering, 36,* 955-966.

Condom, N., Kuper, M., Marlet, S., Valles, V., Kijne, J., 1999. Salinization, alkanization and sodification in Punjab (Pakistan): Characterization of the geochemical and physical processes of the degradation. *Land Degradation Development, 10,* 123-140.

Coulon, E., Bruand, A., 1989. Effects of compaction on the pore space geometry in sandy soils. *Soil and Tillage Research, 15,* 137-152.

Cowe I. A., McNicol, J.W., 1985. Spectral applications. *Applied Spectroscopy, 39*, 257-264.

Cresswell, H.P., Smiles, D.E., Williams, J., 1992. Soil structure, soil hydraulic properties and the soil water balance. *Australian Journal of Soil Research, 30*, 265-283.

Cudahy T. J., Ramanaidou E.R., 1997. Measurement of the Hematite: Geothite ratio using visible and near infrared reflectance spectrometry in channel iron deposits, Western Australia. Journal of Earth Sciences, 44, 411 – 420

Da Costa, L.M., 1979. *Surface soil colour and reflectance as related to physiochemical and mineralogical soil properties*. In: Remote Sensing for Earth Sciences: Manual of Remote Sensing, John Wiley and Sons, London

Dane, J.H., Klute, A., 1977. Salt effects on the hydraulic properties of a swelling soil. *Soil Science Society of America Journal, 41*, 1043-1049.

Davies, T.M.C., Fern, T., 2002. Sorting the wheat from the chaff. *Spectroscopy of Europe 14 (2)*, 16 – 17.

De Jong, S.M., 1994. Applications of reflective remote sensing for land degradation studies in a Mediterranean environment. Utrecht University, The Netherlands, PhD. dissertation. 240 pp.

Dematte, J. A. M., Pereira, H. S., Nanni, R.M., Cooper, M., Fiorio, P., 2003. Soil chemical alterations promoted by fertilizer application assessed by spectral reflectance. *Soil Science, 168*, 730-747.

Deuchers, S.A., Townend, J., Aitkenhead, M.J. and FitzPatrick, E.A. (1999). Changes in soil structure and hydraulic properties in regenerating rain forest. *Soil Use and Management, 15*, 183-187.

Dexter, A.R., 1988. Advances in characterization of soil structure. *Soil and Tillage Research, 11*, 199-238.

Dexter, A.R., 2004. Soil physical quality, Part I. Theory, effects of soil texture, density, and organic matter, end effects on root growth. *Geoderma, 120*, 201-214.

Dexter, A.R., Czyz, E.A. 2000. Effects of soil management on the dispersibility of clay in a sandy soil. *International Agrophysics, 14*, 269-272.

Di Gregorio, A., Jansen, L.J.M., 2000. Land cover classification system (LCCS): classification concepts and user manual. FAO, Italy.

Dingman, L.S., 2002. *Physical hydrology*. (pp 575). Prentice Hall, New Jersey

Dirksen, C., 1999. Soil physics measurements. Catena-Verlag, Reiskirchen.

Doran,J.W., Coleman, D.C., Bezdocek, D.F., Stewart, B.A., 1994. Defining soil quality for sustainable environment. *Soil Science Society of America* (Special Publication).

Draper, D., 1995. Inference and hierarchical modeling in the social science. *Journal of Educational and Behavioral Statistics 20,* 115-147.

Drexel, J. Preiss, W., 1995. The geology of South Australia. Volume 2, the Phanerozoic. South Australian Geological Survey, *Bulletin 54*.

Dwivedi, S.R., Sankari, R.T., Venkataratnam, L., Karale, L.R., Gawande, S.P., Rao, S.V., Senchaudhary, S., Bhaumik, K.R., Mukharejee, K.K., 1997. The inventory and monitoring of eroded lands using remote sensing data. *International Journal of Remote Sensing, 18,* 107-119.

Ellenkamp, G.R., 2004. *Soil variability and landscape in the Machakos district, Kenya*. Unpublished MSc Dissertation. Wageningen University, The Netherlands.

Elrick, D.E., Parkin, G.W., Reynolds, W.D., Fallow, D.J., 1995. Analysis of early-time and steady-state single ring infiltration under falling head conditions, *Water Resources Research 31(8),* 1883-1892.

Elrick, D.E., Reynolds, W.D., 2002. Measuring water transmission parameters in vadose zone using ponded infiltration techniques. *Agricultural Sciences 7,* 17-22.

ERDAS LLC. (2002). *ERDAS IMAGINE® 8.6*, Leica Geosystems, Atlanta, Georgia

Eshel, G., Levy, G.J., Singer, M.J. (2004). Spectral reflectance properties of crusted soils under solar illumination. *Soil Science Society of America Journal, 68,* 1982-1991

Fabiola, N., Giarola, B., da Silva, A.P., Imhoff, S., Dexter, A.R., 2003. Contribution of natural compaction on hardsetting behavior. *Geoderma, 113,* 95-108.

FAO, 1971-1981. *The FAO-UNESCO soil map of the World.* Legend and 9 volumes. UNESCO, Paris.

FAO, 1979. A provisional methodology for soil degradation assessment. Food and Agriculture Organization, Rome.

FAO, ISRIC, 2000. Soil and terrain database, soil degradation status, and soil vulnerability assessments for Central and Eastern Europe (Scale 1:2.5 million; ver 1.0). Land and Water Digital Media Series 10, FAO, Rome.

Farrar, T.J., Nicholson, S.E., Lare, A.R., 1994. The influence of soil type on the relationship between NDVI, rainfall, and soil moisture in semiarid Botswana: II. NDVI response to soil moisture. *Remote Sensing of Environment, 50,* 121-133.

Feddema, J.J., 1998. Estimated impacts of soil degradation on the African water balance and climate. *Climate Research, 10,* 127-141.

Fern T (2000): NIR news. Journal of Near Infrared, 11(6), 14 – 15.

Fies, J.C., Bruand, A., 1998. Particle packing and organization of the textural porosity in clay-silt-sand mixtures. *European Journal of Soil Science, 49,* 557-567.

Flowers, M.D., Lal, R., 1998. Axle load and tillage effects on soil physical properties and soybean grain yield on a Mollic Ochraqualf in Northwest Ohio. *Soil and Tillage Research, 48,* 21-35.

Franzmeier, D.P., Chartres, C.J., Wood, J.T., 1996. Hardsetting soils in Southeast Australia: landscape and profile processes. *Soil Science Society of America Journal, 60,* 1178-1187.

Gerberman D., Neher J., 1979. Reflectance of varying mixtures of clay soil and sand, *Photogrammetric Engineering and Remote Sensing, 45,* 1145 – 1151.

Gardner, W.R., Hillel, D., and Benjamini, Y. (1970). Post Irrigation movement of soil water. I. Redistribution. *Water Resources Research, 6,* 851-861.

GARMIN International. (2002). *GERMIN® 12 XL handheld GPS*, Olathe, Kansas.

Ghassemi, F., Jakeman,. A.J., Nix, H.A., 1995. *Salinization of land and water resources: human causes, extent, management and case studies.* PhD Thesis. The Australian National University, Canberra, Australia.

Gobin, A.M., Campling, P., Deckers, J.A., Poesen, J., Feyen, J., 1999. Soil erosion assessment at the Udi-Nsukka Cuesta (Southeastern Nigeria). *Land Degradation and Devevelopment, 10*, 141-160.

Gourdin, A., Boumahrat, M., 2002. *Applied numerical methods.* (pp. 392). Prentice Hall of India, New Delhi.

Govers, G., 1999. Tillage erosion and tillage translocation. *Soil and Tillage Research*, 51. Special Issue.

Govers, G., Quine, T.A., Desmet, P.J.J., Walling, D.E., 1996. The relative contribution of soil tillage and overland flow erosion to soil redistribution on agricultural land. Earth Surfaces Processes Landforms, 21, 929-946.

Green, E.R., Chong, S.K., 1983. Sorptivity measurement and its application. In *Advances in Infiltration. Proceedings of the National Conference on Advances in Infiltration* (ASAE , Ed.), 12-13 December, 1983, Chicago, Illinois, ASAE, Michigan, pp. 82-91.

Greene, R.S.B., Eggleton, R.A., Rengasamy, P., 2002. Relationship between clay mineralogy and the hardsetting properties of soils in the Carnarvon horticultural district of Western Australia. *Applied Clay Sciences, 20*, 211-223.

Greenland, D.J., 1981. Soil management and soil degradation. *Journal of Soil Science, 32*, 301-322.

Groenevelt, P.H., Grant, C.D., 2004. A new model for the soil-water retention curve that solves the problem of residual water contents. *European Journal of Soil Science, 55*, 479-485.

Gu, D., Gillepsie, A., 1998. Topographic normalization of Landsat TM images of forest based on sub pixel sun-canopy-sensor geometry. *Remote Sensing of Environment, 64*, 166-175.

Gupta, R.K., Abrol, I.P., 1990. Salt-affected soils: Their reclamation and management for crop production. *Advances in Soil Sciences, 5*, 223-287.

Hartemink, A.E., 1998. Soil chemical and physical properties as indicators of sustainable land management under sugarcane in Papua New Guinea. *Geoderma, 85*, 283-306.

Heil, J.W., Jou, A. S.R., McInnes, K.J., 1997. Soil properties influencing surface sealing of some sandy soils in the Sahel. *Soil Science, 162*, 459-469.

Hengl, T., Heuvelink, G.B.M., Stein, A., 2004. A generic framework for spatial prediction of soil variables based on regression-kriging. *Geoderma, 120*, 75-93.

Hesketh, N., Brookes, P.C., Addiscott, T.M., 2001. Effect of suspended material and pig slurry on the facilitated transport of pesticides, phosphate and bromide in sandy soil. *European Journal of Soil Science, 52*, 287-296.

Holtan, H.N. (1961). A concept for infiltration estimates in watershed engineering. *USDAARS Publication, ARS*, 41-45.

Horn, R., Domzal, H., Slowinska-Jurkiewicz, A., and van Ouwerkerk, C. (1995). Soil compaction processes and their effects on the structure of arable soils and the environment. *Soil and Tillage Research, 35*, 23-36.

Horton, R.E. (1933). The role of infiltration in the hydrological cycle. *Transaction f American Geophysics Union, 14*, 446-460.

Hudson, N.W., 1971. *Soil conversion*, Batsford, London.

Hudson, N.W., 1993. Field measurement of soil erosion and runoff. FAO, Rome.

Insightful Corp., 2002. *S Plus*©, Lucent Technologies: New York.

Iqbal, M. (1983). *An introduction to solar radiation*. Toronto, Academic Press.

Janik, L.J., Merry, R.H., Skjemstad, J.O., 1998. Can mid infrared diffuse reflectance analysis replace soil extractions? *Australian Journal of Experimental Agriculture, 38*, 681-696.

Jetten, V., de Roo, A.P.J., Favis-Mortlock, D.T., 1999. Evaluation of field-scale and catchment-scale soil erosion models. *Catena, 37*, 521-541.

Jones, J.A. R., Spoor, G., Thomasson, A.J., 2003. Vulnerability of subsoils in Europe to compaction: a preliminary analysis. *Soil and Tillage Research, 73*, 131-143.

Jones, J.A.R., 2002. Assessing the vulnerability of soil to degradation. In: Pagliai, M., Jones, R. (Eds), *Sustainable Land Management-Environmental Protection- A soil Physical Approach*. Advances in AgroEcology, vol 35. catena-Verlag, Reiskirchen, pp. 33-44. 598 pp.

Johnson, R.A., Wichern, D.W., 1992. *Applied Multivariate Statistical Analysis*. Prentice-Hall International Inc.: New Jersey.

Kottegoda, N.T., Russo, R., 1997. *Statistics, Probability and Reliability for Civil and Environmental Engineers*. McBraw-Hill International Editions: New York.

Kariuki, P.C., Woldai, T., and van Der Meer, F.D. (2001), *Determination of soil activity in Kenyan soils from spectroscopy*. The International Archives for Photogrammetry, Remote Sensing and Spatial Information Science. Vol 24. Part 6/W6.

Karlen, D.L., Mausbach, M.J., Doran, J.W., Cline, R.G., Harris, R.T., Schuman, G.E., 1997. Soil quality: A concept, definition and framework for evaluation. *Soil Science Society of America, 61*, 4-10.

Kostiakov, A.N. (1932). On the dynamics of the coefficient of water percolation in soils and on the necessity for studying it from a dynamic point of view for purposes of amelioration. Transaction of the 6th Commonwealth International Society of Soil Science, Russian Part A: 17-21.

Kunze, R.J. and Kar-Kuri, H.M. (1983). Gravitational flow in infiltration. In *Advances in Infiltration. Proceedings of the National Conference on Advances in Infiltration* (ASAE , Ed.), 12-13 December, 1983, Chicago, Illinois, ASAE, Michigan, pp. 82-91.

Kutilek, M. and Nielsen, D. (1994). *Soil hydrology*. Reiskirchen, CATENA-VERLAG.

Leger R.G., Millere G.J.F. Chomchan S., 1979. The effects of organic matter, iron oxides and moisture on the colour of two agricultural soils of the Quebec, *Canadian Journal of Soil Science, 59,* 191-202.

Lal, R., Sanchez, P.A., 1992. *Myths and science of soils of the tropics*. Soil Science Society of America Journal. Special Publications No. 29.

Lal, R., 1997. Degradation and resilience of soils. *Philosophical Transactions of Royal Society, London (B), 352*, 997-1010.

Lal, R., 1998. Soil erosion impact on agronomic productivity and environmental quality. *Critical Reviews in Plant Sciences, 17*, 319-464.

Lal, R., 2000a. Physical management of soils of the tropics: Priorities for the 21^{st} centaury. *Soil Science, 165*, 191-207.

Lal, R., 2000b. Soil management in the developing countries. *Soil Science, 165*, 57-72.

Lark, R.M., Cullis, B.R., 2004. Model-based analysis using REML for inference from systematically sampled data on soil. *European Journal of Soil Science 55*, 799-813.

Leij, F.L., van Genuchten, M.T., Yates, S.R., Russell, W.B. Kaveh, F., 1992. RETC: A computer program for analyzing soil water retention and hydraulic conductivity data. In: M.T. van Genuchten, F.J. Leij and L.J. Lund (eds), *Indirect Methods for Estimating the Hydraulic Properties of Unsaturated Soils* (pp. 317-328). Riverside, CA: University of California. California, Riverside, CA. pp. 317-328.

Liang, S., 2004. *Quantitative remote sensing of land surfaces*. John Willey and Sons, New Jersey.

Lilly, A., 2000. The relationship between field-saturated hydraulic conductivity and soil structure: development of class pedotransfer fnctions. *Soil Use and Management, 16*, 56-60.

Lindstrom, M.J., Bates, D.M., 1990. Newton-Raphson and EM algorithm for linear mixed-effects models for repeated-measures data (corr: 94v89 p1572), *Journal of the American Statistical Association 83*, 1014-1022.

Mapfumo, E., Chanasyk, D.S., Naeth, M.A., Baron, V.S., 1999. Soil compaction under grazing of annual and perennial forages. *Canadian Journal of Soil Science, 79*, 191-199.

Marshall, T. J., Holmes, J.W., Rose, W.C., 1996. *Soil physics*. Cambridge University Press, London.

McBratney, A.B., Mendonça-Santos, M.L., Minasny, B., 2003. On digital soil mapping. *Geoderma 117*, 3-52.

McCuen, R.H., Rawls,W.J., and Brakensiek, D.L. (1981). Statistical analyses of the Brooks-Corey and Green-Ampt parameters across soil textures. *Water Resources Research, 17*, 1005-1013.

McGarry, D., 1993. Degradation of Soil Structure. In: McTainsh, G.H., Boughton, W.C. (Eds), *Land degradation processes in Australia*. Cheshire, Melbourne, pp. 271-305.

Metternicht, G.I., Zinck, J.A., 2003. Remote sensing of soil salinity: potentials and constraints. *Remote Sensing of Environment*, *85*, 1-20.

Montero S., Irene C., Brimhall G.H., 2001. Semi-Automated Mineral identification Algorithm for Ultraviolet, visible and Near-Infrared Reflectance Spectroscopy, Paper presented in Annual Conference of the international Association for Mathematics in Geology., On 22nd August, 2001, Berlin.

Montgomery S., Baumgardner K., 1974. Reflectance properties of soils, *Advances in Agronomy*, *38*, 1 – 44.

Morgan, K.M., Morris, D.R., Lee, G.B., Keifer, R.W., Bubenzer, G.D., Daniel, T.C., 1980. Aerial photography as an aid to cropland erosion analysis. *Transactions of American Society of Agricultural Engineers*, 907-913.

Mullins, C.E., Young, I.M., Bengough, A.G., Ley, G.J., 1990. hardsetting soils: behaviour, occurrence and management. *Advances in Soil Science*, *11*, 37-108.

Mullins, C.E., Young, I.M., Bengough, A.G., Ley, G.J., 1987. Hardsetting soils. *Soil Use Management*, *3*, 79-83.

Munkholm, L.J., Schjonning, P., 2004. Structural vulnerability of a sandy loam exposed to intensive tillage and traffic in wet conditions. *Soil and Tillage Research*, *79*, 79-85.

Mzezewa, J., Gotosa, J., Nyamwanza, B., 2003. Characterization of a sodic soil catena for reclamation and improvement strategies. *Geoderma*. *113*, 161-175.

Oldeman, L.R., 1998. *Soil degradation: a threat to food security.* ISRIC, Wageningen, The Netherlands.

Oldeman, L.R., Hakkeling, R.T.A., Sombroek, W.G., 1991. *World map of the status of human-induced degradation: an explanatory note.* ISRIC, Wageningen, The Netherlands/UNEP, Nairobi, Kenya, pp. 34.

Omuto, C.T. 2007a. New biexponential model for water retention characteristics. Geoderma (submitted: Manuscript ID-GEODER-S-07-00028)

Omuto, C.T. 2007b. HydroMe Version 1.0 – A package for estimating soil hydraulic parameters using R software. R-project Team. www.cran.r-project.org/contrib/PACKAGES.html

Omuto, C.T. and Shrestha, D.P. 2006. Remote sensing techniques for rapid detection of soil physical degradation. International Journal of Remote Sensing (In Press).

Omuto, C.T., Minasny, B., Mcbratney, A.B., and Biamah, E.K. 2006a. Nonlinear mixed effects modelling for improved estimation of water retention and infiltration parameters. Journal of Hydrology, 330, 748-758.

Omuto, C.T., Minasny, B., and McBratney, A.B. 2006b. Screening soils for physical degradation. European Journal of Soil Science (In Press).

Omuto, C.T. 2003. Rapid mapping of saturated hydraulic conductivity in tropical watersheds. Msc Thesis, University of Nairobi, Kenya.

Ontar Corporation. (2002). *PcModWin 4.0.* Ontar Corporation: North Andover, USA.

Pagliai, M., 1988. Soil porosity aspects. *International Agrophysics, 4,* 215-232.

Pagliai, M., Jones, R., 2002. *Sustainable land management-environmental protection- A Soil physical approach.* Advances in GeoEcology vol. 35. Catena-Verlag: Reiskirchen.

Park. S., Feddema, J.J. and Egbert, S.L. (2004). Impacts of hydrologic soil properties on drought detection with MODIS thermal data. *Remote Sensing of Environment, 89,* 53-62.

Pettit, A.N. and McBratney, A.B., 1993, Sampling designs for estimating spatial variance components. *Applied Statistics, 42,* 185-209.

Philip, J.R. (1957). The theory of infiltration I. The infiltration equation and its solutions. *Soil Science, 83,* 345-357.

Pinheiro, J.C., Bates, D.M., 2000. *Mixed-effects models in S and S-Plus.* Springer-Verlag, New York.

Poesen, J.W.A., Nearing, M.A. 1993. *Soil surface sealing and crusting.* Catena Supplement, vol. 24. Catena-Verlag: Reiskirchen.

Quine, T.A., Govers, S., Walling, D.E., Zhang, X., Desme, P.J.J, Zhangi, Y., Vandaele, K., 1997. Erosion processes and landform evaluation on agricultural land – New perspective from Caesium-137 measurement and topographic-based erosion modeling. *Earth Surface Processes and landforms. 22,* 799-816.

Quirk, J.P., 1986. Soil permeability in relation to sodicity and salinity. *Philosophical Transactions of the Royal Society, A316,* 297-317.

Rees, W.G. (2001). *Physical principles of remote sensing.* New York, Cambridge University Press.

Reynolds, W.D., Elrick, D.E., 1990. Pondend infiltration from a single ring: I. Analysis of steady flow. *Soil Science Society of America Journal, 54,* 1233-1241.

Richards, L.A., 1954. *Diagnosis and improvement of saline and alkali soils.* Agriculture Handbook, vol. 69. USDA, Washington D.C.

Richard, G., Cousin, I., Sillon, J.F., Bruand, A., Guerif, J., 2001. Effect of compaction on the porosity of a silty soil: influence on unsaturated hydraulic properties. *European Journal of Soil Science, 52,* 49-58.

Rogowski, A.S. (1971). Watershed physics: Model of the soil moisture characteristic. *Water Resources Research, 7,* 1575-1582.

Roulier, S., Angulo-Jeramillo, R., Bresson, L.-M., Auzet, A.-V., Gaudet, J.-P., Bariac, T., 2002. Water transfer and mobile water content measurement in a cultivated crusted soil. *Soil Science, 167,* 201-210.

Rousseva, S., Torri, D., Pagliai, M., 2002. Effect of rain on the microporosity at the soil surface. *European Journal of Soil Science, 53,* 83-94.

Salford Systems, 2002. CART user's guide: An implementation of the original CART methodology. San Diego: Salford Systems.

Sanchez, J., Bluda, R., Artigo, A., Colomer, J.C., Morell, C., Tebar, J.I., 1997. Assessment of soil degradation in desertification threatened areas: A case study in Castill-La Mancha (Spain). In: F. Martin de Santa Olalla (Ed.), EFEDA-II Subgroup II Final Report: *Vegetation, Inventory and Impacts: Desertification Processes in the Mediterranean Area and their Interlinks with Global Climate*. pp. 19-58, Universidad de castilla-La Mancha, Albaceta, Spain.

Sanchez, P.A., Palm,C.A., Buol, S.W., 2003. Fertility capability soil classification: A tool to help assess soil quality in the tropics. *Geoderma, 114*, 157-185

Schadlich, S., Gottsche, F.M., Olesen, F.S., 2001. Influence of land parameters and atmosphere on Meteosat brightness temperature and generation of land of land surface temperature maps by temporally and spatially interpolating atmospheric correction. *Remote Sensing of Environment, 75*, 39-46.

Shepherd K. D., Walsh, M. G., 2004. Diffuse reflectance spectroscopy for rapid soil analysis. In: Rattan Lal (Ed.) *Encyclopedia of Soil Science*. New York: Mercel dekker Inc.

Shepherd, K.D., Walsh, M.G., 2002. Development of reflectance spectral libraries for characterization of soil properties. *Soil Science Society of America Journal, 66*, 988-998.

Shepherd, K.D., Palm, C.A., Gachengo, C.N., Vanlauwe B., 2003. Rapid characterization of organic resource quality for soil and livestock management in tropical agroecosystems using near-infrared spectroscopy. *Agronomy Journal, 95*, 1314-1322.

Smedma, L.K., Rycroft, D.W., 1983. Land Drainage: Planning and Design of Agricultural Drainage System, Batsford, London.

Sobieraj, J.A., Elsenbeer, H., Marques, R. Newton, B., 2002. Spatial variability of hydraulic conductivity along a tropical rainforest catena. *Geoderma 108 (1-2)*, 79-90.

Sobrino, J.A., Caselles, V., Becker, F., 1990. Significance of the remotely sensed thermal infrared measurements obtained over a citrus orchard. *ISPRS Photogrammetric Engineering and Remote Sensing, 44*, 343-354.

Sobrino, J.A., Jimenez-Munoz, J.C., Paolini, L., 2004. Land surface temperature retrieval from Landsat TM 5. *Remote Sensing of Environment, 90*, 434-440.

Sakamoto, Y., Ishiguro,M., Kitagawa, G., 1986. *Akaike Information Criterion Statistics*. Reidel: Dordrecht, Holland.

Sombroek, W.G., Braun, H.M.H., van der Pouw, B.J.A., 1982. *Exploratory Soil Map and Agro-climatic Zone Map of Kenya, 1980, Scale 1:1.000.000.* Kenya Soil Survey, Ministry of Agriculture: Nairobi, Kenya.

Stephen, N., 2002. Standardization of soil quality attributes. *Agriculture, Ecosystems and Environment, 88*, 161-168.

Stott, D.E., Kennedy, A.C., Combardella, C.A., 1999. Impacts of soil organism and organic matter in soil structure. In Rattan Lal (eds). *Soil Quality and Soil Erosion*, Soil and Water Conservation Society, CRC Press.

Suresh, R., 2002. Soil and water conservation engineering, Standard Publishers Distributors, Delhi.

Thisted, R.A., 1988. Elements of statistical computing. (pp. 155-258). Chapman and Hall, London.

Thompson, A.M., Witte, J.C., McPeters, R.D., Oltmans, S.J., Schmidlin, F.J., Logan, J.A., Fujiwara, M., Kirchhoff, V.W.J.H., Posny, F., Coetzee, G.J.R., Hoegger, B., Kawakami, S., Ogawa, T., Johnson, B.J., Vömel, H., Labow, G., 2003. Southern Hemisphere Additional Ozonesondes (SHADOZ) 1998-2000 tropical ozone climatology 1. Comparison with Total Ozone Mapping Spectrometer (TOMS) and ground-based measurements. *Journal of Geophysical Research, 108*, No. D2, 8238, doi: 10.1029/2001JD000967.

Tiffen, M., Mortimore, M., Gichuki F., 1994. *More people, less erosion: Environmental recovery in Kenya.* England, Overseas Development Institute: John Willey and Sons.

Triantafilis, J., 1996. *Quantitative assessment of soil salinity in the lower Naomi Valley.* PhD dissertation, University of Sydney, Australia.

Troufleau, D., Sagaard, H., 1998. Deriving surface water status in the Sahel from the Pathfinder AVHRR land data set. *Physics and Chemistry of Earth, 23(4),* 421-426.

Tsai F., Philpot, W., 1998. Derivative Analysis of Hyperspectral Data. *Remote Sensing of Environment 66*, 41 – 51.

UNEP/ISSS/ISRIC/FAO, 1995. Global and national soils and terrain digital databases (SOTER) procedures manual. World Soil Resources Report No. 74. FAO, Rome.

Unganai, L. S., Kogan, F. N., 1998. Drought monitoring and corn yield estimation in southern Africa from AVHRR data. *Remote Sensing of Environment*, *63*, 219-232.

USDA (1974). Border irrigation. Chapter 4, section 15, US Soil Conservation Service National Engineering Handbook, US Government Print Office.

Valentine, C., and Bresson, L.M., 1992. Morphology, genesis and classification of surface crusting loamy and sandy soils. *Geoderma, 55,* 225-245.

Van Beek, C.G.E., Van Breeman, N., 1963. The alkalinity of alcali soils. *Journal of Soil Science, 24,* 129-136.

Van der Knijff, J.M., Jones, R.J.A., Montanarella, L., 1999. *Soil erosion risk map assessment in Italy*. EUR 19044 EN, 52 pp.

Van Genuchten, M. Th., 1980. A closed –form equation for predicting the hydraulic conductivity of unsaturated soils. *Soil Science Society of America Journal, 44,* 892-898.

Van Lynden, G.W.J., 2000. Soil degradation in central and Eastern Europe: the assessment of the status of human-induced degradation (SOVEUR Project version 1.0. Report 2000/05, ISRIC, Wageningen, The Netherlands.

Venables, W.N., Ripley, B.D., 1999. *Modern applied statistics with S-Plus*. New York: Springer.

Wallbrink, P.J., Murray, A.S., Olley, J.M. 1999. Relating suspended sediments to its original soil depth using fallout radionuclides. *Soil Science Society of America Journal, 63,* 369-378.

Watts, C., Dexter, A.R., 1998. Soil friability: theory, measurement and the effects of management and organic carbon content. *European Journal of Soil Science, 49*, 73-84.

West, S.L., White, G.N., Deng, Y., McInnes, K.J., Juo, A.S.R., Dixon, J.B. 2004. Kaolinite, halloyside, and iron oxide influence on physical behavior of formulated soils. *Soil Science Society of America Journal, 68*, 1452-1460.

Whalley, W.R., Dumitru, E., Dexter, A.R., 1995. Biological effects of soil compaction. *Soil and Tillage Research, 35*, 53-68.

Widder, D.V., 2003. *Advanced calculus*. New Delhi: Prentice Hall of India.

Williams, J., Prebble, R.E., Williams, W.T. and Hignett, C.T. (1983). The influence of texture, structure and clay mineralogy on the soil moisture characteristic. *Australian Journal of Soil Research, 21*, 15-32.

Wright, R. J., Boyer, D. G., Winant, W. M., Perry, H.D., 1990. The influence of soil factors on yield differences among landscape positions in an Appalachian cornfield. *Soil Science, 149*, 375-382.

Wu, L., Pan, L., Roberson, J.M. and Shouse, P.J. (1997). Numerical evaluation of ring-infiltraometers under various soil conditions. *Soil Science, 162*, 771-777.

Young, I.M., Crawford, J.W., Rappldt, C., 2001. New methods and models for characterizing structural heterogeneity of soil. *Soil and Tillage Research, 61*, 33-45.

APPENDICES

A1. Theoretical consideration of infiltration characteristics

Water infiltration is the water entry into the soil and is controlled by two factors; 1) the resistance of the soil to the water flow, and 2) the forces acting on each unit of soil-water to cause them to move. Darcy's law, the fundamental equation describing water movement in the soil, relates the flow rate to these two factors. Mathematically, the statement of Darcy's law is given by

$$Flux = \frac{Q}{A} \text{ is proportional to } \frac{\partial \Psi}{\partial z} \qquad \text{(A1.1)}$$

where Q is the infiltration rate, A is the cross-sectional area of the soil column (which is made of textural and structural pore spaces to conduct the infiltrating water), Ψ is the flux potential (which is the sum of the matrix potential ϕ and gravitational potential z), and $\frac{\partial \Psi}{\partial z}$ is the gradient driving the flow of infiltrating water. Since the movement of water is dominantly in the vertical direction downwards, the gravitational potential is often negative. Thus,

$$Flux = \frac{Q}{A} = v = -K(\theta)\left[\frac{\partial(\phi - z)}{\partial z}\right] \qquad \text{(A1.2)}$$

$$Flux = -D(\theta)\frac{\partial \theta}{\partial z} + K(\theta) \qquad \text{(A1.3)}$$

where $D(\theta) = K(\theta)\frac{d\phi}{d\theta}$ and is known as the diffusivity function. Assuming that during the infiltration the soil moisture only changes with depth (but changes with time is insignificant, that is θ and t are independent variables in equation (A1.3), then, for a unit cross-sectional area

$$\partial z = \frac{-D(\theta)}{v(\theta,t) - K(\theta)}\partial\theta$$

and on integration becomes

$$z(\theta,t) = \int_{\theta}^{\theta_1(t)} \frac{D(\theta)}{v(\theta,t) - K(\theta)}\partial\theta \qquad \text{(A1.4)}$$

where $\theta_1(t)$ is the antecedent soil moisture content at time t. Using the principle of conservation of mass for the moisture profile $\partial v/\partial z = \partial\theta/\partial t$, then

$$\int_{0}^{t} Q(t)dt = \int_{\theta_r}^{\theta_1(t)} z(\theta,t)dz \qquad \text{(A1.5)}$$

where $Q(t)$ is the flux value at the soil surface where infiltration process begins. Substituting equation (A1.4) into equation (A1.5) and integrating by changing the limits yields

$$Qt(\theta_1) = \int_{\theta_r}^{\theta_1} \frac{(\theta - \theta_r)D(\theta)}{v(\theta,t) - K(\theta)}d\theta \qquad \text{(A1.6)}$$

where θ_r is the residual moisture content (Vanapali *et al.*, 1998). Equation (A1.5) can also be integrated in parts to determine the time it takes the infiltrating water to pond, t_p as

$$Qt_p + \int_{t_p}^{t} Q(t)dt = \int_{\theta_r}^{\theta_s} \frac{(\theta - \theta_r)D(\theta)}{v(\theta,t) - K(\theta)}d\theta \qquad \text{(A1.7)}$$

where θ_s is the saturation moisture content at ponding. Writing the integration in equation (A1.7) as $u(Q, \theta, \theta_s)$ and differentiating with respect to time yields

$q = \frac{\partial u}{\partial Q}\frac{dQ}{dt}$ which when integrated becomes

$$\int_{t(Q)}^{t_p} dt = \int_{Q}^{Q_p} \frac{1}{Q}\frac{\partial u}{\partial Q} dQ$$

from which the time to ponding can be evaluated as

$$t(Q) - t_p = \int_{Q_p}^{Q} \frac{1}{Q}\frac{\partial u}{\partial Q} dQ \qquad \text{(A1.8)}$$

where Q_p is the infiltration rate at ponding. If the ponding infiltration rate $Q_p > K_s$ the saturated soil hydraulic conductivity and assuming a simple hydraulic conductivity function, equation (A1.6) can be written as

$$\frac{Q}{K_s} t(\theta_1) = \int_{\theta_r}^{\theta_1} \left[\frac{\frac{(\theta-\theta_r)}{(\theta_s-\theta_r)}}{\frac{v}{K_s}\left(\frac{\frac{(\theta-\theta_r)}{(\theta_s-\theta_r)}}{\frac{(\theta-\theta_r)}{(\theta_s-\theta_r)}} \right) - \left(\frac{(\theta-\theta_r)}{(\theta_s-\theta_r)} \right)^2} \right] \frac{D(\theta)(\theta_s-\theta_r)^2}{K_s^2} d\theta \qquad \text{(A1.9)}$$

In equation (A1.9) if

$q = Q/K_s$, $\quad T = K_s^2 t(\theta_1) \big/ \left[D(\theta)(\theta_s - \theta_r)^2\right]$, $\quad S_f = (\theta - \theta_r) \big/ (\theta_s - \theta_r)$

$Int = \int q dT$, and $S_{f1} = (\theta_1 - \theta_r) \big/ (\theta_s - \theta_r)$, then

$$qT = \int_0^{S_f} \frac{S_f}{qS_f / S_{f1} - S_f^2} dS_f \qquad \text{(A1.10)}$$

At ponding when moisture content is approximately θ_s (that is $\theta_1 = \theta_s$) and on integration of equation (A1.10) by parts yields

$$Int(q) = \int_0^1 \frac{S_f}{qS_f - S_f^2} dS_f = -\ln\left[1 - \frac{1}{q}\right] \quad \text{(A1.11)}$$

Substituting in equation (A1.8) and integrating yields

$$T(q) = T_p + \int_{q_p}^{q} \frac{1}{q} \frac{dInt}{dq} dq = \frac{Int(q_p)}{q_p} + Int(q) - Int(q_p) + \frac{1}{q_p} - \frac{1}{q} \quad \text{(A1.12)}$$

when $Q_p >> K_s$ at the instantaneous ponding then $q_p \to \infty$, the equation (A1.12) becomes

$$T(q) = Int(q) - \frac{1}{q} \quad \text{(A1.13)}$$

substituting for $1/q$ in equation (A1.13) from equation (A1.11) yields

$$T(q) = Int(q) - 1 + e^{-Int(q)}$$

or

$$Int(q) = T(q) - e^{Int(q)} + 1$$

or just simply as

$$I(T) = T + 1 - e^{-I} \quad \text{(A1.14)}$$

The Taylor's expansion series for low values of T in equation (A1.14) gives

$$I(T) = T + 1 - \left\{T - \left(\frac{1}{1}T\right)^0 - \left(\frac{1}{2}T\right)^{0.5} - \left(\frac{1}{3}T\right)^1 - \ldots\right\}$$